/
Article / Book Information

( )	
Title(English)	Traffic Estimation with Vehicles Observing Other Vehicles
( )	
Author(English)	Toru Seo
( )	: , : , : 9982 , :2015 9 25 , : , : , , , , ,
Citation(English)	Degree:, Conferring organization: Tokyo Institute of Technology, Report number: 9982 , Conferred date:2015/9/25, Degree Type:Course doctor, Examiner:,,,,,
( )	
Type(English)	Doctoral Thesis

Traffic Estimation with Vehicles Observing Other Vehicles

by

Toru Seo

Submitted to the

Department of Civil Engineering

in partial fulfillment of the requirements for the degree of

Doctor of Engineering

at the

Tokyo Institute of Technology

August, 2015

Abstract

This dissertation is entitled "Traffic estimation with vehicles observing other vehicles" by Toru Seo, submitted to the Department of Civil Engineering in partial fulfillment of the requirements for the degree of Doctor of Engineering at the Tokyo Institute of Technology, August, 2015. The dissertation supervisor is Professor Yasuo Asakura, Department of Civil Engineering, Tokyo Institute of Technology. The examiners are Professor Yasuo Asakura, Professor Tetsuo Yai, Associate Professor Yasunori Muromachi, Associate Professor Shinya Hanaoka, Associate Professor Daisuke Fukuda (Tokyo Institute of Technology) and Professor Takamasa Iryo (Kobe University).

This dissertation summarizes methodology of estimating traffic using probe vehicles which observe other nearby vehicles. It consists of seven chapters.

In chapter 1, the background and objective are summarized. Automobile traffic takes significant roles in today's civilization. In order to achieve high efficiency of traffic, traffic managements are required. The managements require knowledge on current traffic situation. However, knowing traffic situation in anytime and anywhere is not yet possible due to theoretical and practical reasons. The aim of this dissertation is to propose methodology for traffic state estimation that is theoretically and practically applicable for vast time–space domain. To achieve it, this dissertation formulates and validates traffic state estimation method utilizing probe vehicle with spacing measurement equipment.

In chapter 2, related studies are reviewed and summarized. It includes traffic flow theory, traffic data collection methods, traffic state estimation methods and advanced vehicle technology. Traffic flow theory can be summarized by employing the concept of cumulative flow. Then current traffic data collection methods and traffic state estimation methods are reviewed; and their characteristics are described based on the concept of cumulative flow. As a result, a challenging task remained in traffic engineering filed is outlined: traffic state estimation methods that can applicable for vast time–space domain without theoretical discrepancies. Recent developments in advanced vehicle technology include vehicle automation, by which vehicle can observe other nearby vehicles. Spacing,

namely, distance from a vehicle's head to its leading vehicle's one, is typical information collected by such automated vehicles. As a result, a possible approach for the traffic state estimation is pointed out: methods utilizing probe vehicles with spacing measurement equipment.

In chapters 3 and 4, methodology of estimating traffic state utilizing probe vehicles' position and spacing information is formulated. An estimation method are formulated as requiring less exogenous assumptions as possible and consistent with traditional definition in traffic flow theory. These characteristics enable the methods to be applied in various situations without theoretical discrepancies. The method's characteristics, such as accuracy and precision, are investigated analytically. Then, some well-accepted assumptions on traffic flow are integrated to the methods in order to improve the proposed methodology's reasonability in common traffic situations. One of the method estimates traffic state based on the concept of cumulative flow by assuming existence of a conservation law in a link. The other method estimates traffic state by assuming existence of a conservation law and a fundamental diagram whose parameters are endogenously estimated from the probe vehicle data.

In chapters 5 and 6, the proposed methodology is empirically validated. The data for validation are actual probe vehicle data collected via a field experiment conducted in the real world, as well as synthetic data generated by simulation experiment. A simulation experiment-based validation can clarify the methods' characteristics under idealized situation, while a field experiment-based validation can evaluate the method's characteristics under actual traffic environment. As a result, relation among the estimation methods' precision and accuracy, time–space resolution, penetration rate of probe vehicles and assumptions is clarified. Their consistency with analytical results is confirmed. Therefore, the methods' applicability in actual traffic environment is shown.

In chapter 7, achievements and future directions are summarized. The achievements are formulation and validation of methodology of traffic state estimation utilizing probe vehicle with spacing measurement equipment. The future directions include sophistication of the methodology, such as further integration of traffic flow theory.

Acknowledgements

iii

Contents

List of Figures

List of Tables

List of Notations

Following notations are used throughout in this dissertation unless otherwise specified.

q	flow (veh/h)
k	density (veh/km)
v	speed (km/h)
t	time (h)
x	space (km)
$N(t, x)$	cumulative flow at time t and space x (veh)
n	index for a vehicle
m	index for a probe vehicle
$\hat{\ }$	mark for an estimated value
$\mathbf{A}$	time–space region
$|\mathbf{A}|$	area of time–space region $\mathbf{A}$ (km h)
$\mathbf{a}_n(\mathbf{A})$	time–space region between vehicle n and $n-1$ in region $\mathbf{A}$
$\mathbf{N}(\mathbf{A})$	set of all the vehicles in region $\mathbf{A}$
$\mathbf{P}(\mathbf{A})$	set of all the probe vehicles in region $\mathbf{A}$
$t_n(\mathbf{A})$	time spent by vehicle n in region $\mathbf{A}$
$d_n(\mathbf{A})$	distance traveled by vehicle n in region $\mathbf{A}$
$\bar{h}_n(\mathbf{A})$	mean headway experienced by vehicle n in region $\mathbf{A}$
$\bar{s}_n(\mathbf{A})$	mean spacing experienced by vehicle n in region $\mathbf{A}$
u	free-flow speed (km/h)
k_c, k^c	critical density (veh/km)
κ	jam density (veh/km)
μ	mean
σ	standard deviation

List of Abbreviations

Following abbreviations are used throughout in this dissertation.

TSE	Traffic State Estimation
GPS	Global Positioning System
AVT	Advanced Vehicle Technologies
PVSME	Probe Vehicle with Spacing Measurement Equipment
LWR	Lighthill–Whitham–Richards
FD	Fundamental Diagram
CL	Conservation Law
FIFO	First-In First-Out
OD	Origin–Destination
UE	User Equilibrium
SO	System Optimum
CTM	Cell Transmission Model
MFD	Macroscopic Fundamental Diagram
KFT	Kalman Filtering(-like) Techniques
EnKF	Ensemble Kalman Filter
PR	Penetration Rate of probe vehicles in entire vehicles
MAE	Mean Absolute Error
MAPE	Mean Absolute Percentage Error
RMSE	Root Mean Square Error
RMSPE	Root Mean Square Percentage Error
PoI	Percentage of Improvement
C1	Inner Circler Route
JCT	JunCTion
ID	IDentification

Chapter 1 Introduction

1.1 Background

Transportation—"a system for carrying people or goods from one place to another using vehicles, roads, etc." (Hornby et al., 2010)—is one of the most essential elements in civilization. Efficiency of a transportation system must be kept as high as possible. A transportation system consists of

- people who travel within the system based on their decision,
- modes/infrastructures by/on which people travel, and
- information by which people decide,

In general, civil engineers can keep the efficiency high by controlling and regulating modes/infrastructures based on information, and providing information to people. To do so, civil engineers have to answer following questions:

- how many people are there and how fast they are?
- how people decide?

In fact, these are not easy questions. The first point can be answered by collecting information from the transportation system; however, collecting information from the entire system is not always possible due to technological and financial limitations. The second point may be more difficult. If complete rational travelers with perfect information are assumed, it can be answered partially (Sheffi, 1985); however, as mentioned above, the perfect information condition is not always satisfied (and perhaps people are not complete rational). Under such circumstances, people's decision-making should be modeled theoretically and be validated empirically—this requires information, again. In short conclusion, information on transportation system is required as

- basis for coding controls, and

- input data for controls.

Traffic is a special mode in a transportation system, where automobiles travel through one-dimensional roads (Daganzo, 1997). In the modern era, automobiles take significant role in transportation, because of their high flexibility, high speed, low cost and good capability of carrying. It has the same information problem mentioned in above. Ironically, mainly due to their high flexibility, automobiles often cause traffic jams and negative externalities such as time loss, safety issues and environmental issues—user equilibrium (UE) vs social optimum (SO) problem in traffic network (Wardrop, 1952; Braess, 1968). To mitigate these externalities, carefully planed and precisely performed traffic control measures are required. As a consequence, it can be said that traffic data collection can be one of the most essential elements in civilization. From emergence of traffic engineering (Greenshields, 1935), several methodologies have been developed to collect traffic data. Their approaches can be roughly categorized twofold: Eulerian and Lagrangian sensing. Eulerian sensing, also known as fixed observation, collects traffic data at fixed-point on a road; the typical examples are road side traffic detectors and manual counting. They can acquire sufficient traffic data at installed location; however, spatiotemporally wide ranging data collection is difficult due to their installation and maintenance cost. Lagrangian sensing, also known as floating, mobile and probe observation, collects traffic data from a vehicle that moves along the traffic; the typical examples are Global Positioning System (GPS)-equipped probe vehicles. They can only acquire position and speed data; however, spatiotemporally wide ranging data collection is possible due to their nature and low running cost. Still, there are no feasible methodologies that are capable of collecting sufficient traffic information for spatiotemporally wide range. This makes difficult to understand and control traffic.

Recently, advanced vehicle technologies (AVT), such as adaptive cruise control, collision avoidance, and autonomous vehicles, have been developed practically for the driving safety and efficiency purposes (c.f., National Highway Traffic Safety Administration, 2013). These systems automate some of the driving functions of vehicles by recognizing the surrounding environment of a vehicle. Indeed, these technologies

are valuable as they improve efficiency of an individual vehicle's driving; however, it does not always guarantee optimal improvement at social level, just like the UE vs SO problem. Meanwhile, they can be more valuable if they are utilized from social-scale view point. The information collected by them, especially spacing (i.e., vehicle-to-vehicle distance), is valuable from the point of view of traffic data collection—spacing is closely related to traffic state as well as vehicle's decision-making behavior. The information is impossible to be acquired with conventional data collection methods, such as road side traffic detectors and GPS-equipped probe vehicles. Therefore, such advanced vehicles are expected to be utilized as a source of new traffic data and contribute to transportation from social-scale. Fig 1.1 illustrates traffic data collection approaches; a gray arrow represents a vehicle trajectory, orange area represents observable area, and a red dot/line represents observable information.

1.2   Objective

The primal objective of this dissertation is to propose methodology for probe vehicle-based traffic state estimation (TSE) that can collect sufficient traffic data where probe vehicles observe their surrounding vehicles with onboard equipments. In particular, this dissertation proposes methods for estimating the flow, density, and speed based on the spacing and position information collected by the probe vehicles. This dissertation names such probe vehicles "probe vehicles with spacing measurement equipment (PVSME)". The primal objective is achieved by accomplishing following secondary objectives: review (chapter 2), formulation (chapters 3 and 4) and validation (chapters 5 and 6). In the review chapter, background and challenging tasks for this dissertation are clarified. Then, in the formulation chapters, TSE methods using PVSME are formulated considering the review results. In the validation chapters, empirical characteristics of the formulated methods are investigated; and their performance is shown.

Specifically, this dissertation is organized as follows. Chapter 2 reviews existing studies on related topics to this dissertation, that is, traffic flow theory, traffic data
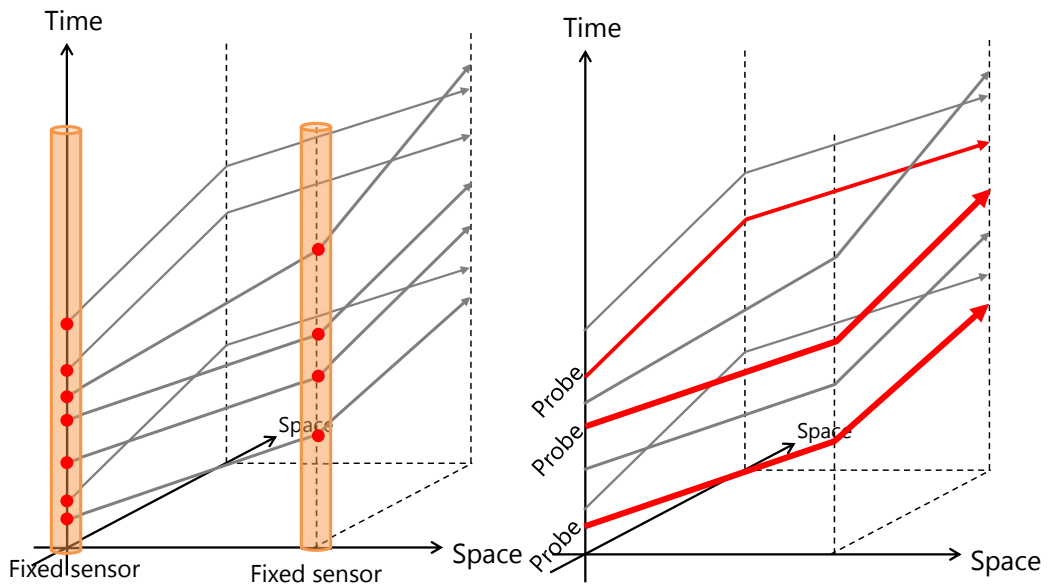
(a) Eulerian sensing (e.g., detectors). Fixed sensors (orange pillars) collect information of travelers (gray arrows).

(b) Conventional Lagrangian sensing (e.g., GPS-equipped probe vehicles). Some of the travelers (red arrows) report information of their own.
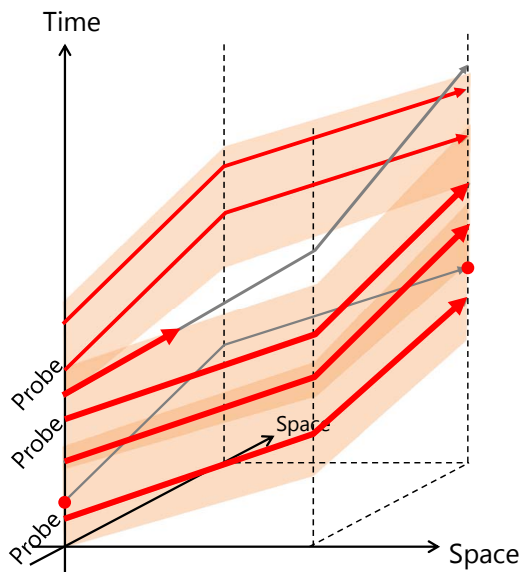
(c) Proposed Lagrangian sensing (i.e., PVSME). Some of the travelers (red arrows and orange belts) collect information of nearby travelers.

Figure 1.1: Transportation system information collection approaches.
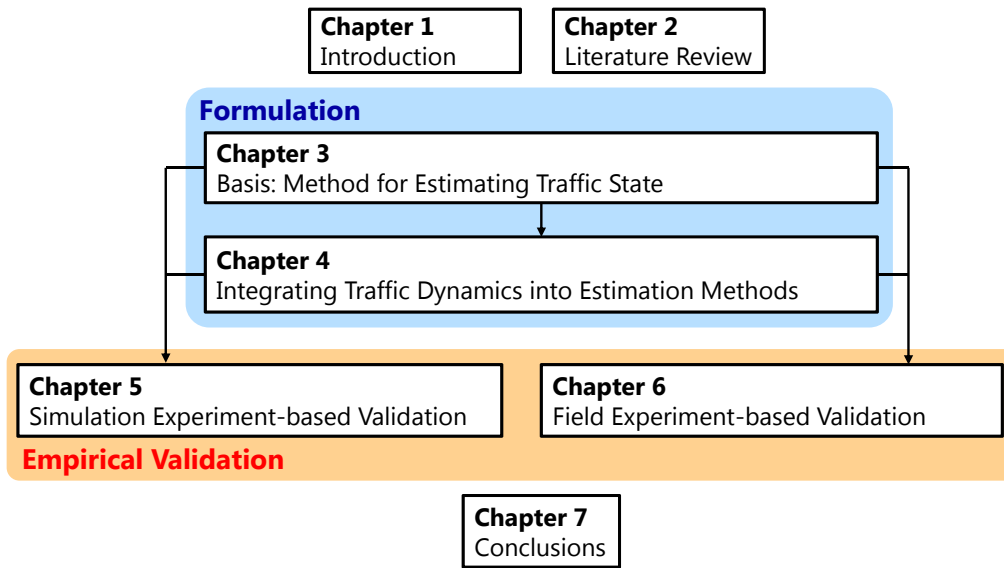
Figure 1.2: Structure of dissertation.

collection, TSE and advanced vehicle technologies. Chapter 3 formulates the basic method for estimating traffic state from the assumed probe vehicle data. It is formulated as much as simple and consistent with traffic flow theory, in order to utilize it as basis of more advanced methods. In addition, the basic method is analytically investigated in order to obtain general insight. Then chapter 4 develops more advanced TSE methods considering other factors in traffic flow theory, especially on those describe traffic dynamics. Chapters 5 and 6 validate the proposed methods in chapters 3 and 4, by using simulation experiment datasets and an actual traffic dataset we collected via a field experiment, receptively. Through the validation, performance of the proposed methodology is shown empirically. Finally, chapter 7 concludes achievements and future direction of the proposed methodology. Fig 1.2 illustrates the structure of this dissertation.

Chapter 2 Literature Review

This chapter reviews existing studies that are related to this dissertation. Section 2.1 summarizes theoretical aspects of traffic flow, from how traffic states are defined to how traffic dynamics are modeled. Section 2.2 classifies existing TSE methods, as well as traffic data collection methods, according to approaches, techniques and technologies employed by them. Finally, section 2.3 reviews recent advancement in the vehicular technologies from a point of view of traffic and transportation engineering.

2.1 Traffic flow theory

This section briefly[*1] reviews how traffic has been theoretically represented and modeled in existing studies.

In order to simplify discussion, following considers sufficiently long length street with single lane without vehicle's overtaking nor merging/diverging sections (i.e., a first-in first-out (FIFO) condition and a conservation law (CL) is satisfied), unless otherwise specified. The space coordinate x increases as downstream direction; the time coordinate t increases as future direction; the vehicle count n increases from leading vehicles to following vehicles.

2.1.1 Traffic state

A traffic state can be defined as *a set of flow q, density k and average speed v*, in macroscopic scale which focuses on aggregated vehicles and does not always distinguish each vehicles. The flow, also known as flow rate and traffic volume, is a number of

---

[*1]See following literatures for the detail on traffic flow theory. Daganzo (1997) provided systematic and detailed introduction to traffic flow theory. Helbing (2001) summarized comprehensive review on traffic flow from various perspective. Wageningen-Kessels et al. (2014) described taxonomy of traffic flow models with excellent artwork.
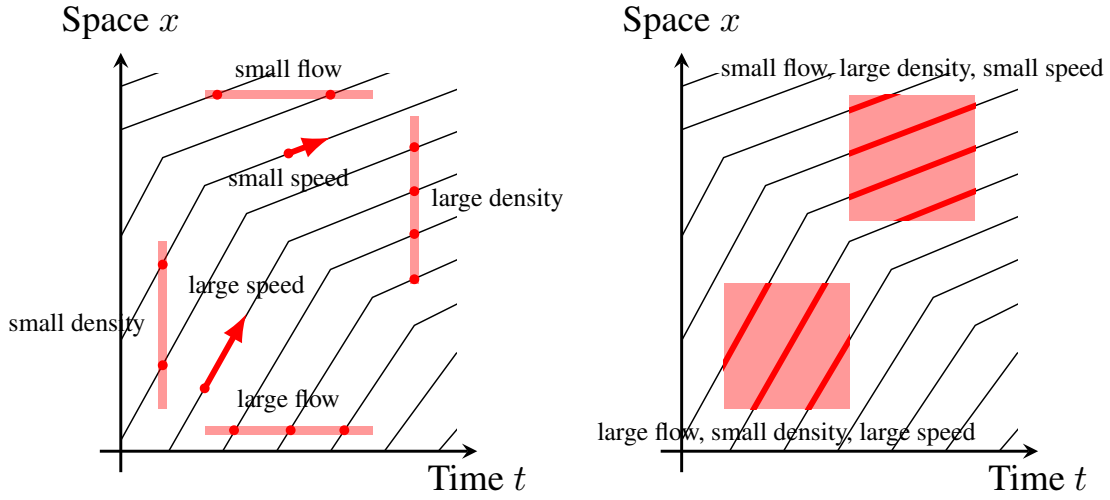
(a) Specified definition often utilized in practical situation

(b) Edie's generalized definition

Figure 2.1: definition of traffic state.

vehicles that pass per unit time; density is a number of vehicles that exist per unit space; and the average speed is a mean of instantaneous speeds among vehicles. In practical situation, point flow in space, space density at a time point and space mean speed are often utilized; they are shown in Fig 2.1a. Edie (1963) proposed generalized definition of traffic state; the traffic state in a time–space region $\mathbf{A}$ can be defined as follows:

$$q(\mathbf{A}) = \frac{d(\mathbf{A})}{|\mathbf{A}|}, \tag{2.1}$$

$$k(\mathbf{A}) = \frac{t(\mathbf{A})}{|\mathbf{A}|}, \tag{2.2}$$

$$v(\mathbf{A}) = \frac{d(\mathbf{A})}{t(\mathbf{A})}, \tag{2.3}$$

where $d(\mathbf{A})$ is the total distance traveled by all of the vehicles in the region $\mathbf{A}$ (veh km), $t(\mathbf{A})$ is the total time spent by all of the vehicles in the region $\mathbf{A}$ (veh h), and $|\mathbf{A}|$ is the time–space area of the region $\mathbf{A}$ (km h). It is shown in Fig 2.1b. These definition include specific definitions mentioned before. Note that the relation of $q = kv$ must be satisfied. They are often utilized for representing macroscopic traffic. Usually, a set of flow, density and speed with high time–space resolution (e.g., minutes- and meters-scale) is referred to
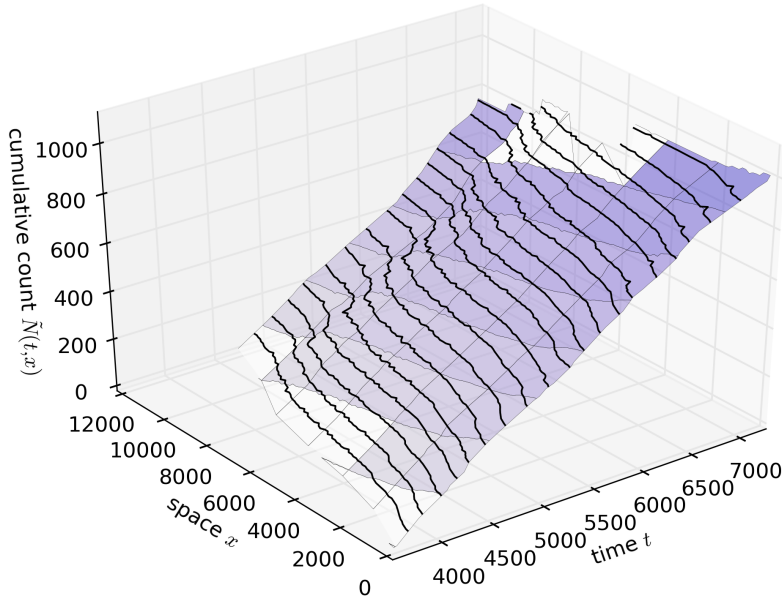
Figure 2.2: Three-dimensional representation of traffic flow using the cumulative flow

a traffic state.

The concept of a cumulative flow can be introduced to generalize above. A cumulative flow $N(t, x)$ is defined as a number of vehicles that passed position x by time t. A cumulative curve or count, which is a cumulative flow at a certain position (i.e., $N(t, x =$ given)), is well-known for analyzing queues. A continuous cumulative flow $\tilde{N}(t, x)$ shapes a continuous and smooth "surface" in vehicle–time–space (n–t–x) domain, in which all the traffic state mentioned above are included (Moskowitz, 1965; Makigami et al., 1971). For example, a contour line of the same $\tilde{N}$ is a vehicle trajectory $X(n, t)$ and $T(n, x)$, a slope of $\tilde{N}$ in the t direction is the flow q, and the slope of $\tilde{N}$ in the $-x$ direction is the density k. Therefore, following equations hold true:

$$q(t, x) = \frac{\partial N(t, x)}{\partial t}, \tag{2.4}$$

$$k(t, x) = \frac{\partial N(t, x)}{\partial x}, \tag{2.5}$$

$$v(t, x) = \frac{q(t, x)}{k(t, x)}. \tag{2.6}$$

Fig 2.2 shows an example of a cumulative flow.

In general, a traffic state can be defined as representation of traffic situation in a certain

time–space domain. In microscopic scale, which focuses on disaggregated vehicles and distinguishes each vehicles, a state of traffic can be defined as position of vehicle n at time t, that is, $X(n, t)$. Its first order derivative, namely, $dX(n, t)/dt = \dot{X}(n, t)$, is instantaneous speed; and its second order derivative $\ddot{X}(n, t)$ is acceleration, respectively, of vehicle n at time t. A spacing of vehicle n, namely, distance to its leading vehicle, is $X(n-1, t) - X(n, t)$. They are often utilized for modeling vehicle driving behaviors. In fact, they are not often referred to "traffic state".

2.1.2 Fundamental diagram

A fundamental diagram (FD), also known as flow–density relation, found by Greenshields (1935), is a relation among the traffic state (i.e., flow, density and speed) in equilibrium state[*2] (i.e., no vehicles have incentive to change their speed and spacing) at a time–space point. An FD can be represented as

$$q(t, x) = Q(k(t, x), t, x), \tag{2.7}$$

where $Q(k, t, x)$ is the FD function that returns flow where density is k at time t and position x. Usually (in single-regime model), an FD in a flow–density plane is a convex curve that has a peak. An FD in a speed–density plane is a weakly monotonic decrease curve. An equilibrium traffic state is a stationary, that is, all the vehicles have the same speed and spacing, if the FD in speed–density plane is strongly monotonic decreasing. Fig 2.3 shows an example of an FD. A traffic state with a density higher than a critical density k_c is considered as congested state; and that lower than or equal to k_c is considered as free-flow state. One of the most widely-used functional form for an FD is triangular

---

[*2]It should be noted that, a flow–density plot, namely, scatter plot that drawn with observed traffic state by traffic detector with fixed time interval, looks like an FD but is not an FD. It is because such flow–density plot can include non-equilibrium states (e.g., the observation duration includes both free-flow state and congested state). The wide scatter often found in flow–density plot is mainly because of this issue; if such non-equilibrium states are removed, an actual data-based flow–density plot will be well-defined bivariately (Cassidy, 1998; Coifman, 2014). Nevertheless, actual FD may have scatter; it is mentioned in later.
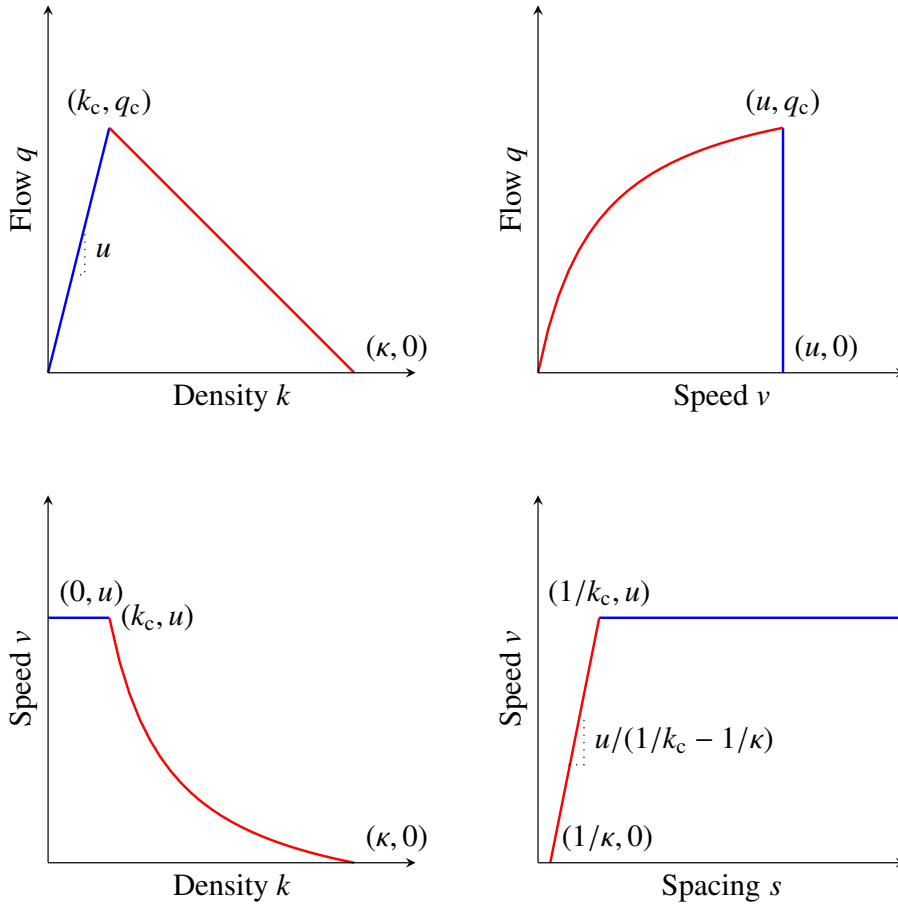
Figure 2.3: Example of triangular FD in four coordinate systems

function (Newell, 1993a), which simplify an FD as piecewise linear function with two lines in flow–density plane, as follows:

$$
q = \begin{cases} uk, & 0 \le k < k_\mathrm{c}, \\ -\frac{uk_\mathrm{c}}{\kappa - k_\mathrm{c}}k + \frac{u}{1/k_\mathrm{c} - 1/\kappa}, & k_\mathrm{c} \le k \le \kappa, \end{cases} \tag{2.8}
$$

where q_c is maximum flow, k_c is critical density, and κ is jam density. For simplicity purpose, backward wave $uk_\mathrm{c}/(\kappa - k_\mathrm{c})$ is sometimes noted using w, and $u/(1/k_\mathrm{c} - 1/\kappa)$ is noted using $1/\tau$. Fig 2.3 illustrates a triangular FD with four coordinate systems, namely, q–k, k–v, q–v and s–v (they are equivalent). The blue lines represent free-flow state and the red lines represent congested state.

Although several studies have investigated FDs characteristics from theoretical, analytical and empirical perspective, there are no complete theory and explanation for
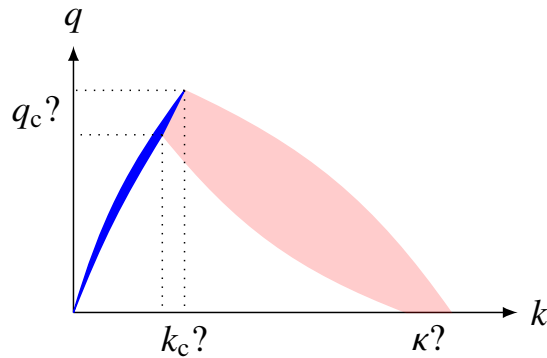
Figure 2.4: Example of realistic FD.

determining an FD; there are only approximations[*3].   This is due to that an FD depends on, ultimately, behavior of drivers whom the traffic consists of. For example, Fig 2.4 illustrates an FD often found in empirical data (Edie, 1961; Treiterer and Myers, 1974). The scatter in congested area is referred to hysteresis phenomenon, which is a phenomenon where trajectories of a transition from lower density to higher and that from higher to lower draw different curves. Its reason is considered to heterogeneity in vehicle's driving style for acceleration and deceleration (Newell, 1962; Treiterer and Myers, 1974; Laval, 2011). The variety in capacity is referred to capacity drop, which is a phenomenon where capacity decreases when free-flow state turns into congested state. Its reason is considered to effect from upstream (Edie, 1961), lane-changing (Daganzo, 2002) and effect of a platoon (Shiomi et al., 2011). Heterogeneity in vehicle length also affects to above phenomena (Coifman, 2015).

2.1.3   Traffic flow model

Representing and modeling dynamics of traffic is important. The modeling approaches can be roughly divided by two: microscopic and macroscopic. In microscopic models, individual vehicle's behavior is disaggregately and explicitly modeled. On the other hand, in macroscopic models, vehicles are approximated as continuous fluid; and behavior of

---

[*3]By employing an approximated functional form, an FD can be estimated empirically based on sufficiently high resolution traffic data (e.g., Chiabaut et al., 2009; Qu et al., 2015).

the fluid is aggregately and explicitly modeled.

(1) Microscopic approach

It is natural that traffic is described from a point of view of a vehicle individually. Car-following models (Pipes, 1953; Kometani and Sasaki, 1958, 1961; Gazis et al., 1961) describe one-dimensional (i.e., longitudinal) movement of individual vehicle behavior by considering interaction among vehicles. In typical car-following models, a vehicle's speed are determined by considering distance to the leading vehicle and speed of it; for example, the car-following model of Kometani and Sasaki (1958) is described as

$$\beta \ddot{X}(n, t) = \dot{X}(n - 1, t - t_{\mathrm{r}}) - \dot{X}(n, t - t_{\mathrm{r}}) \tag{2.9}$$

where β is constant coefficient, and t_{r} is a reaction time (of vehicle n). Newell (2002) connected this model and macroscopic traffic flow model, such as capacity, which is described in later.

Lane-changing models (Gipps, 1986) describe lane-changing (i.e., lateral) movement of individual vehicle behavior by considering interaction among vehicles. In typical lane-changing models, a vehicle determines its lane by considering its desired speed, safety and destination.

Microscopic vehicle behavior (i.e., combination of car-following and lane-changing behavior) has been modeled by using diverse manners, such as gap acceptance decision (Ashton, 1971), behavioral models (Gipps, 1981, 1986), game theory (Kita, 1999) and Markov chained (i.e., dynamic) latent class models (Choudhury and Ben-Akiva, 2013; Yanagihara et al., 2015); because it should be determined considering a lot of objectives and constrains that relate with human behavior, vehicle performance and road alignment. These models are mainly utilized for investigating traffic safety (Kometani and Sasaki, 1958), traffic at merging/diverging section and intersection (Sarvi and Kuwahara, 2007), capacity drop due to platoon (Shiomi et al., 2011), and effects of introducing new types of vehicles such as ADAS (Kikuchi et al., 2003; Talebpour and Mahmassani, 2015)—in other words, where heterogeneity among drivers significantly affects the results and is the

main interest. Their reproductivity in macroscopic scale is not always guaranteed (is not always required), mainly due to their too many parameters, difficulty to be calibrated and mathematical intractability.

(2) Macroscopic approach

From macroscopic point of view, traffic can be approximated as continuous fluid whose flow, density and speed correspond to the original traffic state.

The Lighthill–Whitham–Richards (LWR) model (Lighthill and Whitham, 1955; Richards, 1956), also known as first order traffic flow model and kinematic wave theory, is the simplest and yet sufficient model that describes traffic dynamics. The LWR model employs two principles: an FD and a CL. In the LWR model, a traffic state is assumed to always equilibrates[*4]. The LWR model can be described as following equations:

$$q(t, x) = Q(k(t, x), t, x), \tag{2.10}$$

$$\frac{\partial q(t, x)}{\partial x} + \frac{\partial k(t, x)}{\partial t} = 0, \tag{2.11}$$

where eq (2.10) represents an FD, eq (2.11) represents a CL, and $Q(k, t, x)$ is a fundamental diagram at time–space point (t, x).

One of the objectives of studying macroscopic traffic flow models is to determine the cumulative flow in the time–space area of interest based on given boundary conditions. Therefore, several numerical computation methods for solving the LWR model have been proposed. Numerical computation with time–space discretization (i.e., t–x coordinate system) is a typical approach for solving the LWR model (Daganzo, 1994; Lebacque, 1996). In this approach, the initial condition is the density at a certain time in the road sections and boundary condition is in/outflow to/from the road sections. Other studies

---

[*4]It implies that the vehicle's speed can change instantaneously. It can be flaw in representing realistic traffic phenomena, such as hysteresis phenomena and capacity drop. Some studies developed more complex traffic flow models, such as the second order model (Payne, 1971). However, they may produces some un-preferable phenomena as traffic (Daganzo, 1995); and their tractability may be low. Other studies addressed this issue by modifying the LWR model (Leclercq et al., 2011; Srivastava et al., 2015; Delpiano et al., 2015).

introduced Lagrangian coordinates (i.e., n–t and n–x coordinate system) for solving the LWR model (Leclercq et al., 2007; Laval and Leclercq, 2013). Lagrangian coordinates have following advantages and disadvantages: they can explicitly use vehicle trajectories; however, special treatments are required for dealing non-FIFO situation.

The LWR model can be simplified by assuming that the triangular and constant FD shown in eq (2.8), which have three variables u, k_c and κ (and two auxiliary variables w and τ for concise notation). With this simplification, solving the LWR model based on boundary conditions concludes a minimization problem of two quantities that can be calculated from the boundary cumulative flow, the free-flow speed and the wave speed (Newell, 1993a,b,c). It is referred as Newell's simplified kinematic wave model and Newell's three detector problem. It can be represented as follows:

$$N(t, x_m) = \min \left\{ N\left(t - \frac{x_m - x_u}{u},\ x_u\right),\ N\left(t - \frac{x_d - x_m}{w},\ x_d\right) + \kappa(x_d - x_m) \right\}, \qquad (2.12)$$

where x_m is a position of a detector whose cumulative flow is to be calculated, x_u is a position of an upstream detector, and x_d is a position of a downstream detector. If the first term in $\min\{\cdot\}$ in eq (2.12) is smaller than or equal to the second one, the traffic between x_u and x_m is in free-flow state. Otherwise, it is partially congested and therefore the traffic between x_d and x_m is in congested state.

The cell transmission model (CTM; Daganzo, 1994) is a well-known computation method for the simplified LWR model based on time–space discretization (i.e., the Godunov scheme; Lebacque, 1996). It is described as follows:

$$f_i^{\text{in}}(t) = \min \left\{ N_{i-1}(t),\ \frac{w}{u}(l\kappa - N_i(t)) \right\}, \qquad (2.13a)$$

$$N_i(t + \Delta t) = N_i(t) + f_i^{\text{in}}(t) - f_{i+1}^{\text{in}}(t), \qquad (2.13b)$$

where $f_i^{\text{in}}(t)$ is number of vehicles that enter cell i during timestep t, $N_i(t)$ is number of vehicles in cell i at timestep t (it can be equal to $N(t, il)$), Δt is width of a timestep, and l is length of a cell which must be equal to $u\Delta t$ in order to avoid numerical errors. Eq (2.13a) determines flow based on state of cell i and its upstream cell $i - 1$. If the first term in $\min\{\cdot\}$ in eq (2.13a) is smaller than or equal to the second one, cell i during timestep

t is in free-flow state; and all the vehicles move with the free-flow speed. if not, it is in congested state. Eq (2.13b) represents transmission of vehicles between adjacent cells.

A car-following model that is equivalent to the simplified LWR model was also proposed (Newell's simplified car-following model; Newell, 2002; Daganzo, 2006)—obviously, it can be utilized for computing the model from a microscopic point of view. It can be represented as follows:

$$X(n, t) = \begin{cases} X(n - 1, t - \tau) - \frac{1}{\kappa}, & \text{if } n \text{ is following } n - 1 \\ X(n, t - \Delta t) + u\Delta t, & \text{otherwise} \end{cases} \tag{2.14a}$$

$$= \min\left\{X(n - 1, t - \tau) - \frac{1}{\kappa}, \ X(n, t - \Delta t) + u\Delta t\right\}. \tag{2.14b}$$

In eq (2.14a), "n is following $n - 1$" means that traffic is congested or saturated. As connection with the microscopic models, it showed that relation $0 \leq t_\mathrm{r} \leq \tau$ must be satisfied between an FD and car-following models' reaction time; and $t_\mathrm{r} = \tau/2$ was suggested for usual conditions.

The variational theory (Daganzo, 2005a,b) is efficient computation methodology using the variational method, based on the idea of Newell's three detectors problem, with rigorous mathematical proofs. Then above mentioned calculation methods were generalized for the three coordinate systems including Lagrangian ones (i.e., t–x, n–t and n–x coordinate systems), by applying the theory of Hamilton–Jacobi partial differential equations and the idea of the variational theory (Laval and Leclercq, 2013). It can be summarized as follows:

N-model calculates quantity N at point (t, x):

$$N(t, x) = \min\left\{\min_{y \in B}\{N(0, y) + uk_\mathrm{c}t - k_\mathrm{c}(x - y)\}, \ N\left(t - \frac{x}{u}, 0\right)\right\} \tag{2.15a}$$

$$\simeq \min_{i=-1,0,\ldots,\theta}\left\{N(t - \Delta t, x - i\Delta x) + \Delta x\frac{\theta - i}{\theta + 1}\right\}, \tag{2.15b}$$

where $\Delta x = \Delta n/\kappa$ and $\Delta t = \tau\Delta n$,

T-model calculates quantity T at point (n, x):

$$T(n, x) = \max\left\{T(n, 0) + \frac{x}{u}, \ T\left(0, x + \frac{n}{\kappa}\right) + \tau n\right\} \tag{2.16a}$$

$$\simeq \max\{T(n, x - \Delta x) + \Delta t, \ T(n - \Delta n, x + \Delta x) + \theta \Delta t\}, \qquad (2.16b)$$

where $\Delta t = \Delta x / u$ and $\Delta x = \Delta n / \kappa$,

X-model calculates quantity X at point (n, t):

$$X(n, t) = \min \left\{ \min_{y \in B} \left\{ X(y, 0) + ut - \frac{n - y}{k_{\mathrm{c}}} \right\}, \ X(0, t - \tau n) - \frac{n}{\kappa} \right\} \qquad (2.17a)$$

$$\simeq \min\{X(n, t - \Delta t) + \theta \Delta x, \ X(n - \Delta n, t - \Delta t) - \Delta x\}, \qquad (2.17b)$$

where $\Delta n = \kappa \Delta x$ and $\Delta t = \Delta x / w$,

where B is a boundary (for initial condition) curve of the area of interest, and $\theta = u/w$ is required to be an integer. In eqs (2.15)–(2.17) sub-equations (a) represent general solution; and sub-equations (b) represent corresponding discretized solution (i.e., cellular automata). The Newell's three detector problem and CTM can be regarded as special cases of N-model. The variational theory can be regarded as a special N-model that can efficiently calculate N at arbitrarily (t, x); therefore, it has capability of dealing vehicle trajectories. The Newell's simplified car-following model and some of the existing Lagrangian models can be regarded as special cases of X-model.

More advanced traffic flow models such as that dealing with multi-lane (Daganzo, 2002; Laval and Daganzo, 2006; Zheng, 2014; Shiomi et al., 2015), multi-class (Daganzo, 2002; Wageningen-Kessels et al., 2010), stochastic phenomena (Sumalee et al., 2011) and capacity drop (Leclercq et al., 2011) have been developed.

2.1.4 Area-wide traffic: Macroscopic fundamental diagram

Recently, the concept of an FD is expanded to an area-wide region that includes non-stationary states (Geroliminis and Daganzo, 2008); it is referred to macroscopic fundamental diagram (MFD). An MFD is relation between area-flow and area-density which are defined using Edie's generalized definition. It is conjectured that, under "certain conditions", following features exist in area-wide traffic:

- area-wide traffic is steady,
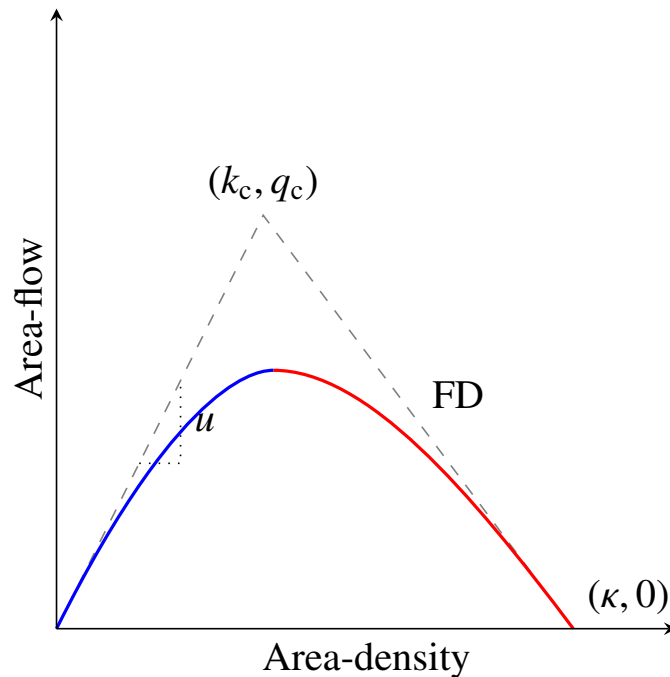
Figure 2.5: Example of well-defined MFD.

- relation between area-flow and area-density is clearly bivariate (except hysteresis
  phenomena mentioned by below), namely, a convex curve with a peak just like an
  FD,

- hysteresis phenomena exist just like an FD, and

- flow at an area's perimeter correlates to its area-flow.

It is referred to "well-defined MFD". These characteristics are expected to enable traffic
control measures that require less information and operation from theoretical and practical
perspectives (Daganzo, 2007; Daganzo et al., 2011, 2012). Fig 2.5 illustrates an example
of well-defined MFD (solid curve) along with an FD (gray dashed curve). The red curve
represents gridlock state, where effect of queue spillover is significant. Note that relation
between the MFD and FD in Fig 2.5 is just a conjecture.

The flaw is that the "certain conditions" for a well-defined MFD are not clarified yet,
although a lot of applications that assumed existence of well-defined MFDs are proposed.
Some of the "certain conditions" were analytically proven, such as homogeneous road

with signals without in/outflow (Daganzo and Geroliminis, 2008), that with stochastic (heterogeneous) schematics and controls (Laval et al., 2015) and two link network with route choice (Leclercq and Geroliminis, 2013; Jin et al., 2013). Other conditions were empirically guessed, such as some-sort-of-homogeneous network (Geroliminis and Daganzo, 2008; Geroliminis and Sun, 2011) and one-to-many network under dynamic user equilibrium (和田・佐津川, 2014). Meanwhile, existence of steady network traffic and therefore steady area-wide traffic were proven under steady traffic demands, supplies and route choice principles (Jin, 2015).

2.2   Traffic data collection and traffic state estimation

2.2.1   Definition

As a preparation for reviewing existing studies, definitions of *traffic data*, *traffic data collection* and *traffic state estimation* in this dissertation and their basic characteristics are described.

(1)   Traffic data

Traffic data are defined as *measured cumulative flow in a certain time–space regions with appropriate origins* in this dissertation. If measurement errors were ignored, the definition can be represented as

$$\mathcal{D}(\mathcal{A}) = \{\{N(t, x) - N(t_0(\mathbf{A}), x_0(\mathbf{A})) \mid (t, x) \in \mathbf{A}\} \mid \mathbf{A} \in \mathcal{A}\} \tag{2.18}$$

where $\mathcal{D}(\mathcal{A})$ is a traffic dataset in time–space regions $\mathcal{A}$, $\mathbf{A}$ is a set of time–space points included in $\mathcal{A}$, N is a global cumulative flow and $(t_0(\mathbf{A}), x_0(\mathbf{A}))$ is a time–space point representing an origin of $\mathbf{A}$ (i.e., reference point for local cumulative flow in $\mathbf{A}$). Note that $\mathbf{A}$ can be closed time–space region, multiple closed region and discrete points. This definition includes common traffic information such as: vehicle flow counts at a fixed position, traffic volume at a fixed position in a time interval, a traffic state with a time–space interval, a vehicle trajectory, and actual travel time between two positions with

starting time. Fig 2.6 visualizes traffic data on time–space diagram, where red lines/dots represent measured integer N, red filled areas represent measuring range of $\mathbf{A}$ (where $\tilde{N}$ is measured), red dotted lines represent connection among regions in one $\mathbf{A}$ (they cannot measure N), and dashed lines represent unobserved vehicles. The details on Fig 2.6 will be described in later.

Traffic data with measurement errors can be represented as

$$
\begin{aligned}
\mathcal{D}'(\mathcal{A}) = \{\{N'(t', x') - N'(t'_0(\mathbf{A}), x'_0(\mathbf{A})) \mid \\
t' = t + \varepsilon^{(t)}_{t,x,\mathbf{A}}, \ x' = x + \varepsilon^{(x)}_{t,x,\mathbf{A}}, \ N'(t, x) = N(t, x) + \varepsilon^{(N)}_{t,x,\mathbf{A}}, \\
t'_0(\mathbf{A}) = t_0(\mathbf{A}) + \varepsilon^{(t)}_{t_0,x_0,\mathbf{A}}, \ x'_0(\mathbf{A}) = x_0(\mathbf{A}) + \varepsilon^{(x)}_{t_0,x_0,\mathbf{A}}, \ (t, x) \in \mathbf{A}\} \mid \mathbf{A} \in \mathcal{A}\} \quad (2.19)
\end{aligned}
$$

where

$$
\begin{cases}
\varepsilon^{(t)}_{t,x,\mathbf{A}} \sim p_t(t, x, \mathbf{A}), \\
\varepsilon^{(x)}_{t,x,\mathbf{A}} \sim p_x(t, x, \mathbf{A}), \\
\varepsilon^{(N)}_{t,x,\mathbf{A}} \sim p_N(t, x, \mathbf{A}),
\end{cases}
$$

and $p_t(t, x, \mathbf{A})$, $p_x(t, x, \mathbf{A})$ and $p_N(t, x, \mathbf{A})$ are probabilistic distributions of measurement errors on t, x and N, respectively, at (t, x) and $\mathbf{A}$.

Traffic data are required for understating, planning and managing traffic and transportation systems. In general, the sufficient characteristics of a traffic data collection method and a TSE method can be described as follows:

1. any two of the traffic state's variables can be simultaneously acquired,
2. a spatially and/or temporally wide-ranging area can be covered,
3. spatial and/or temporal detailed information can be acquired, and
4. accurate information can be acquired.

Using expressions in eq (2.18), above characteristics can be represented as follows:

1. the following is satisfied:

   - $\mathbf{A}$ covers multiple N values (i.e., is not a point nor a line with constant N value), and

(a) Ground truth

(b) Dual detectors/fixed cameras

(c) Aggregated data from dual detectors/fixed cameras

(d) Signal timing

(e) Probe vehicles trajectories

(f) Anonymized probe vehicle data

(g) AVI

(h) A moving observer

(i) Probe vehicles with spacing measurement equipment
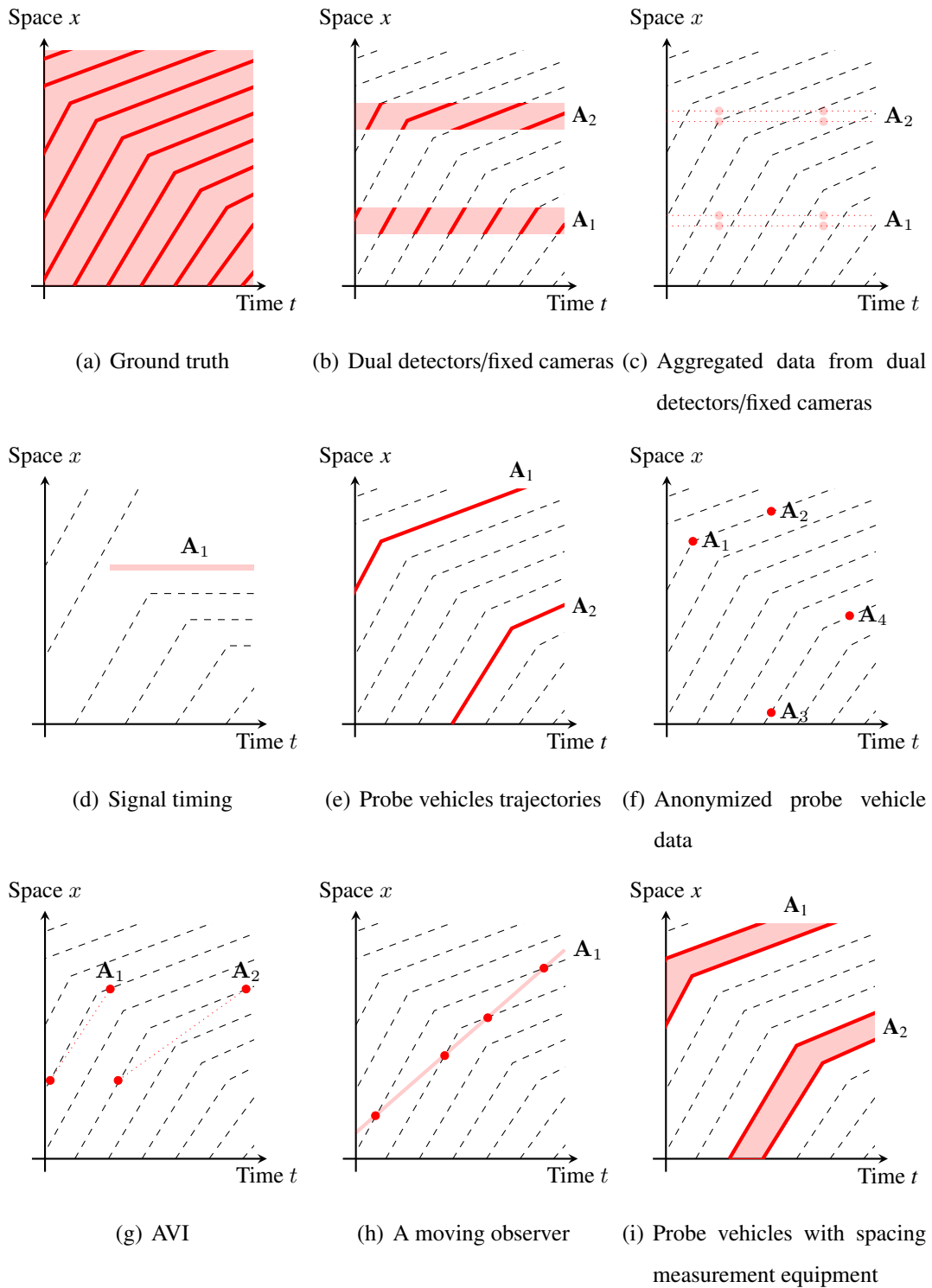
Figure 2.6: Examples of various traffic data.

- $\partial x / \partial t$ at N is available,

2. difference between minimum t (and/or x) and maximum t (and/or x) in all $\mathbf{A}$ in $\mathcal{A}$ is large,

3. the following is satisfied:

   - $\mathbf{A}$ is large region, or

   - a distance between regions (or points, lines) in $\mathbf{A}$ in $\mathcal{A}$ is small,

   and

4. values of N in $\mathcal{D}$ are correct.

However, these characteristics are difficult to achieve simultaneously because of cost and technological limitations. Purposes of utilizing data determine what levels of above characteristics are sufficient. Thus, different data collection and/or TSE methods are applied to specific purposes based on their feasibility and information required.

(2) Traffic data collection

A traffic data collection method is defined as *a method that collects traffic data without significant assumptions* in this dissertation. Assumptions can be regarded as significant if they cannot be derived from knowledge other than traffic flow theory. A traffic data collection method can be represented as a method that collects $\mathcal{D}'(\mathcal{A})$ directly. Therefore, characteristics of a traffic data collection methods depend on definition of collecting range $\mathbf{A}$, measurement errors p_t, p_x, p_N, and operational costs.

(3) Traffic state estimation

Traffic data in unobserved area can be estimated from collected data in observed area—it is referred to TSE. TSE can be defined as *estimation of traffic states at unobserved area and observed area based on data collected at observed area and, if any, exogenous assumptions*. This can be represented as follows:

$$\hat{\mathcal{D}}(\mathcal{B}) = \mathcal{F}(\mathcal{D}'(\mathcal{A}), \boldsymbol{\theta}) \tag{2.20}$$

where $\mathcal{B}$ is a set of time–space regions whose traffic states are estimated, $\hat{\mathcal{D}}(\mathcal{B})$ is estimated traffic data in $\mathcal{B}$, $\mathcal{F}$ is a function representing a TSE method, $\boldsymbol{\theta}$ is a set of exogenous parameters, and $\mathcal{D}'(\mathcal{A})$ is collected traffic dataset in area $\mathcal{A}$. $\mathcal{F}$ and $\boldsymbol{\theta}$ can be regarded as exogenous assumptions for the TSE method. Usually, $\mathcal{A} \subset \mathcal{B}$ is satisfied, meaning that traffic states in unobserved area are estimated. If $\hat{\mathcal{D}}(\mathcal{A}) = \mathcal{D}'(\mathcal{A})$ is satisfied, the observed data are considered to be perfect; otherwise, the observed data may be considered as containing errors and corrected by the TSE method. Operational costs (i.e., computational complexity) of TSE methods can be important if their purposes are real time estimation; otherwise, the costs can be ignored as they are relatively small compared to that of data collection methods.

(4) Remarks

In order to simplify the discussion of this dissertation, following topics are not discussed in detail.

- Traffic data collection can be regarded as a special case of TSE. This is because that data collection procedures require exogenous assumptions to obtain traffic state from sensors' raw signal, even for the most straightforward traffic data collection method (e.g., Coifman et al., 1998). The assumptions are distinguished depending on their significance in this dissertation; however, it is difficult to be quantified.

- Short-term future traffic prediction. It can be regarded as TSE whose $\mathcal{B}$ contains future. It requires demand prediction in addition to standard procedures of TSE methods. For this reason, some studies employed statistical or machine learning approaches which are based on historical data (c.f., Vlahogianni et al., 2014).

- Travel time estimation/prediction. It is studied by numerous studies, since travel time is important information for road user's route choice. It can be regarded as a special case of TSE, because travel time is corresponding to a vehicle trajectory: actual travel time from x_0 to x_1 is defined as $T(n, x_1) - T(n, x_0)$. Meanwhile, it can be regarded as an application of TSE, since travel time can be estimated/predicted

based on TSE results. For these reasons, some studies employed approaches similar to TSE, such as traffic simulation and statistical/machine learning methods (c.f., Oh et al., 2015; Mori et al., 2015).

- Supplemental information regarding TSE such as a confidence interval is sometimes derived in addition to $\hat{\mathcal{D}}(\mathcal{B})$.

2.2.2   Traffic data collection methods

For the efficient collection of traffic data, various methods have been proposed to date. Especially, recent achievements in information and communications technology (ICT) have enabled various information to be acquired by a wide variety of data collection methods.

(1)   Eulerian data

Eulerian data are based on t–x coordinate system and collected by sensors fixed in space. In general, fixed data collection methods can simultaneously acquire all the traffic state variables at their installed points.

Roadside traffic detectors are a typical equipment used for fixed data collection method (c.f., Klein et al., 2006). A detector's sensor detects that whether a vehicle occupies the detector's position or not by using electromagnetic effect of a metal-made vehicle (i.e., inductive loop detector), ultrasonic sensor, etc.; therefore, it can measure flow and time occupancy directly at sensor's position. A detector with single sensor (i.e., single detector) can derive density and speed by assuming a value of the vehicle length. A detector that has two sensor with short space interval (i.e., dual detector) can derive density and speed by assuming steady speed in space between the sensors. Disadvantages of detectors are operation cost and accuracy. Wide-ranging traffic data collection with detectors is difficult due to high cost of installing and maintaining detectors. Accuracy of detector can be low depending on situation—for example, loop detectors often miss or double-count vehicles and ultrasonic detector's sensitivity is affected by air temperature.

This issue requires careful maintenance of detectors and therefore increases the operation cost.

Image data collected by (video) cameras can also be utilized as fixed data collection (Hilbert et al., 1980; Coifman et al., 1998), and provide spatially detailed information near the installed points. Image-based detectors do not require assumptions employed by the loop/ultrasonic detectors; however, they require well trained/calibrated pattern recognition machines. An extreme example of utilizing image data is use of aircrafts, unmanned aerial vehicles (Coifman et al., 2006) and satellites (McCord et al., 2003); however, they may not be feasible in ordinary civil uses due to their high operating (fuel) cost per observation duration.

Signal phase information can be regarded as Eulerian traffic data, since cumulative flow at signal's location must be constant during its red phases.

In general, using the expression in eq (2.18), the characteristics of Eulerian data can be represented as follows. Time coverage of $\mathcal{A}$ is large; but space coverage of $\mathcal{A}$ is small. If the data were disaggregated, $\mathbf{A}$ is defined as a line that is parallel with the time axis or an Eulerian rectangle (i.e., two edges are parallel with the time axis and the other two edges are parallel with the space axis; c.f., Fig 2.6b) whose space length is shorter than that of time. Sometimes the data are aggregated due to limitation of data handling ability; in such cases, $\mathbf{A}$ is defined as points on a line that is parallel with the time axis or vertexes of Eulerian rectangles (c.f., Fig 2.6c). Signal phase information can be represented as a line whose position is the signal and the time is during red sign (Fig 2.6d), Space interval between multiple $\mathbf{A}$ can be large. Deviations of p_t and p_x are neglectable. Deviation of p_N may or may not be small.

In conclusion, the fixed data collection methods can provide temporally detailed information at their installed points. However, information that is spatially detailed and wide-ranging is difficult to be acquired simultaneously; because the observable area of the methods is limited to the vicinity of the sensors' installed positions.

(2)   Lagrangian data

Lagrangian data are based on n–t or n–x coordinate system and collected by sensors moving along with vehicles.

A probe vehicle is defined as having an onboard data collection devices that collects traffic data while the vehicle is in the traffic (Zito et al., 1995; Sanwal and Walrand, 1995; Murakami and Wagner, 1999). Probe vehicle data can be analyzed to acquire wide-ranging and spatiotemporally detailed information; because they are often driven by travelers who range over the entire road network. Today, the most common probe vehicles are the ones equipped with a Global Positioning System (GPS) device to identify their position and speed. From the GPS-equipped probe vehicle data, we can identify the probe vehicles' origins, destinations and routes by overlaid on a road map. Once these information are identified, the probe vehicle data directly provide the speed in road sections that the probe vehicles drove. Mobile communication devices have also been utilized as probes for specific purposes, such as individual tracking (Asakura and Hato, 2004; Asakura and Iryo, 2007). Usually, probe vehicles consists of ordinary road users who are using position identification systems for their own purposes, such as route navigation and fleet management (Liu et al., 2009). Therefore, additional cost regarding the data collection is relatively low compared with the fixed data collection; it only requires data transmission and storage costs. In addition, probe vehicles can collect data while severe disasters such that fixed data collection cannot operate due to blackouts (Hara and Kuwahara, 2015). Probe vehicle data have become popular with advances in ICT, and many studies have utilized them. With penetration rate of few percentage on a highway, they can collect spatiotemporally detailed data compared with usual traffic detectors (Herrera et al., 2010). However, GPS-equipped probe vehicle data do not provide the flow and density information, unless otherwise a PR is 100% or putting strong assumptions such as an FD and a PR. Unfortunately, a 100% PR may be difficult to be achieved due to privacy issues (Antoniou and Polydoropoulou, 2015).

Wardrop and Charlesworth (1954) proposed other type of probe vehicle, that is, a

moving observer method that estimates the speed and flow of predetermined routes by using a single probe vehicle. The original method relied on manually counting the number of vehicles that the probe vehicle overtakes, that overtake the probe vehicle, and that pass in the opposite direction, along with the journey time of the probe vehicle. Special equipments such as laser imaging detection and ranging (LIDAR) can automate this method (Redmill et al., 2011; Coifman and Hall, 2014). However, unfortunately, even with recent technological advancement, this method of estimating flow may be difficult to be automated and often miss-counts vehicles using common equipment, such as video cameras; this may be because of difficulty of using background subtraction against traffic in other lanes where background also moves[*5].

Matching a vehicle (AVI: automatic vehicle (re-)identification) that observed at multiple fixed sensors is sometimes possible. By using the AVI, not only traffic state at sensors position but also OD pair, travel route and average travel speed of some of the vehicles can be acquired. Note that, an AVI system cannot always matches all the vehicles. For example, electromagnetic signature observed by loop detectors (Coifman, 1998), license numbers and visual features observed by cameras (Asakura et al., 2000; Sumalee et al., 2012) can be utilized. Fare collection system can match vehicles based on the user IDs (Ohba et al., 1999; 上田ら, 2014).

In general, using the expression in eq (2.18), the characteristics of GPS-equipped probe vehicle data can be represented as follows. Time and space coverage of $\mathcal{A}$ depend on probe vehicles' movement. Shape of **A** is defined as a line that follows probe vehicle's trajectory (i.e., $N(t, x) = $ const, $(t, x) \in \mathbf{A}$; c.f., Fig 2.6e). In practical, probe vehicle ID may be removed from the probe vehicle data due to privacy concerns; it can be represented as Fig 2.6f. In addition, data from multiple probe vehicles are sometimes aggregated into single average speed datum due to limitation in data handling ability and further privacy concerns; this aggregated data are no longer considered as traffic data defined in

---

[*5]Currently, the idea of the moving observer is employed as analogy for explaining derivation of traffic flow models (Lighthill and Whitham, 1955) and calculation of them (Daganzo, 2005a,b) apart from its original motivation.

this dissertation. Time and space interval between multiple $\mathbf{A}$ depend on probe vehicles' penetration rate (PR). Deviation of p_t is neglectable but that in p_x may be not neglectable. An error on N is zero if the road is single-lane (i.e., $N'(t', x') = N'(t_0'(\mathbf{A}), x_0'(\mathbf{A}))$ is always satisfied). An AVI can be visualized as Fig 2.6g and the moving observer method can be visualized as Fig 2.6h.

In conclusion, the probe vehicle data can provide spatiotemporally wide-ranging and detailed information if the PR is high enough. However, the widely used probe vehicle data, namely, GPS-equipped ones, cannot acquire quantity-related information, namely, flow and density.

2.2.3   TSE methods

Following summarizes some of the existing TSE studies. First, direct utilizations of the traffic flow theory are mentioned. Then, TSE methods considering practical problems, namely traffic flow theory-based and statistical/machine learning-based method, are described.

(1)   Deterministic theory-based methods

According to the definition of TSE, solving the LWR model based on given initial/boundary conditions can be TSE. Such TSE methods can be regarded as deterministic theory-based; because they assume their theories and collected data are perfect and well-posed. In other words, using expressions in eq (2.20), deterministic theory-based methods can be represented as follows: $\mathcal{F}$ represents a computation method for a traffic flow model, $\boldsymbol{\theta}$ represents the model parameters, $\mathcal{D}'(\mathcal{A})$ represents boundary condition for the model, and $\mathcal{B}$ represents area inside $\mathcal{A}$.

Following methods described in section 2.1.3 can be regarded as $\mathcal{F}$ of deterministic theory-based TSE methods, although they did not limit their motives to TSE: Newell's simplified kinematic wave model (referred to Newell's three detector problem; Newell, 1993a,b,c), Eulerian coordinates-based (Godunov scheme) calculation methods of the

LWR model (Daganzo, 1994; Lebacque, 1996), the variational theory (Daganzo, 2005a,b), and Lagrangian coordinates-based calculation methods of the LWR model (Newell, 2002; Laval and Leclercq, 2013). $\boldsymbol{\theta}$ includes parameters of an FD for above methods.

Deterministic theory-based TSE methods may have limitations. Theories only represent abstracted features of actual phenomena, meaning that $\mathcal{F}$ and $\boldsymbol{\theta}$ do not always hold true in actual phenomena. Especially in traffic flow theory, attributes of an FD are uncertain for general traffic, as mentioned in section 2.1.2. Even if the theories were perfect, following issues remain: $\mathcal{F}$ may not be perfect (c.f., numerical errors, non-closed-form expressions); and $\mathcal{D}(\mathcal{A})$ contain measurement errors.

(2) Practical traffic flow theory-based methods

Some TSE methods are based on traffic flow theory as well as collected data and considers discrepancies between theories and actual traffic data appropriately. Basically, they introduce procedures that can handle discrepancies between theories and actual traffic data, by introducing such as stochastic factors (then apply maximum likelihood method) and residual minimization procedures. In these methods, definitions of terms in eq (2.20) are varied. Following describes features of existing these TSE methods regarding to their definitions of $\hat{\mathcal{D}}(\mathcal{B})$, $\mathcal{D}'(\mathcal{A})$, $\mathcal{F}$ and $\boldsymbol{\theta}$.

On $\hat{\mathcal{D}}(\mathcal{B})$, namely, variables to be estimated and areas of interest of TSE. Usually, detailed aggregated data, such as minutes–hundreds meters scale traffic states, are estimated (e.g., Wang and Papageorgiou, 2005). Disaggregated data are sometimes estimated (e.g., Yuan et al., 2012). Network-wide TSE methods and area-wide TSE methods are also developed, such as missing link complementation based on CLs (Castillo et al., 2013) and area-flow estimation assuming that a well-defined MFD exists (Gayah and Dixit, 2013).

On $\mathcal{D}'(\mathcal{A})$, namely, input data for TSE. Eulerian data are often utilized for the input data (e.g., Wang and Papageorgiou, 2005). Lagrangian data are also utilized for newer TSE methods, with recent GPS-equipped probe vehicles' emergence (e.g., Nanthawichit

et al., 2003); however, it should be noted that most of them still uses Eulerian data (e.g., Nanthawichit et al., 2003; Herrera and Bayen, 2010; Mehran et al., 2012; Yuan et al., 2012) as boundary conditions. At signalized intersections, signal timing information can be utilized for input data, since flow at red signal is known to be zero (Ban et al., 2011; Mehran et al., 2012; Comert, 2013; Hao et al., 2013; Sun and Ban, 2013; Lee et al., 2015; Wada et al., 2015). If an estimation method is based on Eulerian coordinate system, aggregated data are utilized (Nanthawichit et al., 2003; Wang and Papageorgiou, 2005; Herrera and Bayen, 2010). Disaggregated data are also utilized in order to reproduce detailed traffic phenomena from vehicles trajectories using Lagrangian coordinates (Yuan et al., 2012; Mehran et al., 2012; Wada et al., 2015). Utilizing disaggregated data may require special treatment on non-FIFO conditions (e.g., a probe vehicle overtaking other probe vehicle will violate the coordinate system; Mehran et al., 2012). For example, Yuan et al. (2012) avoided this issue by reproducing disaggregate data from data aggregated from raw disaggregated data; Mehran et al. (2012) and Wada et al. (2015) assumed that overtaking never happens.

On $\mathcal{F}$ and $\boldsymbol{\theta}$, namely, methodology of TSE. Basically, the methodology introduces stochastic factors based on traffic flow theory and then applies maximum likelihood method or residual minimization procedures to estimate traffic states.

The most typical methodology is Kalman filtering-like techniques (KFT), such as Kalman filter (Kalman and Bucy, 1961), extended Kalman filter, ensemble Kalman filter, particle filter, etc. It may be due to their capability to integrate traffic flow theory and fuse heterogeneous traffic data within a TSE method. General state-space model for KFT can be represented as follows:

$$\mathcal{D}(\mathcal{B}_t) = \mathcal{S}_t(\mathcal{D}(\mathcal{B}_{t-1}), \mathcal{V}_t), \tag{2.21}$$

$$\mathcal{D}'(\mathcal{A}_t) = \mathcal{H}_t(\mathcal{D}(\mathcal{B}_t), \mathcal{W}_t), \tag{2.22}$$

where eq (2.21) is a system equation, eq (2.22) is an observation equation, $\mathcal{B}_t$ is a part of $\mathcal{B}$ those belong to time t, $\mathcal{A}_t$ is a part of $\mathcal{A}$ those belong to time t, $\mathcal{S}_t$ is a system model, $\mathcal{H}_t$ is an observation model, $\mathcal{V}_t$ is a system noise, and $\mathcal{W}_t$ is an observation

noise, at time t, respectively. The objective of KFT-based TSE is to estimate $\mathcal{D}(\mathcal{B})$ based on $\mathcal{D}'(\mathcal{A})$, $\mathcal{S}_t$, $\mathcal{H}_t$, $\mathcal{V}_t$ and $\mathcal{W}_t$; the estimator is $\hat{\mathcal{D}}(\mathcal{B})$. $\mathcal{S}_t$ corresponds to a traffic flow model; and $\mathcal{D}'(\mathcal{A}_t)$, $\mathcal{H}_t$ and $\mathcal{W}_t$ correspond to a data collection method. The disadvantage are such as numerical errors, computation costs and calibration difficulties due to linear approximation, numerical differential, Monte Caro simulation and/or ad hoc parameters. Various combinations of observation and system models have been investigated by existing studies. They can be summarized as follows: aggregated detector data and random walks (Gazis and Knapp, 1971), aggregated speed data of probe vehicles, detector data and second order traffic flow model (Nanthawichit et al., 2003), freeway detector data and second order traffic flow model (Wang and Papageorgiou, 2005), state and parameters estimation using detector data and first order traffic flow model (Lint et al., 2008), state and parameters estimation using detector data and second order traffic flow model (Wang et al., 2009), various heterogeneous data from detector, probe vehicle and AVI (van Lint and Hoogendoorn, 2010), aggregated speed data of probe vehicles, boundary detector data and speed-based traffic flow model (Herrera and Bayen, 2010), and disaggregated probe vehicle data, boundary detector data and Lagrangian-coordinated first order traffic flow model (Yuan et al., 2012). van Lint and Hoogendoorn (2010); El Faouzi et al. (2011) provided reviews including KFT-based TSE methods.

Other methodologies are also employed. For example, the deterministic theory-based methods were modified into practical TSE methods that can handle discrepancies between theories and actual traffic data (Muñoz et al., 2003; Sumalee et al., 2011; Mehran et al., 2012; Laval et al., 2012; Deng et al., 2013; Lei and Zhou, 2014; Wada et al., 2015; Sun et al., 2015), using maximum likelihood method, residual minimization, etc. Naïve extrapolation method with less assumption on traffic flow theory is also useful in some cases (Coifman, 2002).

The concept of an FD (or MFD sometimes) has a significant role in $\mathcal{F}$ (as well as $\mathcal{S}_t$ in KFT) and therefore the TSE method. Most existing TSE methods assume conditions on an FD (e.g., its functional form and parameters) exogenously[*6]. However, as mentioned in section 2.1.2, an FD is a complicated phenomenon that involves various factors and

cannot be described or predicted completely. Therefore, they usually requires careful parameter calibration prior to TSE. Furthermore, in principle, this calibration must require knowledge on traffic states in $\mathcal{B}$—it can be a vicious circle.

(3)   Statistical/machine learning-based methods

Statistical methods and machine learning methods are also utilized for TSE. Basically, they estimate traffic state based on collected current traffic data and some relation (e.g., spatial and/or temporal correlation among data) abstracted from stored historical traffic data. Therefore, $\mathcal{F}$ represents a method for abstracting relation or a traffic state calculation method based on abstracted relation; $\boldsymbol{\theta}$ represents parameters of an abstracting method or abstracted relation. Methods for abstracting the relation are varied. Data required for the methods are also varied, as long as the statistical methods and machine learning methods allow, including both of Eulerian data and Lagrangian data.

These methods are often utilized for short-term future prediction; because the abstracted relation may include changes in demand in short-term future without explicit traveler behavior model (c.f., Karlaftis and Vlahogianni, 2011; Vlahogianni et al., 2014). In short-term future prediction, $\mathcal{A}$ represents current and past at a certain space; and $\mathcal{B}$ represents future at the same space.

They are also utilized for missing link complement problems (花岡ら, 2013; Kataoka et al., 2015). For example, probe vehicles cannot always collect data from every links in a network; therefore, traffic states of such links are required to be estimated. In these problems, $\mathcal{A}$ represents links with probe vehicles at a time; and $\mathcal{B}$ represents links without probe vehicles at the same time.

The shortcoming is that they require long term historical data for abstracting the relation and assume the relation always holds true. It implies that these methods are valid only under ordinal conditions; because extraordinary data, in which the ordinal relation does not hold true, are difficult to be collected[*7]. In addition, they can be black box and

---

[*6]Under special conditions (e.g., detector observes flow and density), the parameters can be estimated along with traffic states by using special procedures (Lint et al., 2008; Wang et al., 2009; Sun et al., 2015).

case-specific which sometimes contradict traffic flow theory.

2.3 Advanced vehicle technologies

2.3.1 Overview

Recently, advanced vehicle technologies (AVT) have began spread in the practical uses. The AVT includes automated vehicles and connected vehicles.

The automated vehicles includes functions, such as adaptive cruise control, collision avoidance and autonomous vehicles (Bengler et al., 2014). Several technologies for the automated vehicles have been developed practically for the driving safety and efficiency purposes (National Highway Traffic Safety Administration, 2013; Diakaki et al., 2015). To realize automated vehicles, the surrounding environment of a vehicle must be recognized using on-vehicle equipments with high accuracy and frequency (Rajamani and Shladover, 2001; Sivaraman and Trivedi, 2013). The typical and essential factor of the surrounding environment of a vehicle is a spacing, namely, distance between a vehicle and its leading vehicle. In fact, spacing measuring technology is not very new development; it have been studied from mid 1990s (Saneyoshi, 1996; Bertozzi and Broggi, 1998) and achieves high performance even with commercialized equipments. For example, Saneyoshi (1996), which utilized stereo camera and was commercialized recently, reported that the precision is within ±0.01 m and ±1 m at distances of 5 m and 100 m, respectively; and the maximum detectable range is 130 m.

The connected vehicles establishes bidirectional information connection among nearby vehicles (i.e., VANET: vehicular ad hoc network) using on-vehicle equipment and/or road-based infrastructure (Hartenstein and Laberteaux, 2008). Basically, it intends to enable efficient information exchange so that driving can be efficient, such as information provision and cooperative vehicle control combined with the automated

---

[*7]The characteristics can be utilized for detecting extraordinary conditions themselves by comparing predicted traffic state and revealed actual traffic state (成岡ら, 2015).

technologies.

Effects of AVT for traffic and transportation are investigated and optimistic results
are often obtained, such as improvements on safety and capacity in both of microscopic
and macroscopic scales (Kikuchi et al., 2003; Talebpour and Mahmassani, 2015; Zhang,
2015; Diakaki et al., 2015).

2.3.2   Utilization for TSE-like purposes

Some of the data collected by AVT satisfy the definition of traffic data in this dissertation.
For example, spacing data collected by automated vehicles are represented as traffic data
whose **A** containing two values of N, namely, the automated vehicle itself and its leading
vehicle. This is the probe vehicle with spacing measurement equipment (PVSME). It can
be visualized as Fig 2.6i.

In fact, several studies investigated utilization of such AVT data to TSE-like purposes.
For example, capacity of road sections can be measured continuously using a vehicle
with spacing measurement equipment (小谷ら, 2003). Image recognition techniques that
measure spacing in order to quantity-related variable estimation were developed (Rabie
et al., 2002; Panmungmee et al., 2012; Yokoi et al., 2013); however, their estimation
outputs as well as estimation methods are not specified. Some studies (Messelodi et al.,
2009; Diaz et al., 2012) called data collected by spacing measurement and visible vehicle
counting functions "extended Floating Car Data (xFCD)". An estimation method for
occupancy was developed based on statistical relation between the xFCD and detector
data (Wilby et al., 2014). Data from connected vehicles can be utilized for traffic density
estimation with some assumptions (Goodall et al., 2014; Darwish and Bakar, 2015).

Chapter 3 Basis: Method for Estimating Traffic State

This chapter[*1] describes the basic method for estimating traffic state from probe vehicle data including position and spacing. The method estimates the flow, density, and speed at a predetermined time and space resolution for a corridor that the probe vehicles drive through. In order to keep it simple and easy to expansion, the method is designed as not relying on significant exogenous assumptions.

Sections 3.1 and 3.2 describe premises for the estimation method. Section 3.3 formulates traffic state estimators based on the premises. Section 3.4 investigates analytical characteristics of the estimators by using approximation. Section 3.5 shows numerical examples of the estimators. Section 3.6 summarizes the chapter and discusses characteristics of the estimators.

3.1 Assumptions and concepts

The proposed estimation method is for traffic state in a corridor. The corridor is assumed to be one-way traffic that can include multi-lane, merging, and diverging sections. Edie's generalized definitions (Edie, 1963) were employed for the traffic flow variables; these define the traffic flow variables (i.e., flow, density, and speed) in a time–space region based on the trajectories of all vehicles in the region and the area of the region. The definitions indicate generalized forms of the well-known traffic variable definitions, such as the spot flow rate, space density, and space mean speed.

The probe vehicle data are used as the inputs for the estimation. The data consist of the following continuously measured variables:

[*1]This chapter is mainly based on joint research with Dr. Takahiko Kusakabe and Prof. Yasuo Asakura, published in *Transportation Research Part C* (Seo et al., 2015a).

- spacing of the probe vehicle (i.e., space headway between the probe vehicle and its leading vehicle in the same lane) and

- position of the probe vehicle.

To simplify the situation, the following conditions are assumed:

- The measurements have no error.

- The route that the probe vehicle drives is identified without error.

- The probe vehicles are randomly distributed in the traffic; the probe vehicle penetration rate (PR) is unknown to analysts.

- The driving behavior of the probe vehicles is the same as that of other vehicles.

The first and second assumptions indicate an error free assumption. The third and fourth assumptions indicate a random sampling assumption.

The traffic state estimation procedure is described as follows.

Step 1 Time–space region subject to the traffic state estimation is divided into multiple discrete time–space regions.

Step 2 The traffic flow variables of every time–space region are estimated independently based on data collected by the probe vehicles in each region.

Fig 3.1 shows a time–space diagram and time–space region, where the horizontally hatched region **A** is a discrete time–space region, the thick solid lines are trajectories of the probe vehicles, the dashed lines are those of non-probe vehicles, the vertically hatched regions $\mathbf{s}_n$ are time–space regions between the n-th probe vehicle and its leading vehicle, and the 5th, 8th and 12th vehicles are probes.

Any rule can be used to divide the time–space region of the traffic flow (step 1). The simplest rules is employed in this method, where the traffic flow is divided into identical size of Eulerian rectangles. This is a familiar coordination in today's traffic flow data, where fixed-point detectors are installed at a certain time and space resolution or interval. This coordination can be represented as follows:

$$\mathbf{A}_i^j = \{(x,t) \mid x_i \le x \le x_{i+1},\ t_j \le t \le t_{j+1}\} \qquad i \ge 0,\ j \ge 0, \tag{3.1}$$
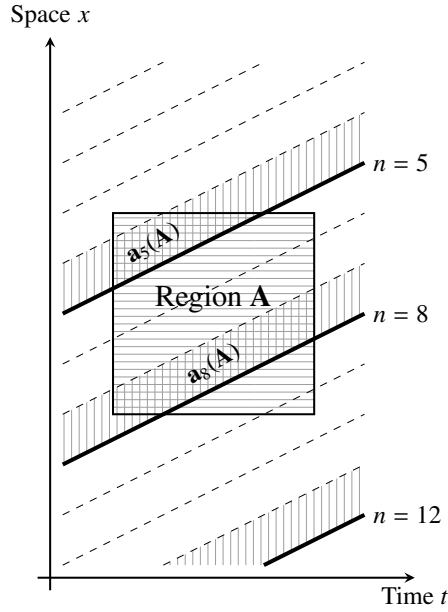
Figure 3.1: Time–space region **A** and probe vehicle data.

$$x_{i+1} = x_i + \Delta x, \tag{3.2}$$

$$t_{j+1} = t_j + \Delta t, \tag{3.3}$$

where i and j are non-negative indices for space and time, respectively, $(x_0,\ t_0)$ is the coordinates of a predetermined origin, $(x_i,\ t_j)$ is the coordinates of the lower-left corner of the region $\mathbf{A}_i^j$, Δx is a predetermined space resolution, and Δt is a predetermined time resolution. Note that $\mathbf{A}_i^j$ is simply written as $\mathbf{A}$ in the rest of this dissertation for the purpose of conciseness.

The estimation method of the step 2 is described in the next subsection.

3.2   Collectable data by PVSMEs

The PVSMEs are supposed to collect their position and spacing as mentioned. In this section, they are defined in mathematical form.

A position is a coordinate in time–space plane. A vehicle trajectory consists of continuous positions of a vehicle. Trajectory of vehicle m can be defined as $X(m, t)$

and $T(m, x)$, where $X(m, t)$ represents position that vehicle m exists at time t and $T(m, x)$ represents time that vehicle m passes position x. Obviously, these two of the same m should be equivalent to each other, and following relation holds true: $x = X(m, T(m, x))$.

A spacing is space distance between a position of a vehicle at a time and that of its leading vehicle at the same time. Then, a spacing of vehicle m at time t can be defined as $X(l(m, t), t) - X(m, t)$, where $l(m, t)$ represents a leading vehicle of vehicle m at time t. If FIFO is satisfied, it can be simplified as $X(m - 1, t) - X(m, t)$.

We define $d_m(\mathbf{A})$: distance traveled by vehicle m in region $\mathbf{A}$, $t_m(\mathbf{A})$: time spent by vehicle m in region $\mathbf{A}$, and $\mathbf{a}_m(\mathbf{A})$: total spacing of vehicle m in region $\mathbf{A}$, as follows:

$$d_m(\mathbf{A}) = \max\{X(m, t) \mid (t, X(m, t)) \in \mathbf{A}\} - \min\{X(m, t) \mid (t, X(m, t)) \in \mathbf{A}\}, \tag{3.4}$$

$$t_m(\mathbf{A}) = \max\{T(m, x) \mid (T(m, x), x) \in \mathbf{A}\} - \min\{T(m, x) \mid (T(m, x), x) \in \mathbf{A}\}, \tag{3.5}$$

$$\mathbf{a}_m(\mathbf{A}) = \{(t, x) \in \mathbf{A} \mid X(m, t) < x < X(l(m, t), t)\}, \tag{3.6}$$

If FIFO is satisfied, $\mathbf{a}_m(\mathbf{A})$ can be simplified as

$$\mathbf{a}_m(\mathbf{A}) = \{(t, x) \in \mathbf{A} \mid X(m, t) < x < X(m - 1, t)\}. \tag{3.7}$$

In practical, data collected by a probe vehicle are discrete, e.g., GPS log with 1 s time interval. Therefore, to obtain $d_m(\mathbf{A})$, $t_m(\mathbf{A})$ and $\mathbf{a}_m(\mathbf{A})$, probe vehicle data must be interpolated somehow. Note that precision of $\mathbf{a}_m(\mathbf{A})$ is significantly affected by quality of interpolation, while those of $d_m(\mathbf{A})$ and $t_m(\mathbf{A})$ are not.

3.3 Estimators

The traffic flow variables defined by Edie (1963), namely, the flow $q(\mathbf{A})$, density $k(\mathbf{A})$, and speed $v(\mathbf{A})$, in a time–space region $\mathbf{A}$ are as follows:

$$q(\mathbf{A}) = \frac{d(\mathbf{A})}{|\mathbf{A}|}, \tag{3.8}$$

$$k(\mathbf{A}) = \frac{t(\mathbf{A})}{|\mathbf{A}|}, \tag{3.9}$$

$$v(\mathbf{A}) = \frac{d(\mathbf{A})}{t(\mathbf{A})}. \tag{3.10}$$

These definitions are easily transformed into eqs (3.11)–(3.13) by summing the spacings and trajectories of each vehicle in the region $\mathbf{A}$:

$$q(\mathbf{A}) = \frac{\sum_{n \in \mathbf{N(A)}} d_n(\mathbf{A})}{\sum_{n \in \mathbf{N(A)}} |\mathbf{a}_n(\mathbf{A})|}, \tag{3.11}$$

$$k(\mathbf{A}) = \frac{\sum_{n \in \mathbf{N(A)}} t_n(\mathbf{A})}{\sum_{n \in \mathbf{N(A)}} |\mathbf{a}_n(\mathbf{A})|}, \tag{3.12}$$

$$v(\mathbf{A}) = \frac{\sum_{n \in \mathbf{N(A)}} d_n(\mathbf{A})}{\sum_{n \in \mathbf{N(A)}} t_n(\mathbf{A})}, \tag{3.13}$$

if $\sum_{n \in \mathbf{N(A)}} |\mathbf{a}_n(\mathbf{A})| > 0$, where $\mathbf{a}_n(\mathbf{A})$ is a time–space region between vehicle n and its leading vehicle in the region $\mathbf{A}$ ($\mathbf{a}_n(\mathbf{A}) = \mathbf{A} \cap \mathbf{s}_n$, cross-hatched regions in Fig 3.1), $\mathbf{N(A)}$ is a set of all vehicles in the region $\mathbf{A}$, $d_n(\mathbf{A})$ is the distance traveled by vehicle n in the region $\mathbf{A}$, and $t_n(\mathbf{A})$ is the time spent by vehicle n in the region $\mathbf{A}$.

By replacing $\mathbf{N(A)}$ in eqs (3.11)–(3.13) with the set of all probe vehicles in region $\mathbf{A}$, namely, $\mathbf{P(A)}$, estimators based on the probe vehicle data can be defined as follows:

$$\hat{q}(\mathbf{A}) = \frac{\sum_{n \in \mathbf{P(A)}} d_n(\mathbf{A})}{\sum_{n \in \mathbf{P(A)}} |\mathbf{a}_n(\mathbf{A})|}, \tag{3.14}$$

$$\hat{k}(\mathbf{A}) = \frac{\sum_{n \in \mathbf{P(A)}} t_n(\mathbf{A})}{\sum_{n \in \mathbf{P(A)}} |\mathbf{a}_n(\mathbf{A})|}, \tag{3.15}$$

$$\hat{v}(\mathbf{A}) = \frac{\sum_{n \in \mathbf{P(A)}} d_n(\mathbf{A})}{\sum_{n \in \mathbf{P(A)}} t_n(\mathbf{A})}. \tag{3.16}$$

These estimators denote the flow, density, and speed of probe vehicles that works informal moving blockade. Note that eqs (3.14)–(3.16) are exactly the same as eqs (3.11)–(3.13) if all of the vehicles were the probe vehicles ($\mathbf{P(A)} = \mathbf{N(A)}$).

3.4 Analytical characteristics of estimators

It is valuable to investigate characteristics of the estimators in analytical way prior to applied them to empirical data; because it gives general insights. The estimation procedures can be described as random process of selecting probe vehicles with a certain probability. For example, flow estimator (3.14) can be represented as

$$\hat{q}(\mathbf{A}) = \frac{\sum_{n \in \mathbf{N(A)}} b_n d_n(\mathbf{A})}{\sum_{n \in \mathbf{N(A)}} b_n \mathbf{a}_n(\mathbf{A})}, \tag{3.17}$$

$$b_n \sim B(P), \tag{3.18}$$

where $B(P)$ is Bernoulli distribution which is equal to 1 with probability P and 0 otherwise, and P is PR of probe vehicle. In general, indices for accuracy (i.e., bias) and precision are defined as

$$\text{Bias}(\hat{q}(\mathbf{A})) = E[\hat{q}(\mathbf{A}) - q(\mathbf{A})], \tag{3.19}$$

$$\text{RMSE}(\hat{q}(\mathbf{A})) = \sqrt{E[(\hat{q}(\mathbf{A}) - q(\mathbf{A}))^2]}. \tag{3.20}$$

where $\text{Bias}(\hat{\theta})$ is the bias, which is an accuracy index of an estimator $\hat{\theta}$, where $\text{RMSE}(\hat{\theta})$ is the root mean square error, which is a precision index of an estimator $\hat{\theta}$. Unfortunately, eqs (3.17)–(3.20) are difficult to be expressed in closed form. Therefore, following discusses the bias and precision by using approximations that hold true in special cases, and Taylor approximations.

The estimators represented in eqs (3.14) and (3.15) are not unbiased in general. With third-order Taylor expansion, the bias in the flow and density estimators shown in eqs (3.14) and (3.15) can be approximated as:

$$\text{Bias}(\hat{q}(\mathbf{A})) \simeq \frac{1}{|\mathbf{P}(\mathbf{A})|} \frac{Var[\bar{h}_n(\mathbf{A})]}{E[\bar{h}_n(\mathbf{A})]^3}, \tag{3.21}$$

$$\text{Bias}(\hat{k}(\mathbf{A})) \simeq \frac{1}{|\mathbf{P}(\mathbf{A})|} \frac{Var[\bar{s}_n(\mathbf{A})]}{E[\bar{s}_n(\mathbf{A})]^3}, \tag{3.22}$$

where $\bar{h}_n(\mathbf{A})$ and $\bar{s}_n(\mathbf{A})$ are the mean time and space headway, respectively, of vehicle n in the region $\mathbf{A}$ (see section 3.4.1 for their derivation). According to these equations, an inverse correlation exists between the bias and number of probe vehicles in the region. Therefore the bias tends to be mitigated as the size of the region is increased (i.e., time/space resolution is lowered) or the PR is increased. The bias also correlates to the variance of all of the vehicles' mean time/space headway, which depends on the traffic flow characteristics. There is no bias in the speed estimator.

In a similar way, the precision of the flow and density estimators shown in eqs (3.14) and (3.15) can be approximated as

$$\text{RMSE}(\hat{q}(\mathbf{A})) \simeq \frac{1}{E[\bar{h}_n(\mathbf{A})]^2} \sqrt{\frac{Var[\bar{h}_n(\mathbf{A})]}{|\mathbf{P}(\mathbf{A})|}}, \tag{3.23}$$

$$\text{RMSE}(\hat{k}(\mathbf{A})) \simeq \frac{1}{E[\bar{s}_n(\mathbf{A})]^2} \sqrt{\frac{Var[\bar{s}_n(\mathbf{A})]}{|\mathbf{P}(\mathbf{A})|}}, \tag{3.24}$$

(see section 3.4.2 for their derivation). The tendencies in the precision are quite similar to those in the bias; namely, the precision of the flow increases as the number of probe vehicles in a region increases and the variance in the mean time headway decreases.

3.4.1 Derivation of the approximated bias

The approximation of $|\mathbf{a}_n(\mathbf{A})| \simeq d_n(\mathbf{A})\bar{h}_n(\mathbf{A})$ can be appropriate for most situations, such as when the size of region $\mathbf{A}$ is sufficiently larger than the spacing. With this approximation, the true flow in eq (3.11) can be transformed to

$$q(\mathbf{A}) \simeq \frac{E[d_n(\mathbf{A})]}{E[d_n(\mathbf{A})\bar{h}_n(\mathbf{A})]}. \tag{3.25}$$

We assumed that $d_n(\mathbf{A})$ and $\bar{h}_n(\mathbf{A})$ are independent from each other. Therefore,

$$q(\mathbf{A}) \simeq \frac{1}{E[\bar{h}_n(\mathbf{A})]}. \tag{3.26}$$

In the same way, the flow estimator in eq (3.14) can be transformed to

$$\hat{q}(\mathbf{A}) \simeq \frac{1}{E_{\mathbf{P}(\mathbf{A})}[\bar{h}_n(\mathbf{A})]}, \tag{3.27}$$

where $E_{\mathbf{P}(\mathbf{A})}[\theta_n]$ is the mean of θ_n for each vehicle in $\mathbf{P}(\mathbf{A})$. The expected value of the estimator is

$$E[\hat{q}(\mathbf{A})] \simeq E\left[\frac{1}{E_{\mathbf{P}(\mathbf{A})}[\bar{h}_n(\mathbf{A})]}\right]. \tag{3.28}$$

The third-order Taylor expansion of $f(X) = 1/X$ around $E[X]$ is derived as

$$\frac{1}{X} \simeq \frac{1}{E[X]} - \frac{1}{E[X]^2}(X - E[X]) + \frac{1}{E[X]^3}(X - E[X])^2 - \frac{1}{E[X]^4}(X - E[X])^3. \tag{3.29}$$

We can then obtain

$$E\left[\frac{1}{E_{\mathbf{P}(\mathbf{A})}[\bar{h}_n(\mathbf{A})]}\right] \simeq \frac{1}{E[E_{\mathbf{P}(\mathbf{A})}[\bar{h}_n(\mathbf{A})]]} + \frac{Var[E_{\mathbf{P}(\mathbf{A})}[\bar{h}_n(\mathbf{A})]]}{E[E_{\mathbf{P}(\mathbf{A})}[\bar{h}_n(\mathbf{A})]]^3}, \tag{3.30}$$

by taking the expectations and substituting $E_{\mathbf{P(A)}}[\bar{h}_n(\mathbf{A})]$ for X. If the probe vehicles are randomly sampled from all of the vehicles, $E[E_{\mathbf{P(A)}}[\bar{h}_n(\mathbf{A})]] = E[\bar{h}_n(\mathbf{A})]$ and $Var[E_{\mathbf{P(A)}}[\bar{h}_n(\mathbf{A})]] \simeq Var[\bar{h}_n(\mathbf{A})]/|\mathbf{P(A)}|$ are satisfied. Therefore, eq (3.30) can be transformed to

$$E\left[\frac{1}{E_{\mathbf{P(A)}}[\bar{h}_n(\mathbf{A})]}\right] \simeq \frac{1}{E[\bar{h}_n(\mathbf{A})]} + \frac{1}{|\mathbf{P(A)}|}\frac{Var[\bar{h}_n(\mathbf{A})]}{E[\bar{h}_n(\mathbf{A})]^3}. \tag{3.31}$$

From eqs (3.26), (3.28), and (3.31), the relation between flow and its estimator can be approximated as

$$E[\hat{q}(\mathbf{A})] \simeq q(\mathbf{A}) + \frac{1}{|\mathbf{P(A)}|}\frac{Var[\bar{h}_n(\mathbf{A})]}{E[\bar{h}_n(\mathbf{A})]^3}. \tag{3.32}$$

3.4.2　Derivation of the approximated precision

The index for the precision, that is, root mean square error (RMSE), is represented as follows:

$$
\begin{aligned}
\mathrm{RMSE}(\hat{q}(\mathbf{A})) &= \sqrt{E[(q(\mathbf{A}) - \hat{q}(\mathbf{A}))^2]}\\
&\simeq \sqrt{E\left[\left(\frac{1}{E[\bar{h}_n(\mathbf{A})]} - \frac{1}{E_{\mathbf{P(A)}}[\bar{h}_n(\mathbf{A})]}\right)^2\right]}\\
&= \sqrt{E\left[\frac{1}{E[\bar{h}_n(\mathbf{A})]^2}\right] - E\left[\frac{2}{E[\bar{h}_n(\mathbf{A})]E_{\mathbf{P(A)}}[\bar{h}_n(\mathbf{A})]}\right] + E\left[\frac{1}{E_{\mathbf{P(A)}}[\bar{h}_n(\mathbf{A})]^2}\right]}\\
&= \sqrt{\frac{1}{E[\bar{h}_n(\mathbf{A})]^2} - \frac{2}{E[\bar{h}_n(\mathbf{A})]}E\left[\frac{1}{E_{\mathbf{P(A)}}[\bar{h}_n(\mathbf{A})]}\right] + E\left[\frac{1}{E_{\mathbf{P(A)}}[\bar{h}_n(\mathbf{A})]^2}\right]}\\
&\simeq \sqrt{\frac{1}{E[\bar{h}_n(\mathbf{A})]^2} - \frac{2}{E[\bar{h}_n(\mathbf{A})]}\left(\frac{1}{E[\bar{h}_n(\mathbf{A})]} + \frac{1}{|\mathbf{P(A)}|}\frac{Var[\bar{h}_n(\mathbf{A})]}{E[\bar{h}_n(\mathbf{A})]^3}\right) + E\left[\frac{1}{E_{\mathbf{P(A)}}[\bar{h}_n(\mathbf{A})]^2}\right]}\\
&= \sqrt{E\left[\frac{1}{E_{\mathbf{P(A)}}[\bar{h}_n(\mathbf{A})]^2}\right] - \frac{1}{E[\bar{h}_n(\mathbf{A})]^2} - \frac{2}{|\mathbf{P(A)}|}\frac{Var[\bar{h}_n(\mathbf{A})]}{E[\bar{h}_n(\mathbf{A})]^4}}. \tag{3.33}
\end{aligned}
$$

The third-order Taylor expansion of $f(X) = 1/X^2$ around $E[X]$ is derived as

$$\frac{1}{X^2} \simeq \frac{1}{E[X]^2} - \frac{2}{E[X]^3}(X - E[X]) + \frac{3}{E[X]^4}(X - E[X])^2 - \frac{4}{E[X]^5}(X - E[X])^3. \tag{3.34}$$

We can then obtain

$$E\left[\frac{1}{E_{\mathbf{P(A)}}[\bar{h}_n(\mathbf{A})]^2}\right] \simeq \frac{1}{E[E_{\mathbf{P(A)}}[\bar{h}_n(\mathbf{A})]]^2} + \frac{3Var[E_{\mathbf{P(A)}}[\bar{h}_n(\mathbf{A})]]}{E[E_{\mathbf{P(A)}}[\bar{h}_n(\mathbf{A})]]^4},\qquad(3.35)$$

by taking the expectations and substituting $E_{\mathbf{P(A)}}[\bar{h}_n(\mathbf{A})]$ for X. If the probe vehicles are randomly sampled from all of the vehicles, this can be transformed to

$$E\left[\frac{1}{E_{\mathbf{P(A)}}[\bar{h}_n(\mathbf{A})]^2}\right] \simeq \frac{1}{E[\bar{h}_n(\mathbf{A})]^2} + \frac{3}{|\mathbf{P(A)}|}\frac{Var[\bar{h}_n(\mathbf{A})]}{E[\bar{h}_n(\mathbf{A})]^4}.\qquad(3.36)$$

From eqs (3.33) and (3.36), the precision can be approximated as

$$\mathrm{RMSE}(\hat{q}(\mathbf{A})) \simeq \frac{1}{E[\bar{h}_n(\mathbf{A})]^2}\sqrt{\frac{Var[\bar{h}_n(\mathbf{A})]}{|\mathbf{P(A)}|}}.\qquad(3.37)$$

3.5   Numerical examples

In order to investigate general behavior of the estimators, and validity of the approximations for their accuracy/precision, numerical examples on the flow estimator is shown. In the numerical examples, traffic is assumed to be steady as follows.

Distribution of mean time headway of a vehicle, $\bar{h}_n(\mathbf{A})$, is assumed to follow the Gamma distribution, which is often employed for representing the headway distribution (c.f., Katakura, 1971; Zhang et al., 2007), with parameters $k = k_h$ and $\theta = \theta_h$. Variable $d_n(\mathbf{A})$ is also assumed to follow the Gamma distribution with parameters $k = k_d$ and $\theta = \theta_d$, and is independent of $\bar{h}_n(\mathbf{A})$. Note that $d_n(\mathbf{A})$ is actually almost independent of $\bar{h}_n(\mathbf{A})$ where $\mathbf{A}$ has long time length comparing to the space length and the vehicle speed, such that all the vehicles in $\mathbf{A}$ travel distance of the space length of $\mathbf{A}$.

The probability density function of the Gamma distribution is

$$f(x) = x^{k-1}\frac{e^{-x/\theta}}{\Gamma(k)\theta^k},\qquad(3.38)$$

where k and θ are parameters of the distribution, and Γ is the Gamma function. The mean and variance are $k\theta$ and $k\theta^2$, respectively.

The parameters of the distributions (mean $\mu(\cdot)$ and standard deviation $\sigma(\cdot)$), the total number of vehicles $\mathbf{N(A)}$, and the number of probe vehicles $\mathbf{P(A)}$ are given for numerical

Table 3.1: Parameters for numerical examples

	$\mu(\bar{h}_n(\mathbf{A}))$ (s)	$\sigma(\bar{h}_n(\mathbf{A}))$ (s)	$\mu(d_n(\mathbf{A}))$ (m)	$\sigma(d_n(\mathbf{A}))$ (m)
(a)	1.5	0.5	100	5
(b)	3	2	100	5
(c)	3	2	100	20
(d)	8	9	100	20

examples. If the mean of $\bar{h}_n(\mathbf{A})$ was large, it means that the flow is low. If the variance of $\bar{h}_n(\mathbf{A})$ was large, it implies that the flow is in free-flow state. If the variance of $d_n(\mathbf{A})$ was large, it implies that the variance of speed is large. If $\mathbf{N}(\mathbf{A})$ was large, it implies that size of $\mathbf{A}$ is large, namely, the estimation resolution is low. If $\mathbf{P}(\mathbf{A})$ was large compared to $\mathbf{N}(\mathbf{A})$, it means that PR is high.

The parameters of time headway distribution were adopted from field data described by Katakura (1971), while that of speed were assumed. Three combination of the distribution parameters values were employed as shown in Table 3.1, where (a) represents near-saturated state, (b) represents free-flow state, (c) represents free-flow state with larger speed variance and (d) represents sparse free-flow state. The value of $\mathbf{N}(\mathbf{A})$ is either 100 veh or 5000 veh, which represents high and low resolution, respectively. The $\mathbf{P}(\mathbf{A})$ is selected from various values. Note that congested states are not validated in this section, since mean headway variance in congested states can be significantly smaller than that of free-flow states so that the estimation accuracy/precision may be high.

Errors defined by eqs (3.17)–(3.20) are numerically computed using Monte Carlo simulation (i.e., simulated random sampling of b_n where $d_n(\mathbf{A})$ and $\mathbf{a}_n(\mathbf{A})$ are given for all n). Then, they are compared with the analytically approximated ones (3.21) and (3.23). Figs 3.2 and 3.3 show the results. Each subfigure shows relation between errors and PR under specific state and resolution. Errors include numerical computed bias and RMSE (blue lines), and analytically approximated ones (red lines). According to the figure, the numerical computed errors decrease as PR increases, resolution lowers, and variances in headway and speed lowers. The effect of speed variance is relatively

(a) Near-saturated state (2400 veh/h)

(b) Free-flow state (1200 veh/h)

(c) Free-flow state (1200 veh/h) with larger speed
variance

(d) Sparse free-flow state (450 veh/h)
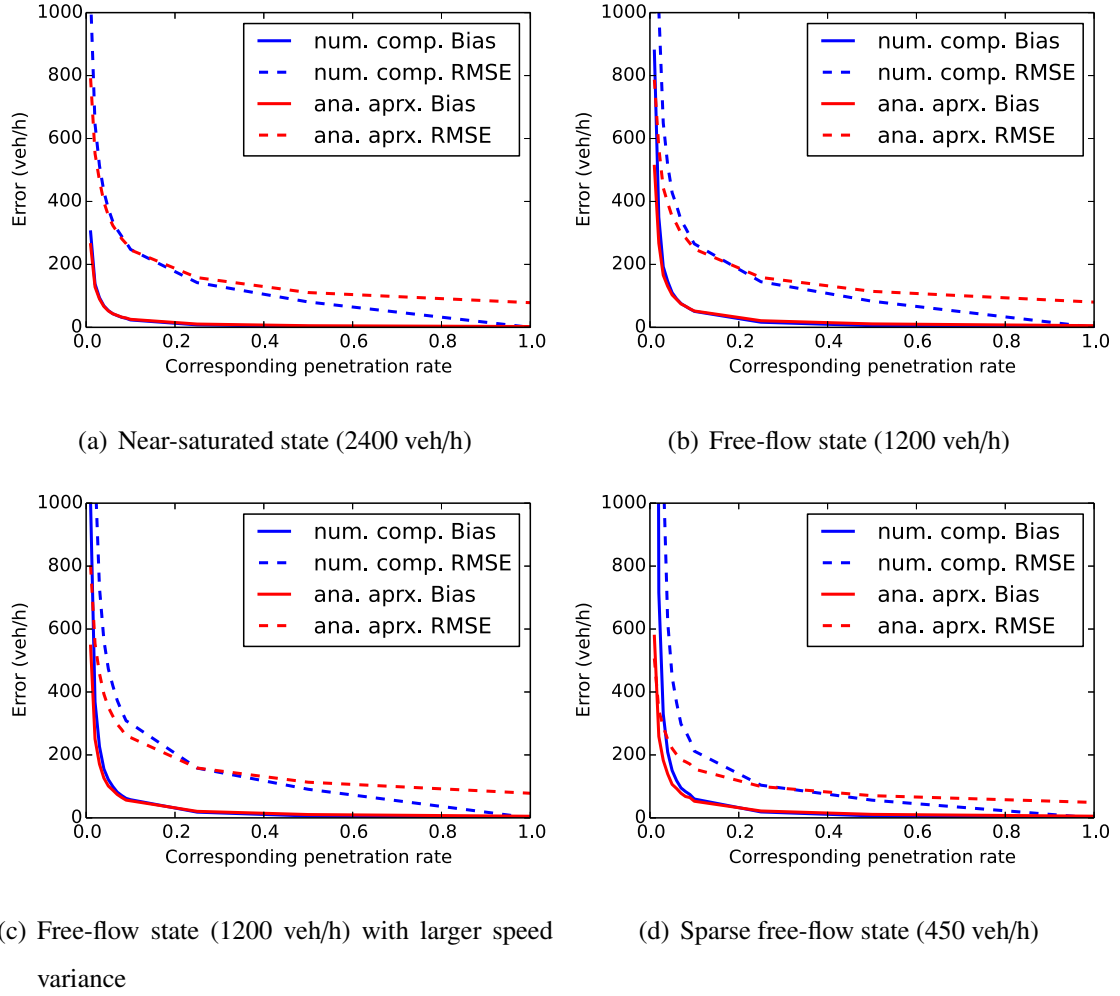
Figure 3.2: Numerical examples of error of the flow estimator with high resolution.

insignificant. The tendencies of the numerical computed errors are the same to the analytical approximated ones. In addition, the analytical approximated errors are fairly close to the numerical computed ones under some conditions, such as in low resolution, in dense state, for bias, etc. Therefore, they can be valid and useful for predicting the accuracy/precision of the TSE method in prior to applications under such conditions. On the other hand, the approximation is not appropriate under high penetration rate or sparse traffic flow conditions. It may be due to third order Taylor approximation and approximation $Var[E_{\mathbf{P(A)}}[\bar{h}_n(\mathbf{A})]] \simeq Var[\bar{h}_n(\mathbf{A})]/|\mathbf{P(A)}|$.

(a) Near-saturated state (2400 veh/h)

(b) Free-flow state (1200 veh/h)

(c) Free-flow state (1200 veh/h) with larger speed variance

(d) Sparse free-flow state (450 veh/h)
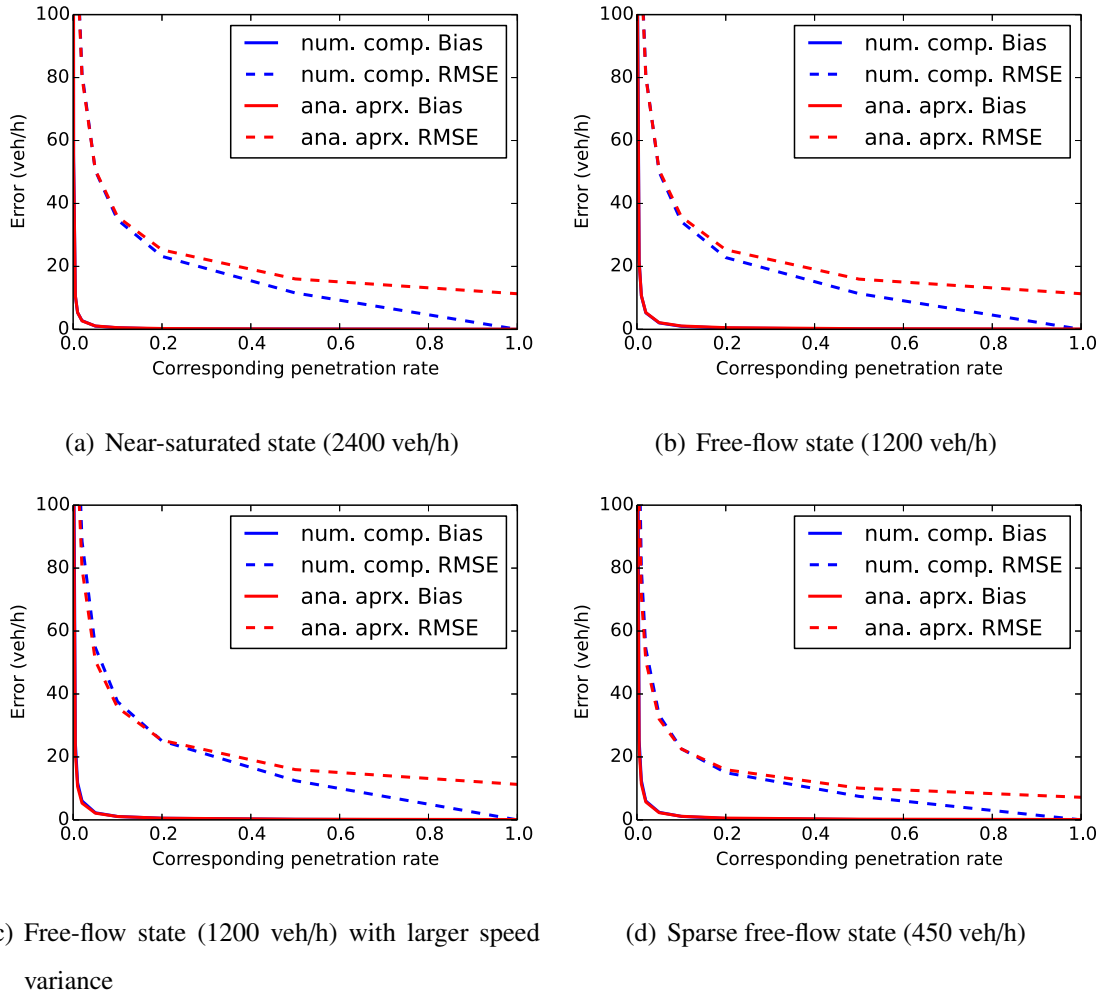
Figure 3.3: Numerical examples of error of the flow estimator with low resolution.

3.6   Discussions

With the method we can estimate the flow, density, and speed depending only on probe vehicle data. This characteristic is valuable for a TSE method because it makes wide-ranging state estimation easy, as noted in chapter 2. The method does not presume an FD, which is often used to estimate the traffic state in existing studies (e.g., Nanthawichit et al., 2003; Yuan et al., 2012; Mehran et al., 2012). Because of this independency from an FD, the results obtained with this method are robust against unpredictable or uncertain factors of traffic flow, such as traffic incidents. In addition, the results can be utilized to

(a) Higher resolution   (b) Lower resolution   (c) Area-wide resolution
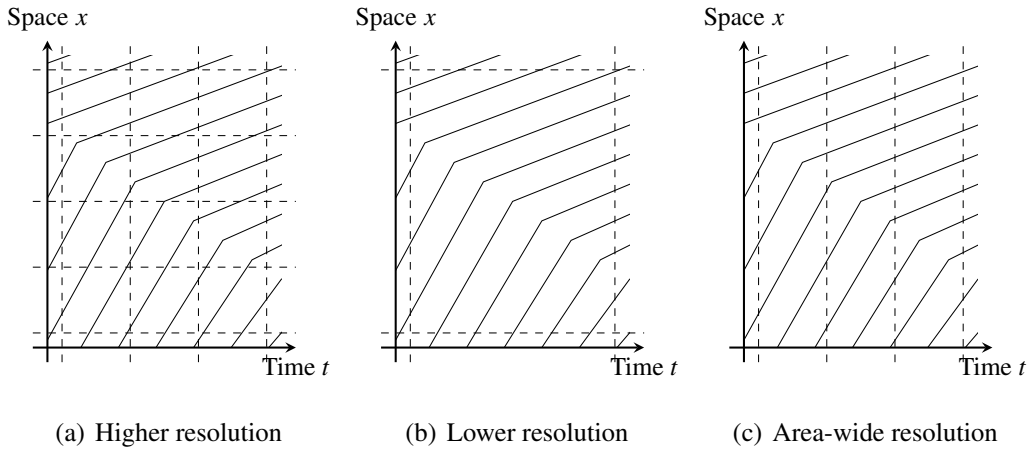
Figure 3.4: Examples of **A** shapes.

estimate or calibrate traffic flow models, including FDs.

The resolution of the estimation (Δt and Δx) can be adjusted to the requirements by the planners and analysts. As shown in eqs (3.21)–(3.24) and section 3.5, there is a tradeoff between the estimation accuracy and precision and resolution, as well as a positive relation between the accuracy and precision and PR. Therefore, analysts can choose a desired resolution depending on the estimation purpose and the number of probe vehicles in order to maintain the required accuracy and precision. Fig 3.4 illustrates examples of the shapes of **A** where the dashed lines represent each boundaries of **A**s. If the number of probe vehicles is sufficiently large, a high resolution can be set—detailed and dynamic changes in traffic states can be recognized (Fig 3.4a). In contrast, even if the number of probe vehicles is very small, analysts can still obtain some knowledge on the traffic by setting a low resolution, such as an hourly traffic volume (Fig 3.4b) and area-flow/density (Fig 3.4c).

Section 3.5 shows numerical examples of the accuracy/precision depending on traffic situation, estimation resolution and PR by assuming simple spacing and speed distributions; and suggested naïve benchmarks on the capability of the proposed method and validity of the analytically approximated errors. In order to investigate these characteristics under more realistic traffic situation, in which speed and spacing are

described by nonlinear traffic phenomena, they are quantitatively analyzed based on data collected via simulation experiments and a field experiment in chapters 5 and 6

The proposed method relies on assumptions that may not always satisfied in the real world, namely, the error free and random sampling assumptions. The error free assumption can be reasonable except in situations with very sparse traffic where leading vehicles are not often detectable. The reasons are as follows. Small errors in position measurement[*2] do not significantly affect accuracy and precision of the proposed method. If the size of the time–space region $\mathbf{A}$ is larger enough than expected error in position measurement, errors in $d_n(\mathbf{A})$, $t_n(\mathbf{A})$ and $\mathbf{a}_n(\mathbf{A})$ can be neglectable. On the other hand, errors in spacing measurement directly affect $\mathbf{a}_n(\mathbf{A})$ and therefore accuracy and precision of the proposed method. However, errors in spacing measurement should be small because practically implemented spacing measurement technologies have to provide good features in order to guarantee the safety of the ADAS. Although the spacing measurement requires assumption on vehicle length, this can be only a weak assumption; because variation of vehicle length is expected to be relatively smaller comparing to that of the spacing.

Leading vehicles are not always detectable due to technical problems, such as excessive distance. This "missing spacing" issue always exist, and is more significant at sparse traffic. This issue may arise over estimation if such data were discarded; therefore, it cannot be neglected. For example, ratio of missing spacing under traffic condition described in section 3.5, 80 km/h average speed, and maximum detectable range 130 m (Saneyoshi, 1996) is calculated as follows: (a) 0.0%, (b) 9.2%, (c) 9.6% and (d) 44.4%. Therefore, for practical purposes, imputation methods for missing spacing are desirable[*3].

The random sampling assumption may not always satisfied in the real world. This

---

[*2]Usual GPS-based map-matching techniques' accuracy is around 10 m (Quddus et al., 2007).

[*3]The amount of flow over estimation caused by discarding missing spacing data in the example are as follows: (a) 0.0, (b) 213.6, (c) 226.3 and (d) 1110.1 veh/h—they are far more than neglectable. If the missing spacing data are simply substituted by the maximum detectable range, flow over estimation can be mitigated to (a) 0.0, (b) 64.9, (c) 77.6 and (d) 482.9 veh/h.

means that the probe vehicles may have different driving behaviors compared with other vehicles. In general, the estimation biases caused by biases in probe vehicles' driving behavior can be explained as follows. If average speed of probe vehicles is larger than that of all the vehicles, the flow and speed will be proportionally overestimated. If average spacing of probe vehicles is larger than that of all the vehicles, the flow and density will be proportionally overestimated. Note that the biases are difficult to be specified in prior due to the nonlinear relation between speed and spacing.

Chapter 4 Integrating Traffic Dynamics into Estimation Methods

This chapter[*1] describes how the basic method can be integrated with dynamics of traffic. Traffic is dynamic phenomena that propagates over time and space. If conditions describing such dynamics were integrated into TSE methods, their accuracy and precision can be improved while keeping them consistent with traffic flow theory. For example, the negative effect by local fluctuation in microscopic vehicular traffic, such as vehicle platoons and lane-changing, can be mitigated. This chapter develops two TSE methods integrated with traffic dynamics based on the basic method formulated at chapter 3.

Section 4.1 describes some directions of integrating dynamics of traffic into TSE methods. Sections 4.2 and 4.3 describe TSE methods integrated with a CL and with both of an FD and a CL, respectively. Both sections consist of the method's concept, its formulation and its summary. Finally, section 4.4 provides qualitative comparison among the three TSE methods, namely, the basic method (chapter 3), the method with CL (section 4.2) and the method with FD and CL (section 4.3).

4.1 Directions

Basically, traffic dynamics can be described with a fundamental diagram (FD) and a conservation law (CL) (c.f., the LWR model, chapter 2). An FD represents relation among flow, density and speed in equilibrium traffic. A CL means that vehicles do not warp, appear and disappear without specific sinks and sources.

The following develops two TSE methods. One of them utilizes the condition of a

---

[*1]This chapter is mainly based on joint research with Dr. Takahiko Kusakabe and Prof. Yasuo Asakura, published in *Journal of JSCE* (瀬尾ら, 2013), *ISTTT21*, *Transportation Research Part C* (Seo and Kusakabe, 2015, in press) and *IEEE ITSC 2015* (Seo et al., 2015b, accepted).

CL where a CL must be satisfied (i.e., road sections that do not have merging/diverging sections). The other utilizes the conditions of an FD and a CL; a functional form of an FD is given exogenously while its parameters are endogenously estimated from probe vehicle data. Note that methods with an FD but without a CL is not considered here; because it is theoretically pointless for TSE purposes in a corridor[*2].

4.2   Method with CL

This section develops a method that estimates the traffic state based on the collected spacing and position data of probe vehicles by considering a CL to represent the traffic dynamics. On the other hand, it does not use an FD in order to eliminate exogenous factors.

4.2.1   Concept

The proposed method estimates traffic states in a road section where some of the vehicles in the flow are probes that measure the geographic position and spacing of the vehicle ahead without any errors. The road section's schematics are assumed to be known to analysts. The probe vehicles' driving behavior is assumed to be the same as that of non-probe vehicles, i.e., the probes are randomly sampled from all of the vehicles. In addition, the traffic flow is assumed to be single-lane traffic that satisfies the FIFO condition in order to simplify the situation.

The spacing observed by a vehicle at a point depends on microscopic vehicular phenomena that depend on macroscopic traffic flow phenomena. For example, the spacing of a vehicle takes a volatile value that is mainly determined by whether the vehicle or not is the leader of a platoon; meanwhile, the development of the platoon is determined by the global traffic state. Therefore, aggregation is needed in order to estimate the traffic state from the observed vehicular variables. In this method, the observed vehicular variables

---

[*2]Methods with an FD without a CL may be interesting in terms of area-wide traffic state estimation, namely, methods with MFD.

are aggregated based on the CL. Specifically, the number of vehicles between two specific probe vehicles is a constant along a section where flow discontinuity points (e.g., a node in a road network) do not exist. This number of vehicles is estimated by aggregating the data observed by the two boundary probe vehicles. The estimation procedure is as follows:

Step 1 The number of vehicles between two consecutive probe vehicles and two consecutive discontinuity points is estimated based on the observed data of the two probe vehicles.

Step 2 The cumulative flow at the probe vehicle trajectories is calculated from the estimated number of vehicles.

Step 3 The continuous cumulative flow over the entire time–space region is estimated by interpolating the cumulative flow at the probe vehicle trajectories.

Step 4 The traffic state (i.e., flow, density and speed) is derived by partially differentiating the continuous cumulative flow.

Fig 4.1 visualizes the relation among the cumulative flow, vehicle trajectory, and traffic state (for details, see Makigami et al., 1971); the height is the continuous cumulative flow $\tilde{N}$, the contour line of $\tilde{N}$ is a vehicle's trajectory, the slope of $\tilde{N}$ in the t direction ($\partial\tilde{N}/\partial t$) is the flow q, and the slope of $\tilde{N}$ in the $-x$ direction ($-\partial\tilde{N}/\partial x$) is the density k. This method can be regarded as based on rectangles on the n–x coordinate plane, which is similar to the n–t Lagrangian coordinates of Leclercq et al. (2007); Wageningen-Kessels et al. (2013) and is identical to coordinates of T-model by Laval and Leclercq (2013), because the primary subject of estimation is the number of vehicles in the n–x rectangles.

4.2.2 Estimation method for cumulative flow at probe vehicle's trajectory

Consider the time–space region $\mathbf{A}_m^j$ (c.f., Fig 4.2) surrounded by the

- trajectory of the m-th probe vehicle,
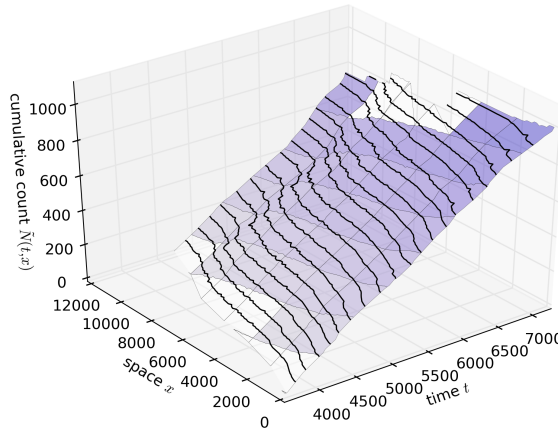
Figure 4.1: Three-dimensional representation of traffic flow.
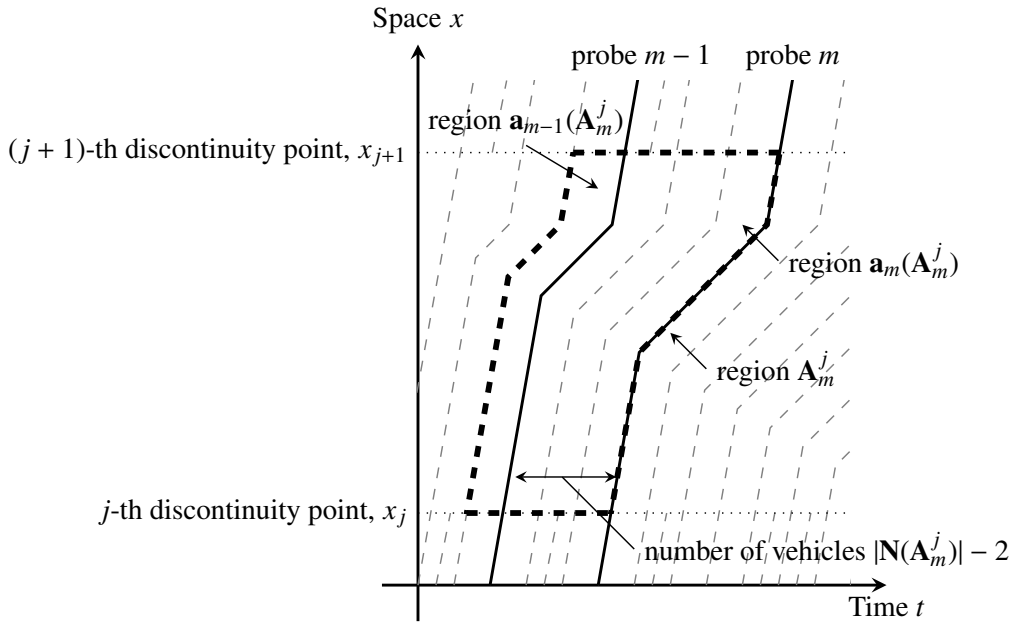
Figure 4.2: Method conceptualized as time–space diagram.

- trajectory of the leading vehicle of the $(m-1)$-th probe vehicle,

- position of the j-th discontinuity point, and

- position of the $(j+1)$-th discontinuity point.

Because of this definition and the FIFO assumption, the number of vehicles in the region $\mathbf{A}_m^j$ is always identical to the number of vehicles between the m-th probe vehicle and the leading vehicle of the $(m-1)$-th probe vehicle. The following notations are employed to

represent the time and space coordinates: x_m^t is the position of the m-th probe vehicle at the time point t, t_m^x is the time point of the m-th probe vehicle at the position x, and x_j is the position of the j-th discontinuity point.

The cumulative flow $N(t, x)$ at a probe vehicle's trajectory—with the 0th probe vehicle[*3] as a reference point—is described by using the number of vehicles between two probe vehicles as follows:

$$N(t_0^x, x) = 0, \tag{4.1a}$$

$$N(t_m^x, x) = N(t_{m-1}^x, x) + |\mathbf{N}(\mathbf{A}_m^j)| - 2 \qquad (m \geq 1, \ x_j < x < x_{j+1}), \tag{4.1b}$$

where $\mathbf{N}(\mathbf{A})$ is the set of all vehicles in the time–space region $\mathbf{A}$ and $|\mathbf{N}(\mathbf{A})|$ is the number of vehicles of $\mathbf{N}(\mathbf{A})$. Eq (4.1) means that the number of vehicles between the m-th and $(m-1)$-th probe vehicles at the position x (i.e., $N(t_m^x, x) - N(t_{m-1}^x, x)$) is identical to the number of vehicles in the region $\mathbf{N}(\mathbf{A}_m^j)$ minus two[*4] (i.e., $|\mathbf{N}(\mathbf{A}_m^j)| - 2$) if the position x is between the j-th and $(j + 1)$-th discontinuity points.

The only unknown variable in eq (4.1) is $\mathbf{N}(\mathbf{A}_m^j)$. This can be estimated from the probe vehicle data as follows:

$$|\hat{\mathbf{N}}(\mathbf{A}_m^j)| = \frac{|\mathbf{A}_m^j|}{\left(|\mathbf{a}_{m-1}(\mathbf{A}_m^j)| + |\mathbf{a}_m(\mathbf{A}_m^j)|\right)/2}, \tag{4.2}$$

where $\mathbf{a}_m(\mathbf{A})$ is the time–space region between the m-th probe vehicle and its leading vehicle in region $\mathbf{A}$, which should be observed by the probe vehicle, and $|\mathbf{A}|$ is the area of the region $\mathbf{A}$. Eq (4.2) means that all vehicles in time–space region $\mathbf{A}_m^j$ are distributed with a time–space interval of $(|\mathbf{a}_{m-1}(\mathbf{A}_m^j)| + |\mathbf{a}_m(\mathbf{A}_m^j)|)/2$, which is the average of the two probe vehicle's intervals. This is consistent with the generalized definitions of Edie (1963). It also implies that the number of vehicles between two vehicles is determined by the two vehicles' spacing at a road section without discontinuity points. By using the estimated value, the cumulative flow at a probe vehicle's trajectory (4.1) can be calculated as follows:

$$\hat{N}(t_0^x, x) = 0, \tag{4.3a}$$

[*3]This vehicle is to be specified by an analyst

[*4]the $(m - 1)$-th probe vehicle and its leading vehicle

$$\hat{N}(t_m^x, x) = \hat{N}(t_{m-1}^x, x) + |\hat{\mathbf{N}}(\mathbf{A}_m^j)| - 2 \qquad (m \geq 1, \ x_j < x < x_{j+1}). \tag{4.3b}$$

4.2.3 Estimation method for traffic state

The flow, which is defined as $q = \partial \tilde{N} / \partial t$, can be estimated as

$$\hat{q}(t, x) = \frac{\hat{N}(t_m^x, x) - \hat{N}(t_{m-1}^x, x)}{t_m^x - t_{m-1}^x} \qquad (t_{m-1}^x < t \leq t_m^x). \tag{4.4}$$

The continuous cumulative flow $\tilde{N}$ is estimated from

$$\hat{\tilde{N}}(t, x) = \int_{t_0^x}^t \hat{q}(\tau, x) \mathrm{d}\tau. \tag{4.5}$$

In fact, eqs (4.4) and (4.5) mean that $\hat{\tilde{N}}$ is linearly interpolated from the discrete $\hat{N}$ of eq (4.3) over the t-axis (Fig 4.3a) where uniform distribution of the vehicles between t_m^x and t_{m-1}^x is assumed.

Once the continuous cumulative flow is obtained, the density and speed can be estimated as

$$\hat{k}(t, x) = -\frac{\partial \hat{\tilde{N}}(t, x)}{\partial x}, \tag{4.6}$$

$$\hat{v}(t, x) = \frac{\hat{q}(t, x)}{\hat{k}(t, x)}, \tag{4.7}$$

based on their definitions, namely, $k = -\partial \tilde{N} / \partial x$ and $v = q/k$, except at the discontinuity points.

The estimation procedure can also be visualized as Fig 4.3. First, the number of vehicles between two convective probe vehicles $|\hat{\mathbf{N}}(\mathbf{A}_m^j)| - 2$ is estimated based on the observed data from probe vehicles. Then, the cumulative flow $\hat{N}(t_{m-1}^x, x)$, $\hat{N}(t_m^x, x)$ and continuous cumulative flow $\hat{\tilde{N}}(t, x)$ are estimated along with the cumulative flow's slope on the n–t plane, which means the flow $\hat{q}(x, t)$ between t_{m-1}^x and t_m^x, as shown in Fig 4.3a. By using the continuous cumulative flow $\hat{\tilde{N}}(t, x)$, the density $\hat{k}(x, t)$ can be estimated as the slope of $\hat{\tilde{N}}(t, x)$ on the n–x plane, as shown in Fig 4.3b and c.
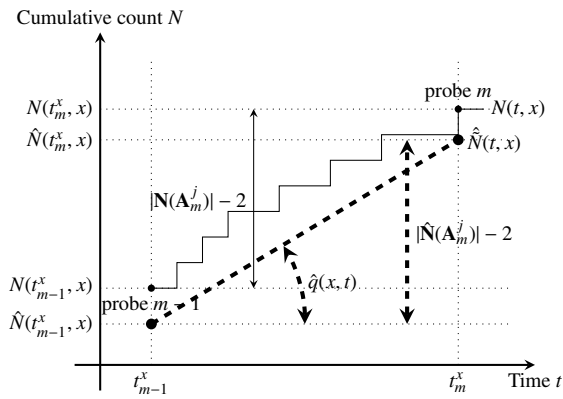
(a) n–t cumulative curve at certain point x in space (x_j, x_{j+1}).
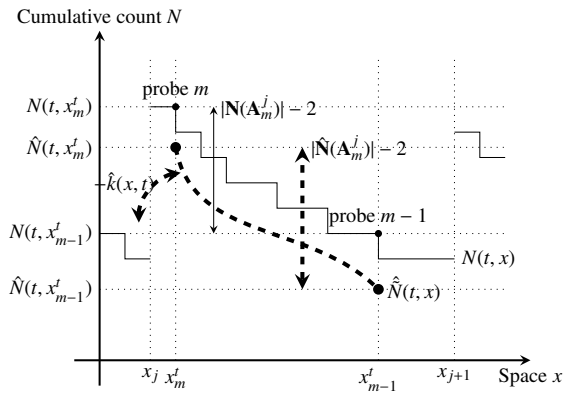
(b) n–x cumulative curve at certain time point t where $x_j \leq x_m^t < x_{m-1}^t \leq x_{j+1}$ is satisfied.
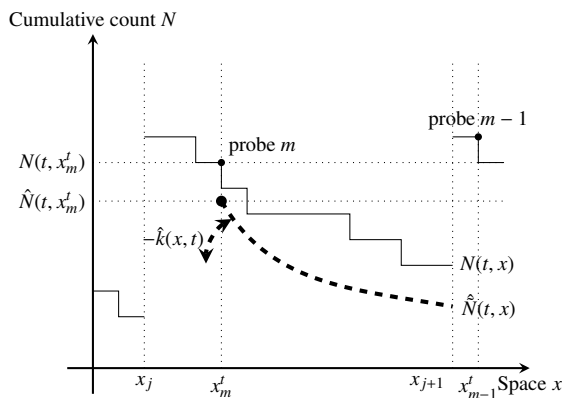
(c) n–x cumulative curve at certain time point t where $x_j \leq x_m^t < x_{j+1} < x_{m-1}^t$ is satisfied.

Figure 4.3: Illustrated examples of estimation method on cumulative curves.

4.2.4 Discussions

The proposed method can derive the flow, density, and speed without an explicit FD, meaning that no exogenous assumptions on an FD. Therefore, the proposed method can easily be applied to various traffic conditions, especially when an FD is unknown or unpredictable. Its independence from an FD also means that the proposed method can be utilized to estimate the FD itself. In fact, estimating the cumulative flow based on eq (4.2) is identical to estimating the area-flow (c.f., MFD; Geroliminis and Daganzo, 2008; Daganzo and Geroliminis, 2008) between two merging/diverging positions and two consecutive probe vehicles. It implies that if a well-defined MFD exist in the region (Daganzo and Geroliminis (2008); Laval et al. (2015) prove this fact under certain conditions such as a link with constant FD), the proposed method could be accurate.

The proposed method utilizes the CL in order to estimate the traffic state from vehicles' spacing. This means that the traffic state of a certain time point and position is estimated based on spacings observed by the same vehicle over a wider area of time and space. Therefore, the precision of the estimated traffic state is relatively robust against fluctuations in microscopic vehicular phenomena (e.g., vehicle platoons, lane-changing) comparing to the basic method proposed of chapter 3, which does not consider the CL. As noted earlier, equation (4.2) is identical to estimating the area-flow from the probe vehicle data based on Edie's generalized definition. Therefore, the accuracy and precision of $|\hat{\mathbf{N}}(\mathbf{A}_m^j)|$ can be analytically approximated based on eqs (3.21) and (3.23) of the basic method, as follows:

$$E\left[|\hat{\mathbf{N}}(\mathbf{A}_m^j)|\right] - |\mathbf{N}(\mathbf{A}_m^j)| \simeq \frac{|\mathbf{A}_m^j|\,\sigma\left(\bar{h}_n(\mathbf{A})\right)^2}{2(x_{j+1} - x_j)\mu\left(\bar{h}_n(\mathbf{A})\right)^3}, \tag{4.8}$$

$$\mathrm{RMSE}\left(|\hat{\mathbf{N}}(\mathbf{A}_m^j)|\right) \simeq \frac{|\mathbf{A}_m^j|}{(x_{j+1} - x_j)\mu\left(\bar{h}_n(\mathbf{A})\right)^2}\sqrt{\frac{\sigma\left(\bar{h}_n(\mathbf{A})\right)^2}{2}}, \tag{4.9}$$

where $\mu()$ represents the mean, $\sigma()^2$ represents the variance, $\bar{h}_n(\mathbf{A})$ represents the mean headway of a vehicle n in the region $\mathbf{A}_m^j$, and RMSE is root mean square error and taken as an index for precision. Eqs (3.21) and (3.23) mean that the accuracy and precision of

the estimated cumulative flow N are improved as mean of the vehicle's mean headways increases and the variance of the vehicle's mean headways decreases. Therefore, the accuracy and precision of the estimated traffic state have similar tendencies.

The basic method estimates a traffic state in a short road segment using data collected from the segment itself; therefore, estimation error can be large because vehicles may keep a platoon formed in the segment (i.e., $\sigma(\bar{h}_n(\mathbf{A}))^2$ may be large). In contrast, the proposed method in this section estimates a traffic state in a position using data collected from the entire link; therefore, estimation error can be smaller because platoons may be newly formed and/or declined in the link (i.e., $\sigma(\bar{h}_n(\mathbf{A}))^2$ may be smaller).

The deficiencies of the proposed method are as follows. First, single-lane traffic and FIFO condition were assumed in order to estimate the number of vehicles between two probe vehicles; such assumptions are not always satisfied in the real world. However, the proposed method can be applied to traffic where these conditions are not satisfied if the probe vehicle's driving behavior is the same as other vehicles. This is because the expected number of vehicles that overtake a probe vehicle and number that are overtaken by a probe vehicle is equal to each other. In addition, estimation error may sometimes decrease under non-FIFO condition; because a platoon, by which mean headway variances increase, will be formed and/or declined frequently under such condition. Note that if the road has multiple lanes, the cumulative number (4.3) needs to be multiplied by the number of lanes. Second, the linear interpolation of the cumulative flow over time is limited in its ability to reproduce shockwaves. Another deficiency is that real-time states cannot be estimated. Therefore, short-term future prediction is required in order to obtain the real-time states[*5].

[*5]This prediction can be based on the estimated traffic state and an FD that can be estimated with the proposed method.

4.3 Method with FD and CL

This section develops a method that estimates the traffic state based on the observed spacing and position data of probe vehicles by considering an FD and CL to represent the traffic dynamics.

4.3.1 Concept

The following conditions are assumed for traffic that is subject of TSE in this method. The road schematics (e.g., position and length of links, link connectivity, position of nodes, number of lanes) are pre-given information for the proposed method. Probe vehicles are randomly distributed in traffic with unknown penetration rate. The probe vehicles are PVSMEs, which continuously collect data including spacing (i.e., distance between probe vehicle and its leading vehicle ahead) and position without error.

The procedure of the proposed TSE method can be described as follows. First, time–space resolution for TSE, time–space resolution for FD's parameter estimation, and FD's functional form are set by analysts. Then, traffic states and FD parameters are respectively derived (i.e., observed) from the probe vehicle data. Finally, by using a data assimilation technique, traffic states are updated from the observed traffic states, the observed FD parameters, estimated traffic states in the previous timestep, and a traffic flow model.

Specifically, the basic TSE method is utilized for observing traffic states. FD parameters are derived by regressing spacing and headway (spacing divided by speed) relation in the probe vehicle data. The cell transmission model (CTM; Daganzo, 1994), a numerical computation method for solving the LWR model, is applied for the traffic flow model. As a data assimilation technique, Ensemble Kalman Filter (EnKF; Evensen, 1994) is employed due to its capability for dealing nonlinear phenomena in traffic (the system model). Note that the observation model of the proposed TSE method can be represented by a linear system; therefore, EnKF is an appropriate way for this problem. Fig 4.2 summarizes the procedures of the proposed method.
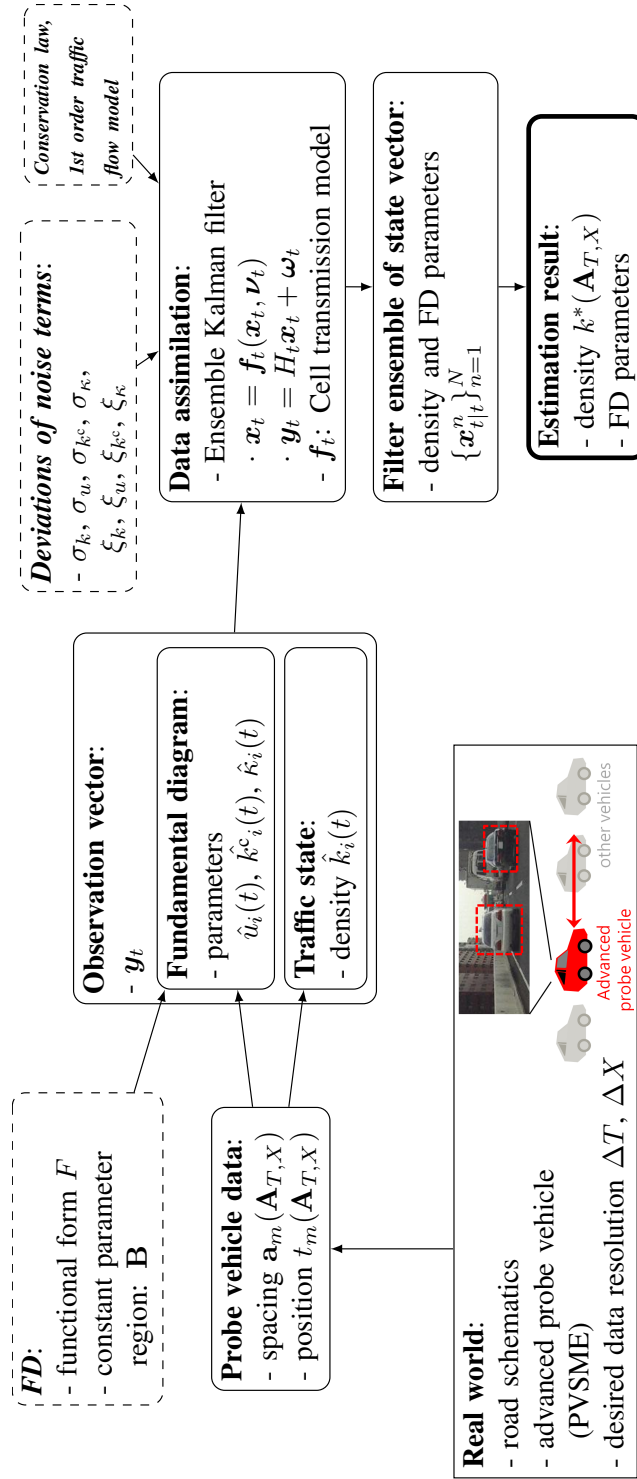
Figure 4.4: Illustrated concept of the procedure of the proposed TSE method.

4.3.2 Ensemble Kalman filter

This part briefly describes EnKF by employing the expressions from 樋口 (2011).

A state–space model for EnKF can be described as follows

$$\boldsymbol{x}_t = \boldsymbol{f}_t(\boldsymbol{x}_t, \boldsymbol{\nu}_t), \tag{4.10}$$

$$\boldsymbol{y}_t = H_t \boldsymbol{x}_t + \boldsymbol{\omega}_t, \tag{4.11}$$

where eq (4.10) is a system equation, eq (4.11) is an observation equation, $\boldsymbol{x}_t$ is a state vector, $\boldsymbol{f}_t$ is a system model, $\boldsymbol{\nu}_t$ is a system noise vector, $\boldsymbol{y}_t$ is an observation vector, H_t is an observation matrix, and $\boldsymbol{\omega}_t$ is an observation noise vector, at timestep t respectively. The observation noise vector $\boldsymbol{\omega}_t$ follows normal distribution whose average is 0 and variance-covariance matrix is R_t, namely, $\boldsymbol{\omega}_t \sim \mathcal{N}(0, R_t)$.

The general procedure of EnKF can be described as follows:

Step 1 Generate an ensemble of the initial states $\{\boldsymbol{x}_{0|0}^n\}_{n=1}^N$. Let $t \leftarrow 1$.

Step 2 Prediction step:

> **Step 2.1** Generate an ensemble of the system noises $\{\boldsymbol{\nu}_t^n\}_{n=1}^N$.
>
> **Step 2.2** Calculate $\boldsymbol{x}_{t|t-1}^n = \boldsymbol{f}_t(\boldsymbol{x}_{t-1|t-1}^n, \boldsymbol{\nu}_t^n)$ for each n.

Step 3 Filtering step:

> **Step 3.1** Generate an ensemble of the observation noises $\{\boldsymbol{\omega}_t^n\}_{n=1}^N$.
>
> **Step 3.2** Obtain the filter ensemble $\{\boldsymbol{x}_{t|t}^n\}_{n=1}^N$ for each n, by calculating eq (4.12) based on $\boldsymbol{y}_t$, H_t, R_t, $\{\boldsymbol{x}_{t|t-1}^n\}_{n=1}^N$, $\{\boldsymbol{\omega}_t^n\}_{n=1}^N$.

Step 4 Increment the timestep, $t \leftarrow t + 1$. Go back to Step 2 until $t = t_{\max}$.

The filter ensemble in Step 3.2 can be derived as follows:

$$\boldsymbol{x}_{t|t}^n = \boldsymbol{x}_{t|t-1}^n + \hat{K}_t \left(\boldsymbol{y}_t + \breve{\boldsymbol{\omega}}_t^n - H_t \boldsymbol{x}_{t|t-1}^n \right), \tag{4.12}$$

where,

$$\hat{K}_t = \hat{V}_{t|t-1} H_t' \left(H_t \hat{V}_{t|t-1} H_t' + R_t \right)^{-1}, \tag{4.13a}$$

$$\hat{V}_{t|t-1} = \frac{1}{N-1} \sum_{j=1}^{N} \breve{x}_{t|t-1}^{j} (\breve{x}_{t|t-1}^{j})', \tag{4.13b}$$

$$\breve{x}_{t|t-1}^{n} = x_{t|t-1}^{n} - \frac{1}{N} \sum_{j=1}^{N} x_{t|t-1}^{j}, \tag{4.13c}$$

$$\breve{\omega}_{t}^{n} = \omega_{t}^{n} - \frac{1}{N} \sum_{j=1}^{N} \omega_{t}^{j}. \tag{4.13d}$$

In this method, following mean vector of the filter ensemble is defined as an "estimation result" at timestep t:

$$\bar{x}_{t|t} = \frac{1}{N} \sum_{n=1}^{N} x_{t|t}^{n}, \qquad \forall t. \tag{4.14}$$

4.3.3 TSE method formulation

In this subsection, the TSE method is formulated by specifying the terms and the function in eqs (4.10) and (4.11).

(1) System model

A nonlinear system equation that represents traffic dynamics is formulated.

The state vector x_t is defined as follows:

$$x_t = (k_1(t), k_2(t), \dots, k_i(t), \dots k_M(t),$$
$$u_1(t), u_2(t), \dots, u_i(t), \dots u_M(t),$$
$$k_1^c(t), k_2^c(t), \dots, k_i^c(t), \dots k_M^c(t),$$
$$\kappa_1(t), \kappa_2(t), \dots, \kappa_i(t), \dots \kappa_M(t)) \tag{4.15}$$

where, $k_i(t)$ is a density, $u_i(t)$ is a free-flow speed, $k_i^c(t)$ is a critical density, and $\kappa_i(t)$ is a jam density, of cell i at timestep t respectively. Note that $k_i(t)$ is the traffic state and $u_i(t), k_i^c(t), \kappa_i(t)$ are the FD parameters. The number of elements in vector x_t is $4M$, where M is total number of discretized spaces (cells) in the system model.

The system model f_t consists of two parts: on traffic state dynamics and on FD parameters. The first part of the system model f_t (on traffic state dynamics) is the CTM
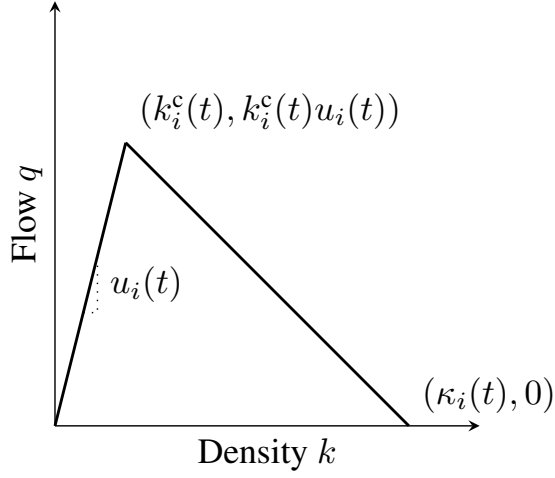
Figure 4.5: Triangular FD and its parameters in cell i at time t.

with noise term. It is described as follows:

$$Q_i^{\text{in}}(t) = \varepsilon_i^k(t) \min \left\{ \begin{array}{l} l_{i-1}k_{i-1}(t), \\ \frac{k_i^c(t)}{\kappa_i(t)k_i^c(t)}(l_i\kappa_i(t) - l_ik_i(t)) \end{array} \right\}, \tag{4.16a}$$

$$k_i(t+1) = k_i(t) + Q_i^{\text{in}}(t)/l_i - Q_{i+1}^{\text{in}}(t)/l_i, \tag{4.16b}$$

where $Q_i^{\text{in}}(t)$ is a number of vehicles that enters cell i at timestep t, l_i is the length of cell i, and $\varepsilon_i^k(t)$ is a system noise of cell i at timestep t that is expressed as $\varepsilon_i^k(t) \sim \mathcal{N}(1, \sigma_k^2)$ (truncated to non-negative values). Triangular FD is employed by eq (4.16); the relation between triangular FD and its parameters is shown in Fig 4.5. The original CTM represents traffic dynamics by solving the LWR model (partial differential equation system of continuous fluid approximated traffic) using the Godunov scheme; it can be represented as eq (4.16) without the noise term, $\varepsilon_i^k(t)$.

The CTM requires time and space discretization. The size of the CTM's timestep is Δt. The cell length should be equal to the timestep size multiplied by the free-flow speed in the cell (i.e., $l_i = \Delta t u_i$) in order to keep consistency with the LWR model; and should be larger than the value in order to satisfy the CFL condition. The detailed discretization method is described later, namely, eq (4.23) and Fig 4.6; because it has significant relation with the observation.

The other part of the system model $\boldsymbol{f}_t$ (on FD parameters) is assumed to be random
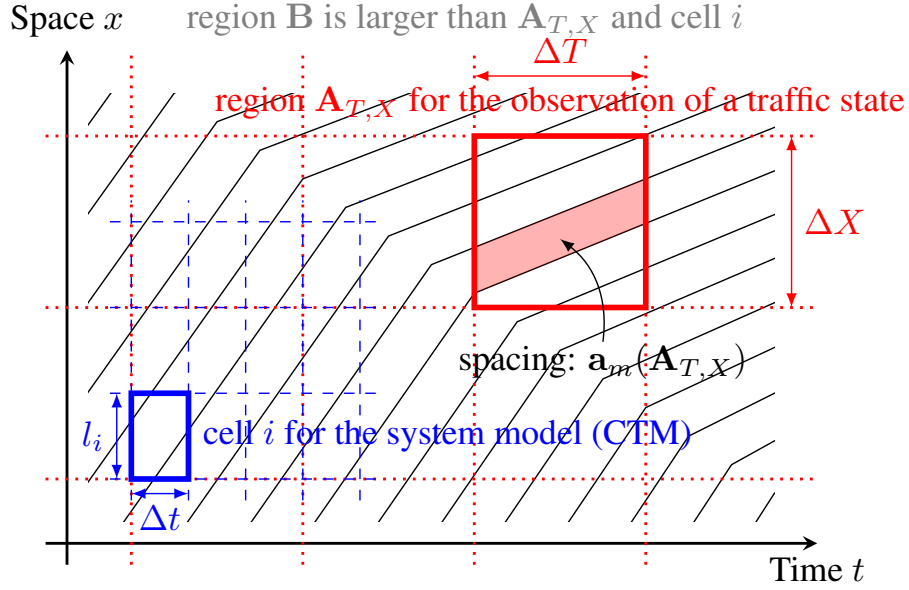
Figure 4.6: Coordinates for the method with FD and CL and the probe vehicle data.

walks. They can be represented as

$$u_i(t + 1) \sim \mathcal{N}(u_i(t), \sigma_u^2), \tag{4.17a}$$

$$k_i^c(t + 1) \sim \mathcal{N}(k_i^c(t), \sigma_{k^c}^2), \tag{4.17b}$$

$$\kappa_i(t + 1) \sim \mathcal{N}(\kappa_i(t), \sigma_\kappa^2), \tag{4.17c}$$

where σ_u, σ_{k^c} and σ_κ are deviations for the random walks. The size of the deviations are given by the analysts.

The system noise vector $\boldsymbol{\nu}_t$ is assumed to be consists of σ_k, σ_u, σ_{k^c} and σ_κ without time, space nor flow dependency.

(2) Observation

A linear observation equation can be formulated based on the basic method.

The observation vector $\boldsymbol{y}_t$ is defined to have the same property with the state vector $\boldsymbol{x}_t$ as

$$\boldsymbol{y}_t = (\,\ldots, \hat{k}_i(t), \ldots, \hat{u}_i(t), \ldots, \hat{k}^c_i(t), \ldots, \hat{\kappa}_i(t), \ldots\,) \tag{4.18}$$

where the $\hat{}$ mark indicates that the variable is directly derived (i.e., observed) from the probe vehicle data. The number of elements in vector y_t is also $4M$.

From the probe vehicle data, a density in a time–space region can be derived as follows:

$$\hat{k}(\mathbf{A}_{T,X}) = \frac{\sum_{m \in \mathbf{P}(\mathbf{A}_{T,X})} t_m(\mathbf{A}_{T,X})}{\sum_{m \in \mathbf{P}(\mathbf{A}_{T,X})} |\mathbf{a}_m(\mathbf{A}_{T,X})|}. \tag{4.19}$$

This is equivalent to eq (3.15). This is the observed state. The definition of $\mathbf{A}_{T,X}$ is

$$\mathbf{A}_{T,X} = \{(x,t) \mid X \le x \le X + \Delta X,\ T \le t \le T + \Delta T\} \tag{4.20}$$

where ΔT and ΔX are predetermined resolutions for time and space, respectively. Eq (4.20) means that region $\mathbf{A}_{T,X}$ is a rectangle in time–space plane with time length ΔT and space length ΔX (c.f., Fig 4.6).

The FD parameters are derived from regression of headway–spacing relation in the probe vehicle data. Values of $\hat{u}_i(t)$, $\hat{k}^c_i(t)$, $\hat{\kappa}_i(t)$ are assumed to be constant in a pre-determinded time–space region $\mathbf{B}$ (i.e., the observed FD parameters are constant in $\mathbf{B}$). They can be determined as

$$\hat{u}_i(t) = u(\mathbf{B}), \qquad\qquad\qquad \forall(t,i) \in \mathbf{B} \tag{4.21a}$$

$$\hat{k}^c_i(t) = w(\mathbf{B})\kappa(\mathbf{B})/(u(\mathbf{B}) + w(\mathbf{B})), \qquad\qquad \forall(t,i) \in \mathbf{B} \tag{4.21b}$$

$$\hat{\kappa}_i(t) = \kappa(\mathbf{B}), \qquad\qquad\qquad \forall(t,i) \in \mathbf{B}, \tag{4.21c}$$

where $u(\mathbf{B})$, $w(\mathbf{B})$ and $\kappa(\mathbf{B})$ are the free-flow speed, the wave speed and the jam density, respectively, in time–space region $\mathbf{B}$. The values of $u(\mathbf{B})$, $w(\mathbf{B})$ and $\kappa(\mathbf{B})$ are the solution of the following optimization problem:

$$\underset{u(\mathbf{B}),w(\mathbf{B}),\kappa(\mathbf{B})}{\operatorname{argmin}} \sum_{(m,\tau) \in \mathbf{P}(\mathbf{B})} D\left(h_{m,\tau}, s_{m,\tau}, u(\mathbf{B}), w(\mathbf{B}), \kappa(\mathbf{B})\right)^2,$$

$$\text{s.t. } u(\mathbf{B}) \ge 0,\ w(\mathbf{B}) \ge 0,\ \kappa(\mathbf{B}) \ge 0, \tag{4.22}$$

where $h_{m,\tau}$ and $s_{m,\tau}$ are stationary headway and spacing, respectively, of vehicle m at time τ, D is a function that returns the minimum distance from a point $(q,k) = (1/h_{m,\tau}, 1/s_{m,\tau})$ to a curve $q = F(k, u(\mathbf{B}), w(\mathbf{B}), \kappa(\mathbf{B}))$, and F is a function representing a triangular

FD. Therefore, problem (4.22) finds FD parameter values that minimizes total distance between observed stationary headway–spacing points and the FD curve. Stationary means that the change rates of these variables in small time duration $\Delta\tau$ (e.g., $(h_{m,\tau}-h_{m,\tau-\Delta\tau})/h_{m,\tau}$) are small enough. This procedure is required because a theoretical FD is defined under stationary condition and an empirical FD can be clear triangular relation under stationary condition Cassidy (1998).

The relation between region $\mathbf{A}_{T,X}$ for the observation and cell i at timestep t in the system model are as follows. The resolution of the observation and that of the system model can be different; because that of the observation depends on the analysts purposes, while that of the system model depends on the timestep and free-flow speed in the CTM. In this method, the size of region $\mathbf{A}_{T,X}$ is set to includes one or multiple cell(s) and timestep(s) completely (i.e., without extending a cell and a timestep over multiple regions for the observation) in order to make the coordinate system concise and to avoid causing numerical errors. Specifically, the value of ΔT, Δx, Δt and l_i are determined as follows:

$$l_i = \alpha \hat{u}_i(t)\Delta t, \qquad \forall (t,i) \in \mathbf{B} \tag{4.23a}$$

$$\Delta T = \beta \Delta t, \tag{4.23b}$$

$$\Delta X = \gamma l, \tag{4.23c}$$

where α is a coefficient larger than or equal to 1 (equal to 1 is desirable), and β and γ are natural numbers. Fig 4.6 shows an example with $\alpha = 1$, $\beta = 3$ and $\gamma = 2$. In the figure, solid curves represent vehicle trajectories, dotted grid represents regions for the observation, and dashed gird represents cells for the system model. The analysts can select appropriate values for Δt, α, β and γ according to their interests. Following definitions are introduced in order to represent the relation between region $\mathbf{A}_{T,X}$ and cell i at timestep t:

$$\mathbf{A}_i(t) = \mathbf{A}_{T,X}, \qquad \text{if } T \le t\Delta t < (t+1)\Delta t \le T + \Delta T$$

$$\text{and } X \le x_i < x_i + l \le X + \Delta X \tag{4.24}$$

where x_i is a space coordinate of the upstream edge of cell i. Therefore, following relation

holds true:

$$\hat{k}_i(t) = \hat{k}(\mathbf{A}_i(t)) = \hat{k}(\mathbf{A}_{T,X}). \tag{4.25}$$

The variance of observation noise ω_t, namely, R_t, is determined as follows. Section 3.4 showed that the precision of the estimator (4.19) in a region $\mathbf{A}_{T,X}$ is approximately in inverse proportion to the number of the probe vehicles in $\mathbf{A}_{T,X}$, namely, $|\mathbf{P}(\mathbf{A}_{T,X})|$. Therefore, deviations of traffic state observation noises are assumed to be inversely proportional to $|\mathbf{P}(\mathbf{A}_{T,X})|$. As a result, element (a, b) of the matrix R_t is defined as

$$R_t(a, b) = \begin{cases} \frac{\xi_k^2}{|\mathbf{P}(\mathbf{A}_a(t))|}, & \text{if } a = b \text{ and } a \le M \\ \xi_u^2, & \text{if } a = b \text{ and } M < a \le 2M \\ \xi_{k^c}^2, & \text{if } a = b \text{ and } 2M < a \le 3M \\ \xi_\kappa^2, & \text{if } a = b \text{ and } 3M < a \le 4M \\ 0, & \text{otherwise}, \end{cases} \tag{4.26}$$

where ξ_k is deviation for observing traffic state, and ξ_u, ξ_{k^c} and ξ_κ are deviations for observing respective FD parameters. The size of the deviations are given by the analysts.

An element (i, i) of the observation matrix H_t represents whether the cell i is observed or not. Therefore, element (a, b) of H_t is defined as

$$H_t(a, b) = \begin{cases} 1, & \text{if } a = b \text{ and } a \le M \text{ and } |\mathbf{P}(\mathbf{A}_a(t))| > 0 \\ 1, & \text{if } a = b \text{ and } a > M \\ 0, & \text{otherwise}, \end{cases} \tag{4.27}$$

according to the presence of probe vehicles.

4.3.4 Discussions

As results of the filtering steps, the filter ensemble's mean vector $\bar{x}_{t|t}$ can be obtained. The density elements (1st to M-th elements) in the mean vectors $\bar{x}_{t|t}$ are the final output of the TSE procedure. This estimated density is declared as $k^*(\mathbf{A}_{T,X})$ with resolution of ΔT and ΔX.

The proposed TSE method estimates traffic density $k^*(\mathbf{A}_{T,X})$ from the probe vehicle data. The probe vehicle data consist of continuous position and spacing of probe vehicles, namely, $t_m(\mathbf{A}_{T,X})$ and $\mathbf{a}_m(\mathbf{A}_{T,X})$ $\forall m \in \mathbf{P}(\mathbf{A}_{T,X})$ $\forall T, X$. The framework of EnKF with the CTM is employed for the estimation procedure. The functional form of the FD is assumed to be triangular. On the other hand, the parameters of the FD are not required to be assumed; they are endogenously estimated from probe vehicle data. Note that the proposed approach possibly employs FDs with other functional forms; and use time and/or space varying FD parameters by defining appropriate $\mathbf{B}$. The parameters regarding to time–space resolution (i.e., cell and timestep size for CTM, $\mathbf{A}$ for state observation, $\mathbf{B}$ for FD parameters observation) of the estimation are given by the analysts according to their interest. The size of the noise terms are required to be given. Note that the other variables of a traffic state, namely, flow and speed, can be easily derived from the estimated density and FD.

The method assumes that probe vehicles are representing whole traffic without biases, so that the FD parameters and traffic states can be estimated without biases. However, in mixed traffic condition with traditional vehicles and automated ones, probe vehicles may have biased driving behavior and therefore the proposed TSE method will be biased.

The method treats traffic in a link—no merging/diverging sections exist in the middle of the link. Traffic in a network with multiple links can be treated by implementing a node conservation law and a merging/diverging model in the proposed approach.

For large-scale real world application, the method may be not very costly in terms of computation and data-handling. EnKF requires less computation costs compared with other techniques like the particle filter. Data required for the method are position and spacing, which are calculated by distributed on-vehicle systems for their own purposes; therefore, not heavy data analyses, transmission and storage are required.

The method may be easy to be incorporated with other traffic data collection methods (e.g., detectors, GPS-equipped probe vehicles), since the method is based on data assimilation. It can be achieved by following procedures: incorporating the collected data to $\boldsymbol{y}_t$, and defining appropriate H_t and R_t considering characteristics of the data collection

methods.

4.4   Comparison among three TSE methods

Chapter 3 and this chapter proposed three methods for TSE, namely, the basic method, the method with CL, and the method with FD and CL. This section qualitatively compares the three methods and discusses their expected characteristics.

The basic method estimates traffic state in an arbitrary region using data collected from the region. Since it only assumes random sampling condition, it can be applicable without theoretical discrepancies regardless of traffic condition. However, the resolution of estimated traffic state is identical to the data collection area. Therefore, amount of data will be limited if an analyst estimates high resolution traffic state. It implies that the basic method is not robust against local fluctuations in microscopic traffic, such as platoon and lane-changing.

The method with CL estimates traffic state in an arbitrary point in a certain region. The region is product of predetermined space, which is assumed to be satisfy a CL, and area between two probe vehicles. Therefore, amount of data for TSE is relatively large compared with the basic method; it may improve precision of estimating high resolution traffic state. On the other hand, a CL is not completely satisfied under non-FIFO condition, such as in multi-lane and multi-class traffic.

The method with FD and CL estimates traffic state in an arbitrary region. Traffic dynamics, which means that traffic propagation between adjacent regions, is explicitly considered by assuming an FD and a CL. The FD's parameters are endogenously estimated from the probe vehicle data. Therefore, amount of data for TSE is relatively large compared with the method with CL as well as the basic method. The method employs traffic flow model with an Eulerian coordinate system. It means both advantage and disadvantage: the method cannot utilize information of probe vehicle trajectories, while the method is not severely affected by the discrepancies under non-FIFO condition. Assuming existence of constant FD means that the method is not robust against

(a) The basic method   (b) The method with CL   (c) The method with FD and CL
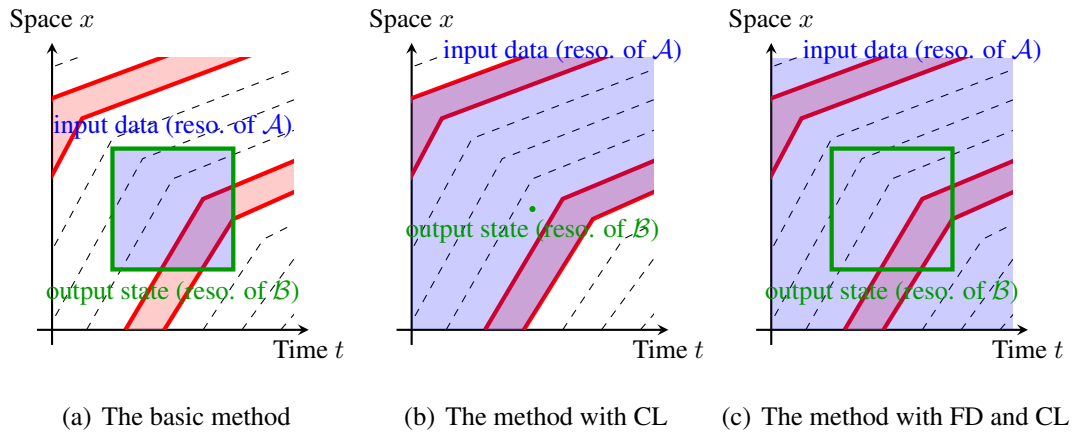
Figure 4.7: Illustrated comparison of three TSE methods.

unpredicted traffic phenomena, such as incident.

Fig 4.7 and Table 4.1 summarize above mentioned characteristics of the three TSE methods. In Fig 4.7, resolution of input data for TSE (i.e., size of an element in the set $\mathcal{A}$ in eq (2.20)) and resolution of estimated traffic state (i.e., that of $\mathcal{B}$) are illustrated along with the probe vehicle data.

Table 4.1: Summary of three TSE methods

Proposed TSE method	Assumption ($\mathcal{F}$)	Data collection range (an element of $\mathcal{A}$)	Resolution of estimated traffic state (an element of $\mathcal{B}$)
The basic method	• Random sampling	Predetermined arbitrary time–space region **A**	Identical to **A**
The method with CL	• Random sampling • Satisfaction of a CL in predetermined time–space area	Region **A** that is a product of the predetermined space and an area between two probe vehicles	Point in **A**
The method with FD and CL	• Random sampling • Satisfaction of a CL in predetermined time–space area • Existence of constant FDs in predetermined time–space areas • Functional form of the FDs • Noise terms (θ)	Region **B** that is identical to the predetermined area with constant FD	Predetermined arbitrary region **A** in **B**

Chapter 5 Simulation Experiments-based Validation

This chapter[*1] describes an empirical analysis of the proposed methods based on synthetic traffic data generated by a microscopic traffic simulator. The simulation experiments-based validation have some advantages compared with the field experiment-based validation that is described by chapter 6. For example, measurement errors and biases in probe vehicles driving behavior can be eliminated in simulation. Therefore, this validation complements the limitations of the field experiment-based validation of chapter 6. However, simulation experiments have limitations in the model and scenario setting. The simulation model describing vehicle behavior is car-following model, which controls the input variable of the proposed TSE methods directory. In addition, scenario setting of simulation, namely, demand and supply to road sections, is given ad hoc.

Sections 5.1, 5.2 and 5.3 describe validation results of the basic estimation method, the estimation method with CL, and that with FD and CL, respectively, based on synthetic traffic data generated by a microscopic traffic simulator.

5.1 The basic method

5.1.1 Simulation Scenario

An experiment environment is prepared as follows. To generate traffic conditions investigated in a validation analysis, Aimsun (TSS-Transport Simulation Systems), microscopic traffic simulator based on a car-following of Gipps (1981) and lane-changing model of Gipps (1986), is employed. The parameters of the car-following model are

---

[*1]This chapter is mainly based on joint research with Dr. Takahiko Kusakabe and Prof. Yasuo Asakura, published in *ISTTT21*, *Transportation Research Part C* (Seo and Kusakabe, 2015, in press) and *IEEE ITSC 2015* (Seo et al., 2015b, accepted).

Table 5.1: Parameters of the model in simulation

Parameter name	Mean	Deviation
Desired speed (km/h)	60	10.0
Max acceleration (m/s^2)	3	0.2
Normal deceleration (m/s^2)	4	0.5
Max deceleration (m/s^2)	6	0.5
Min spacing	1	0.3
Length (m)	4	0.5

shown in Table 5.4. The road is a homogeneous freeway that has a bottleneck at the end of the section. It has two lanes and 3 km length. Based on the above setting, traffic condition for 1 hour with a queue was generated. The average value of ground truth traffic states are 2162.8 veh/h, 128.5 veh/km and 32.6 km/h for flow, density and speed, respectively.

The bias and the root mean square error (RMSE) are employed as accuracy and precision indices, where $\text{Bias}(\hat{\theta}) = E[\hat{\theta} - \theta]$ and $\text{RMSPE}(\hat{\theta}) = \sqrt{E[((\hat{\theta} - \theta))^2]}$. Variable θ denotes a ground truth traffic flow variable (one of q, k and v) at a certain time and space calculated based on Edie's definition; and variable $\hat{\theta}$ is one of those estimated from the probe vehicle data. The parameters set for scenarios were PR P (%), time resolution Δt (min), and space resolution Δx (km). The PR P is selected from 10.0%, 5.0% and 0.1%. The time resolution Δt is selected from 1 min or 60 min; and the space resolution Δx is selected from 0.1 km or 3 km. The error indices are calculated from the results of 20 estimation iterations. In each iteration, probe vehicle data for the estimation were composed of different combinations of probe vehicles whose PR was expected to be the scenario parameter P. Traffic state in a region $\mathbf{A}_i^j$ where probe vehicles do not exist is substituted by that of its neighborhood region, $\mathbf{A}_i^{j-1}$.

5.1.2 Results

Fig 5.1 visualized estimated traffic state by the basic method and corresponding ground truth as time–space diagrams, where plot color represents value of traffic state.[*2] The scenario parameters are $(P, \Delta t, \Delta x) = (10, 0.1, 1)$. The error indices are RMSE$(q) = 719.2$, Bias$(q) = 158.1$, RMSE$(k) = 23.6$, Bias$(k) = 6.2$, RMSE$(v) = 4.8$, and RMSE$(v) = -0.1$. According to the figure, estimation errors are relatively large at free-flow state and relatively small in congested state. These phenomena can be explained by the headway and spacing distribution (c.f., sections 3.4 and 3.6); it is known that they tend to be large in free-flow state in general.

Table 5.2 summarizes the results of the estimation. The precision and bias often improves as P, Δt and Δx increased; these are reasonable features and as analytically expected (c.f., sections 3.4 and 3.6). The biases are positive in most of the scenarios. However, negative biases are also found, such as $(P, \Delta t, \Delta x) = (0.1, 0.1, 1)$ scenario. This may be caused by following two reasons: random error due to small number of samples (simulation iterations), and the interpolation method for regions without probe vehicles.

In order to validate the analytically expected bias and precision shown in eqs (3.21)–(3.24), they are calculated from all the vehicle data and compared with actual errors. The results on density are shown in Table 5.3. $\widehat{\text{Bias}}(\hat{k})$ and $\widehat{\text{RMSE}}(\hat{k})$ represent the analytically expected bias and precision, respectively, of estimated density. The analytically expected errors and the actual ones seems to be corresponded well in $P = 5.0, \ 10.0 \ (\%)$ scenarios. This implies that the analytical approximations discussed at section 3.4 may be reliable in such situations, which are much generalized conditions than that of required for strict satisfaction of eqs (3.21)–(3.24).

[*2]The figure (and most of other similar figures in this dissertation) employs the color scheme developed by Kusakabe et al. (2010), which aims appropriate visualization of traffic data, in both of printing and electrical presentation.

Table 5.2: Precision and bias indices over estimation scenarios.

Scenario parameters			Flow (veh/h)		Density (veh/km)		Speed (km/h)	
P (%)	Δt (min)	Δx (km)	RMSE(q)	Bias(q)	RMSE(q)	Bias(k)	RMSE(q)	Bias(v)
0.1	1	0.1	1102.3	−622.8	112.1	−70.9	18.2	5.1
0.1	60	0.1	849.8	323.6	58.7	12.1	13.9	5.5
0.1	1	3.0	1140.9	−684.9	76.3	−10.3	12.3	−2.6
0.1	60	3.0	522.1	120.3	46.4	12.8	3.9	0.3
5.0	1	0.1	809.5	117.4	33.4	5.2	5.9	−0.3
5.0	60	0.1	202.3	12.8	11.9	1.2	1.2	0.1
5.0	1	3.0	540.7	126.4	38.0	11.8	3.8	−0.2
5.0	60	3.0	147.5	50.1	10.9	2.6	0.6	0.1
10.0	1	0.1	719.2	158.1	23.6	6.2	4.8	−0.1
10.0	60	0.1	121.9	15.4	7.4	1.7	0.8	0.0
10.0	1	3.0	414.9	96.2	26.9	6.8	2.5	0.0
10.0	60	3.0	82.8	−23.0	7.0	−1.5	0.5	0.0

Table 5.3: Analytically expected precision and bias.

Scenario parameters			Precision (veh/km)		Bias (veh/km)	
P (%)	Δt (min)	Δx (km)	$\widehat{\text{RMSE}}(\hat{k})$	RMSE($\hat{k}$)	$\widehat{\text{Bias}}(\hat{k})$	Bias($\hat{k}$)
0.1	1	0.1	112.1	159.8	585.9	−70.9
0.1	60	0.1	58.7	81.4	88.8	12.1
0.1	1	3.0	76.3	261.9	639.0	−10.3
0.1	60	3.0	46.4	89.8	87.6	12.8
5.0	1	0.1	33.4	26.6	16.0	5.2
5.0	60	0.1	11.9	11.6	1.8	1.2
5.0	1	3.0	38.0	33.6	11.7	11.8
5.0	60	3.0	10.9	12.7	1.8	2.6
10.0	1	0.1	23.6	18.8	8.0	6.2
10.0	60	0.1	7.4	8.2	0.9	1.7
10.0	1	3.0	26.9	23.7	5.8	6.8
10.0	60	3.0	7.0	9.0	0.9	−1.5

(a) Estimated flow

(b) Ground truth flow

(c) Estimated density

(d) Ground truth density

(e) Estimated speed

(f) Ground truth speed
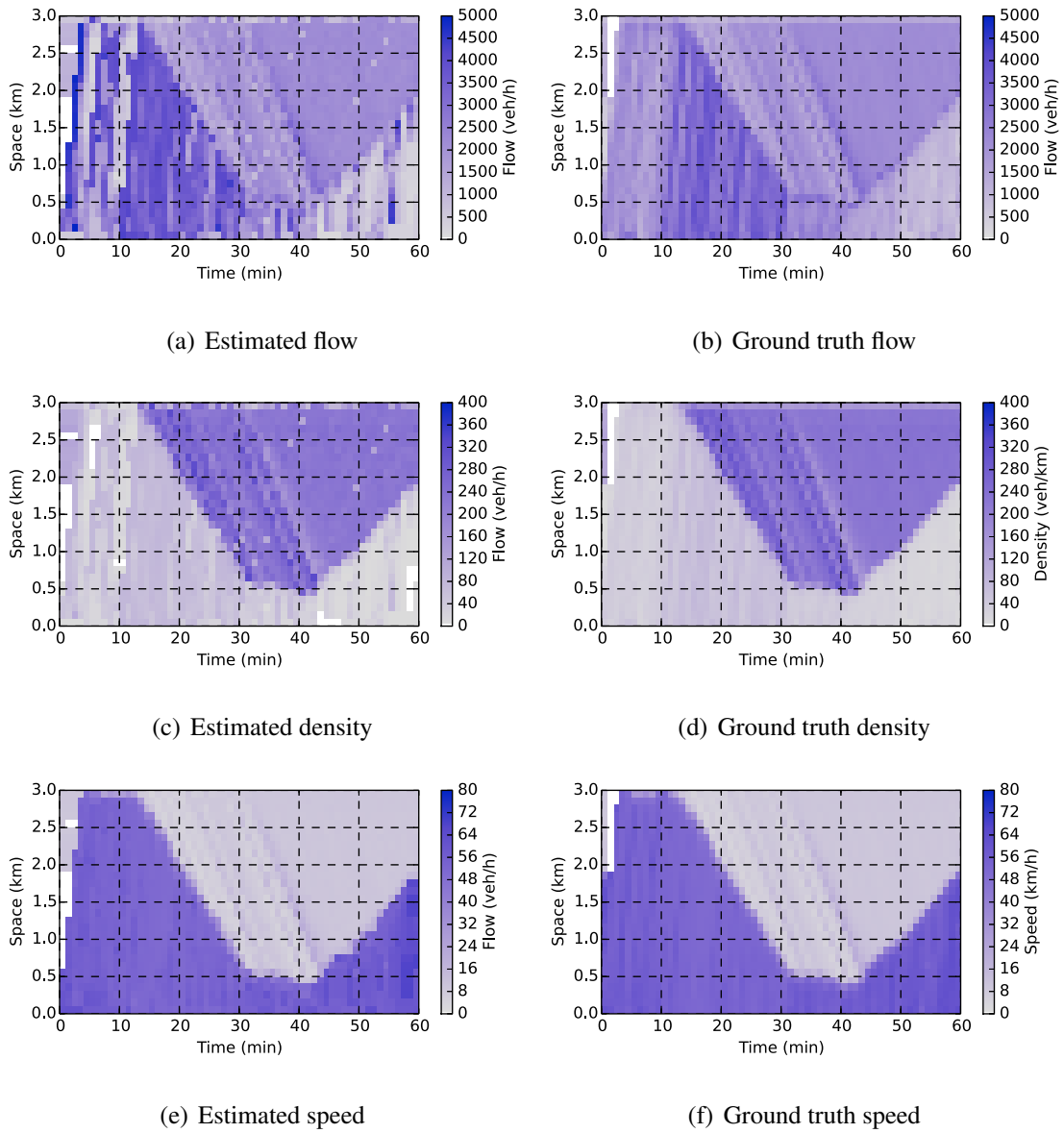
Figure 5.1: Results of the basic method visualized as time–space diagrams.

5.2 The method with CL

This section presents the validation of the proposed TSE method with CL though a simulation experiment.

Table 5.4: Vehicle behavior parameter setting in simulation.

Parameter name	Mean	Deviation
Desired speed (km/h)	80	10.0
Max acceleration (m/s^2)	3	0.2
Normal deceleration (m/s^2)	4	0.25
Max deceleration (m/s^2)	6	0.5
Min spacing (m)	1	0.3
Vehicle length (m)	4	0.5

5.2.1   Simulation scenario

A microscopic traffic flow simulator called AIMSUN (TSS-Transport Simulation Systems), which is based on the car-following model of Gipps (1981) and the lane-changing model of Gipps (1986), was employed for the simulation. The road section in the simulation had a single-lane and length of 5 km with homogeneous geometry except for a bottleneck at the end of the section. Note that this road setting always satisfies the assumptions of the proposed method[*3]. The vehicles in the simulation had heterogeneous driving behaviors, such as the desired speed. Table 5.4 summarizes the parameters. The probe vehicles were randomly sampled from all the vehicles to simulate a given PR. The position and spacing of the probe vehicles with 1 s interval were used for estimating a traffic state.

We generated a traffic situation with a queue by setting the demand from upstream of the section and the capacity at the bottleneck at the end of the section. A ground truth state was available because this was a simulation experiment. Fig 5.2a–d show the ground truth state (flow q, density k, speed v) and cumulative flow $\tilde{N}$ as time–space diagrams. The contour lines of $\tilde{N}$ were drawn at intervals of 100 veh. By applying the proposed method to the generated traffic situation, the characteristics of the proposed method in a various traffic situations (e.g., free-flow, congested flow, flow with backward wave and flow with

---

[*3]Except the first vehicle enters the road; because it does not have its leader. We removed it from candidates for the probe vehicles.

forward wave) can be investigated.

5.2.2 Results

The estimated variables were the traffic state at certain time–space resolutions (i.e., the intervals for the central differences) and the cumulative flow in the section. The cumulative flow was calculated at 1 min time intervals and 100 m space intervals according to eq (4.5). The density $\hat{k}$ was calculated based on the central differences at 100 m intervals according to eq (4.6).

Fig 5.2e–h show the estimated traffic state $(\hat{q}, \hat{k}, \hat{v})$ and cumulative flow $\hat{\tilde{N}}$ as a time–space diagram where the probe vehicle penetration is 3.5%. The contour lines of $\hat{\tilde{N}}$ were drawn at intervals of 100 veh. Through comparison with the ground truth shown in Fig 5.2a–d, the estimation can be used to acquire tendencies of the ground truth, such as the queue propagation and dissolution. More detailed phenomena such as stop-and-go waves were partially captured, but with some errors. This is a deficiency of the method of interpolating the continuous cumulative flow in the proposed methods, namely, liner interpolation over the time.

Fig 5.3 compares the estimated variables and ground truth as scatter diagrams. The estimated variables well corresponded at most of true states although the values were slightly overestimated, as suggested by the analytically expected bias in eq (3.23). In Fig 5.3d, a notable bias can be found around $\tilde{N} \in [800, 1000]$. According to Fig 5.2d, this value of $\tilde{N}$ is located at the area with rapidly diminishing queue, namely, around $t \in [30, 40]$. It implies that, at the area, a probe vehicle may experience much different traffic state from its preceding probe vehicle's experience. Therefore, the headway variance may increases, so that the bias becomes large.

Table 5.5 summarizes the error indices of the traffic state estimation for different combinations of the PR P. The RMSPE and bias were employed as error indices, which are defined as $\mathrm{RMSPE}(\hat{\theta}) = \sqrt{E[((\hat{\theta} - \theta)/\theta)^2]}$ and $\mathrm{Bias}(\hat{\theta}) = E[\hat{\theta} - \theta]$, respectively. The error indices of each scenario were calculated from 100 iterations under different
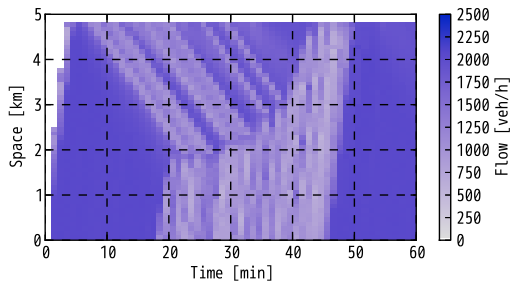
(a) Ground truth flow q.
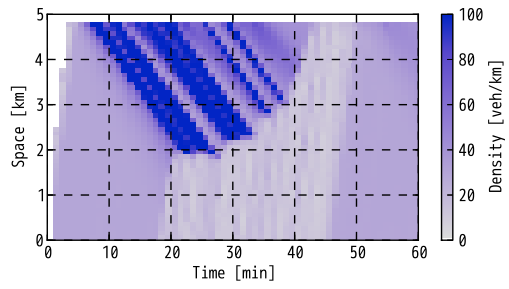
(b) Ground truth density k.
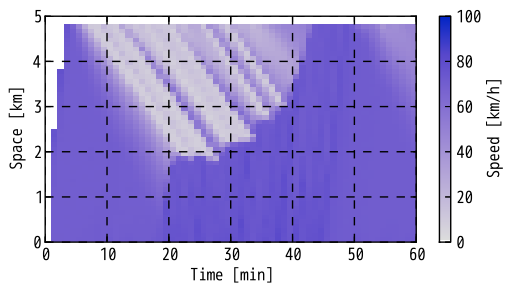
(c) Ground truth speed v.
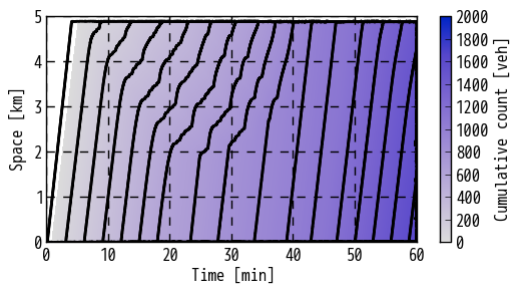
(d) Ground truth cumulative flow $\tilde{N}$.
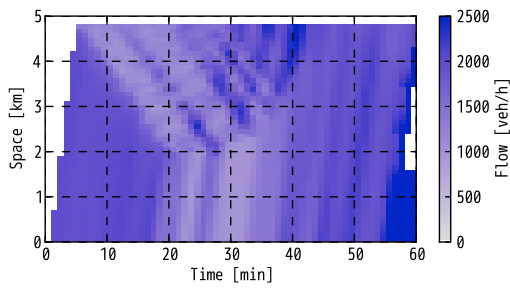
(e) Flow $\hat{q}$ estimated with proposed method.
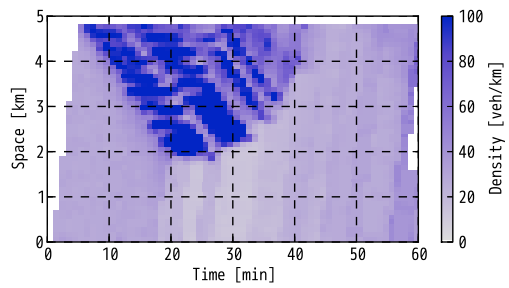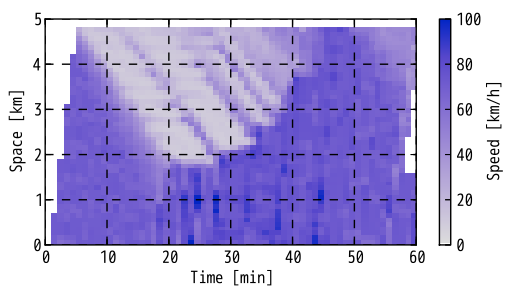
(f) Density $\hat{k}$ estimated with proposed method.

(g) Speed $\hat{v}$ estimated with proposed method.
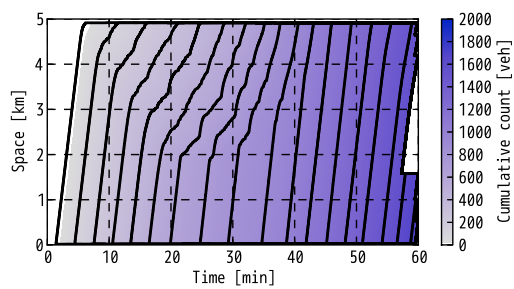
(h) Cumulative flow $\hat{\tilde{N}}$ estimated with proposed method.

Figure 5.2: Time–space diagrams of traffic state and cumulative flow.

(a) Flow q.

(b) Density k.

(c) Speed v.

(d) Cumulative flow $\tilde{N}$.
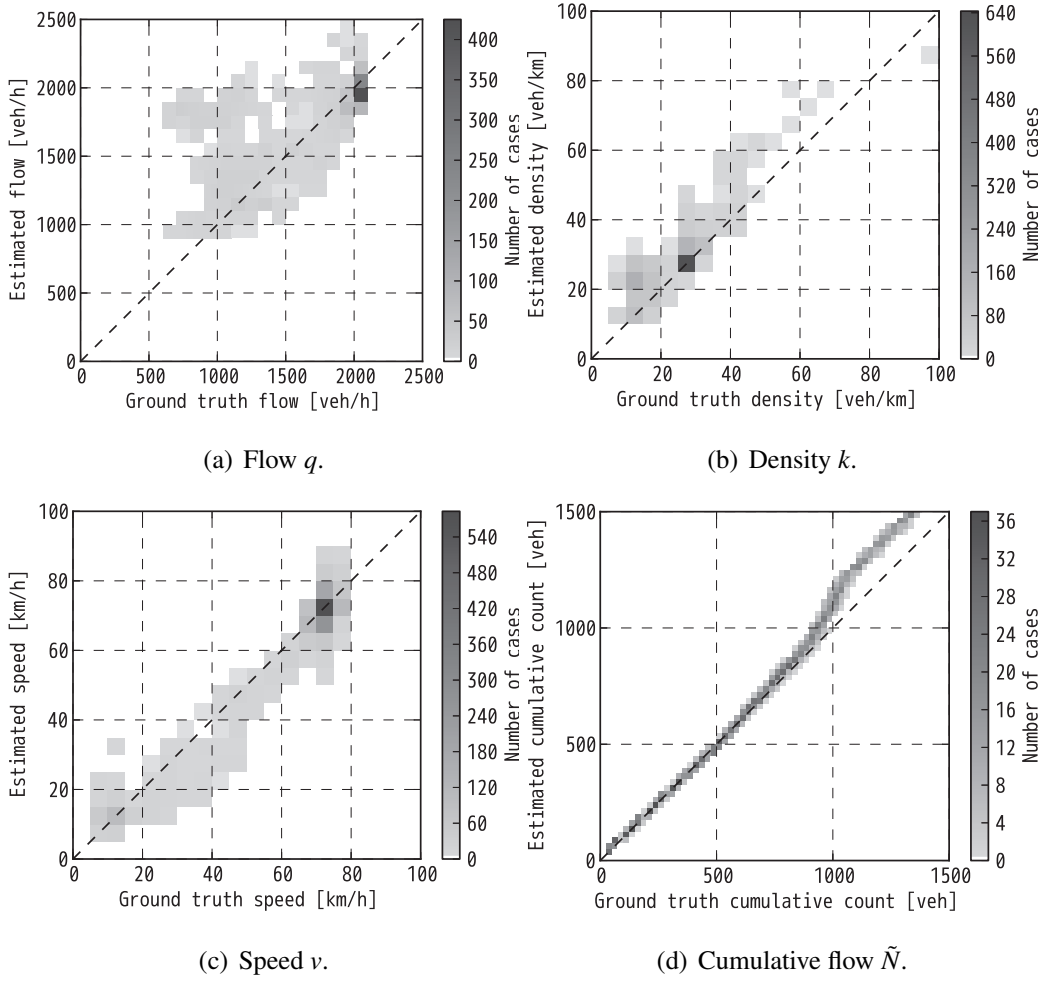
Figure 5.3: Scatter diagrams of estimated variables vs. ground truth variables.

samplings of probe vehicles. The results showed clear improvements in the estimation accuracy and precision as the PR was increased. Almost all of the scenarios overestimated the states similar to Fig 5.3d and for the same reasons.

5.2.3 Effect of incorporating CL

In order to investigate the effect of incorporating the CL, the flow was estimated using the basic method which does not consider the CL but uses the same probe vehicle data. This is defined as $\hat{q}_{\text{withoutCL}}$ in this section. The time and space resolution for calculating $\hat{q}_{\text{withoutCL}}$ were identical to the intervals of the central difference in the proposed method:

Table 5.5: Error indices for scenarios with proposed method.

PR	Flow (veh/h)		Density (veh/km)		Speed (km/h)	
P	RMSPE($\hat{q}$)	Bias($\hat{q}$)	RMSPE($\hat{k}$)	Bias($\hat{k}$)	RMSPE($\hat{v}$)	Bias($\hat{v}$)
0.2%	59%	151.0	107%	−1.6	134%	1.1
1.0%	55%	134.8	87%	2.2	61%	−2.1
3.5%	42%	83.6	52%	2.1	36%	−0.7
5.0%	38%	69.6	48%	2.4	36%	−0.2
10.0%	33%	63.8	45%	2.4	38%	0.7

Table 5.6: Comparison between the method with CL and the basic method.

P	RMSPE($\hat{q}$)	RMSPE($\hat{q}_{\text{withoutCL}}$)	PoI
0.2%	59%	66%	12%
1.0%	55%	63%	7%
3.5%	42%	59%	27%
5.0%	38%	53%	38%
10.0%	33%	52%	43%

1 min and 100 m. Table 5.6 presents the results of the comparison. The percentage of improvement (PoI) is defined as $(\text{RMSPE}(\hat{q}_{\text{withoutCL}}) - \text{RMSPE}(\hat{q}))/\text{RMSPE}(\hat{q})$ and is an index that represents the positive effect of incorporating the CL. According to the results, incorporating the CL clearly improved the estimation precision.

5.3   The method with FD and CL

In this section, numerical characteristics of the proposed TSE method with FD and CL are investigated.

5.3.1   Simulation scenario

Road schematics and vehicle behavior models for this experiment environment are identical to that in section 5.1.1.

The PR P was selected from 5%, 1% and 0.5%. Two types of time–space resolution for observation were selected, namely, $(\Delta T, \Delta X) \in \{(1 \text{ min}, 300 \text{ m}), (10 \text{ min}, 1000 \text{ m})\}$.

The observation error (i.e., precision of the basic method) is expected to be smaller as the observation resolution increased as shown in chapter 3 and section 5.1. In order to simplify the discussion, region **B** is set to be the entire time–space region—the FD parameters are assumed to be constant throughout the simulation.

A timestep width in the system model, Δt, was set to 0.111 min. The other variables on the resolution of the system model, namely, α, β, and γ, were set to certain values such that the cell length l_i is identical to 100 m; their exact values vary in estimation iterations depending on observed free-flow speed u and given observation resolution ΔT and ΔX. With these setting, the value of α is almost always slightly larger than 1; therefore, the CFL condition is expected to be satisfied. Above mentioned parameters are set to satisfy the conditions mentioned in section 4.3.3, eq (4.23).

The size of the noise terms were set ad hoc as follows: $\sigma_k = 0.1$, $\sigma_u = 0.5$ (m/s), $\sigma_{k^c} = 0.002$ (veh/m), $\sigma_\kappa = 0.01$ (veh/m), $\xi_k = 0.01$ (veh/m), $\xi_u = 5.0$ (m/s), $\xi_{k^c} = 0.1$ (veh/m) and $\xi_\kappa = 0.2$ (veh/m). The reason for such larger size of the observation noises was that general traffic does not always follow the triangular FD, especially at a microscopic scale. Criteria for stationary headway–spacing determination is set as less than 10% change rate during 5 s (= $\Delta\tau$). In general, if this criteria is strict, precision of FD observation will be increased. However, if the criteria is too strict compared with the total amount of data, amount of data that passes the criteria becomes few so that the precision can be low. The number of ensembles N was set to 200. In general, larger N value makes accuracy of EnKF's Monte Carlo simulation better at the cost of computation.

5.3.2   Results

Fig 5.4 shows traffic density as time–space diagrams, whose horizontal axes represent time, vertical axes represent space, and color represents density[*4]. In Fig 5.4, a represents the ground truth value k, b represents observed value $\hat{k}$ with $(P, \Delta T, \Delta X) = (5\%, 1 \text{ min}, 300 \text{ m})$, and c represents estimated value k^* with the identical resolution. According to Fig 5.4, the noises in the observation were reduced in the filtering result,
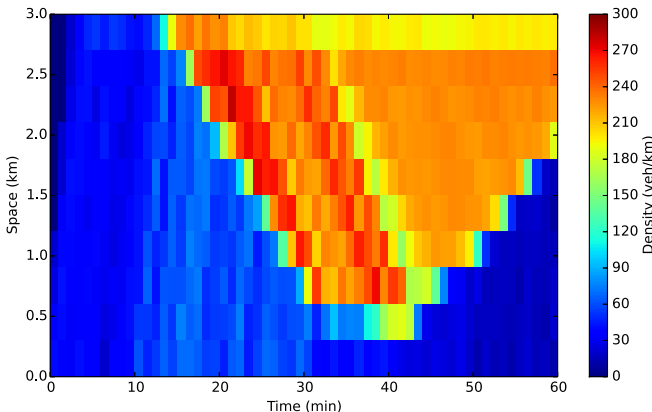
(a) ground truth traffic state k
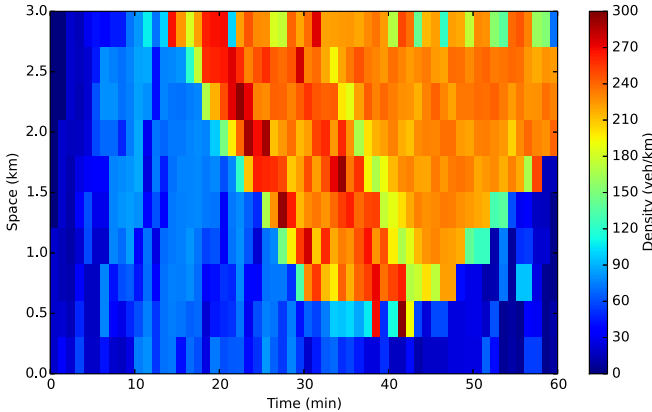
(b) observed traffic state $\hat{k}$
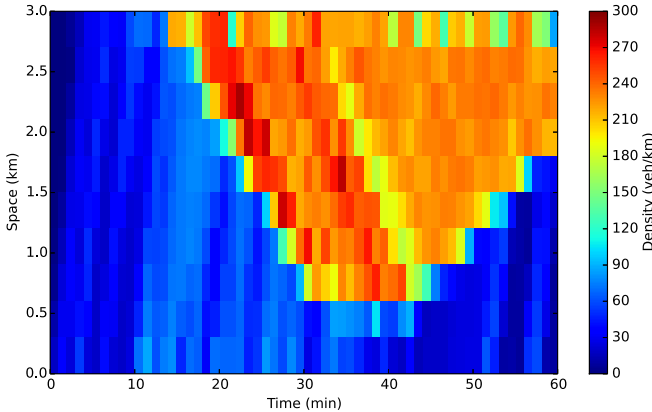
(c) estimated traffic state k^*

Figure 5.4: Typical estimation results visualized as time–space diagrams.
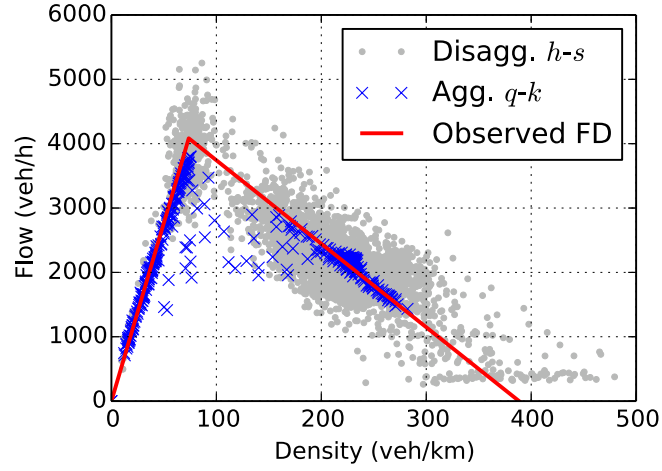
Figure 5.5: Observed FD, disaggregated headway–spacing relation and aggregated flow–density relation.

especially at free-flow areas, such as traffic before 10 min. On the other hand, difference between observed and estimated states in a congested area was not so remarkable—both were close to the ground truth states.

Fig 5.5 shows observed FD by probe vehicles (red line), disaggregated headway–spacing relation of vehicles (gray dots) and aggregated flow–density relation in time–space regions (blue crosses), with $(P, \Delta T, \Delta X) = (5\%, 1\,\text{min}, 300\,\text{m})$. The observed FD's parameter values were $\hat{u} = 55.4$ (km/h), $\hat{k}^c = 73.7$ (veh/km) and $\hat{\kappa} = 388.5$ (veh/km). The disaggregated relation is widely scattered due to the high fluctuation and heterogeneity in microscopic vehicle behaviors. On the other hand, observed FD is closed to the aggregated relation which is clearly bivariate.

Table 5.7 summarizes the estimation performance. The root mean square error (RMSE) and mean absolute percentage error (MAPE) were employed as precision indices on estimated density. Their definitions were as follows: $\text{RMSE}(k^*) = \sqrt{1/S \sum_{\forall (T,X)} \left(k(\mathbf{A}_{T,X}) - k^*(\mathbf{A}_{T,X})\right)^2}$, $\text{MAPE}(k^*) = 1/S \sum_{\forall (T,X)} |k(\mathbf{A}_{T,X}) - k^*(\mathbf{A}_{T,X})|/k(\mathbf{A}_{T,X})$, where S is total size of the results (i.e., combination of (T, X)). The simulation were performed for 50 times in order to get the average performance. In addition, the

---

[*4]In order to emphasize the difference between results, color scheme for this figure is different to the other figures.

Table 5.7: Summary on the estimation performance

Scenario parameters			Precision indices		Percentage of improvement	
P	ΔT (min)	ΔX (m)	RMSE (veh/km)	MAPE	PoI(RMSE)	PoI(MAPE)
0.5%	1	300	65.0	68.5%	8.4%	16.2%
0.5%	5	500	45.6	34.6%	8.3%	19.0%
0.5%	10	1000	31.0	12.7%	−4.3%	13.5%
1.0%	1	300	49.7	58.7%	12.6%	19.0%
1.0%	5	500	32.3	22.9%	6.5%	24.4%
1.0%	10	1000	11.6	7.5%	15.1%	21.2%
5.0%	1	300	20.3	23.0%	20.0%	29.6%
5.0%	5	500	13.6	9.4%	−6.8%	16.7%
5.0%	10	1000	7.4	3.8%	5.8%	15.3%

percentage of improvement (PoI) was employed for evaluate the effect of the data assimilation. It was defined as $\text{PoI}(p) = (p(\hat{k}) - p(k^*))/p(\hat{k})$, where p is a precision index, namely RMSE or MAPE. The value of PoI represents improvement of estimated density k^* compared to observed density $\hat{k}$; if the value is positive, the data assimilation worked positively for precision. According to Table 5.7, distinguishable trends can be found for precision. The precision is increased as probe vehicle penetration rate increases and time–space resolution lowers. In addition, according to PoI value, the data assimilation almost always reduced estimation error, especially on MAPE.

5.3.3   Effect of incorporating FD and CL

The results showed that the estimation precision improved due to the data assimilation in the most cases. According to Fig 5.5, FD parameters were precisely observed by PVSMEs; therefore, the prediction steps by the traffic flow model are expected to work well. Then, according to Fig 5.4 and Table 5.7, improvements of the estimation precision due to the filtering steps were confirmed. Especially, they were remarkable at low density regime; for example, free-flow area shown in Fig 5.4 and PoI(MAPE) in Table 5.7. This is a preferable feature for a TSE method with the PVSMEs; because the precision of

the basic method was relatively low at low density traffic. Contrary, the precision in high density (congested) regime was not improved significantly. This may be due to that the vehicular fluctuation are low in congested regime, since vehicle movements are restricted by the jam. These implied that estimation errors caused by high fluctuations in microscopic vehicular traffic were reduced as intended.

Chapter 6 Field Experiment-based Validation

This chapter[*1] describes an empirical analysis of the proposed methods based on actual traffic data collected via a field experiment. The advantage of a field experiment-based validation is singular: it can be realistic. This is the most preferable feature for the proposed TSE methods; because not all factors in the microscopic vehicle behavior, which determines spacing of vehicle in traffic, can be represented by existing traffic flow models, as described in chapter 2. In addition, traffic condition, namely, demand and supply of the route, is also realistic.

Section 6.1 describes the details of a field experiment we conducted at an urban expressway in Tokyo. Sections 6.2 and 6.3 describes the validation of the basic method of chapter 3 and the method with CL of section 4.2, respectively, based on the data collected via the experiment. Note that the method with FD and CL of section 4.3 is not validated here because of technical limitations of the field experiment—the resolution of the data was not sufficient for it.

6.1   Field experiment

The field experiment was conducted on Tuesday, September 24, 2013, from 15:00 to 16:00. The location was the counterclockwise direction in the Inner Circular Route of the Metropolitan Expressway, which is an urban expressway in Tokyo, Japan. The weather was cloudy with occasional light rain. Twenty probe vehicles equipped with spacing and position measurement devices were employed.

[*1]This chapter is mainly based on joint research with Dr. Takahiko Kusakabe and Prof. Yasuo Asakura, published in *the 34th JSTE Conference* (瀬尾ら, 2014), *ISTTT21* (Seo and Kusakabe, 2015, in press) and *Transportation Research Part C* (Seo et al., 2015a; Seo and Kusakabe, 2015, in press).

6.1.1   Inner Circular Route

The Inner Circular Route (i.e., C1) is a ring-shaped urban expressway located in central Tokyo. In the experiment, the probe vehicles ran in the counterclockwise direction. The loop length is 14.2 km, and most sections have two lanes for cruising and passing. The speed limit is 50 km/h. Figures 6.1 and 6.2 show a map and a schematic of C1, respectively. The space coordinates denoted in Fig 6.2 are used throughout this chapter. In Fig 6.2, a junction is abbreviated as JCT, arrows on the upper side represent the merging from or diverging to other highway routes, and arrows on the lower side represent on/off ramps. Note that the survey section was limited to an 11 km length section from the 0 km point to the 11 km point, because a series of tunnels at the 11–14.2 km disturbed the GPS functions.

A large number of dual supersonic traffic detectors are installed in C1. They enable us to obtain highly detailed and accurate data on the traffic flow variables[*2]. The traffic detectors observed the flow, spot speed, and spot occupancy directly, and these were converted to density and speed for validation of the proposed method. The observation with the traffic detectors is performed at a time resolution of 1 min and average space resolution of 250 meters per lane. In this experiment, these detector observed data are used for comparison purposes. Fig 6.3 shows the density observed by the detectors in the cruising lane as a time–space diagram; where the horizontal axis indicates the time and future is to the right, the vertical axis indicate space and downstream is in the upward direction. Some remarkable events were occurred during the experiment. For example, Edobashi JCT at the 8 km point become a merging bottleneck and caused a 3 km queue was formed at 15:50. Queue spillovers from other highway routes were observed via Takebashi JCT at the 10 km point and Hamazakibashi JCT at the 3.8 km point.

[*2]白石ら (2012) reported that measurement error in 5 min flow of a dual supersonic traffic detector was usually less than 10%.
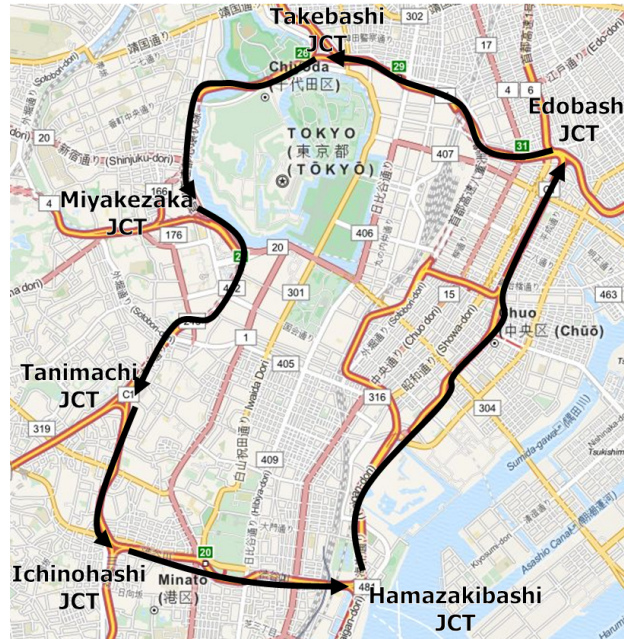
Figure 6.1: Map of the Inner Circular Route.
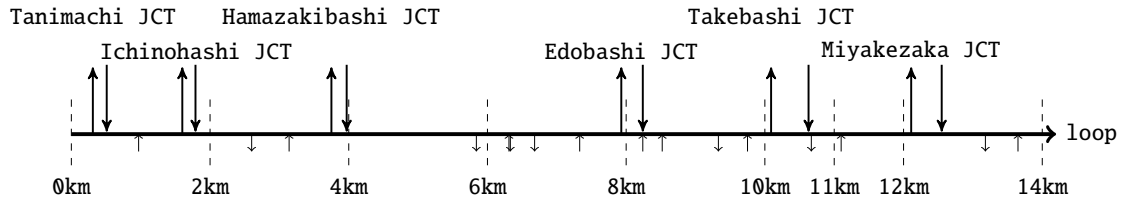
Figure 6.2: Schematic of the Inner Circular Route (counterclockwise direction).
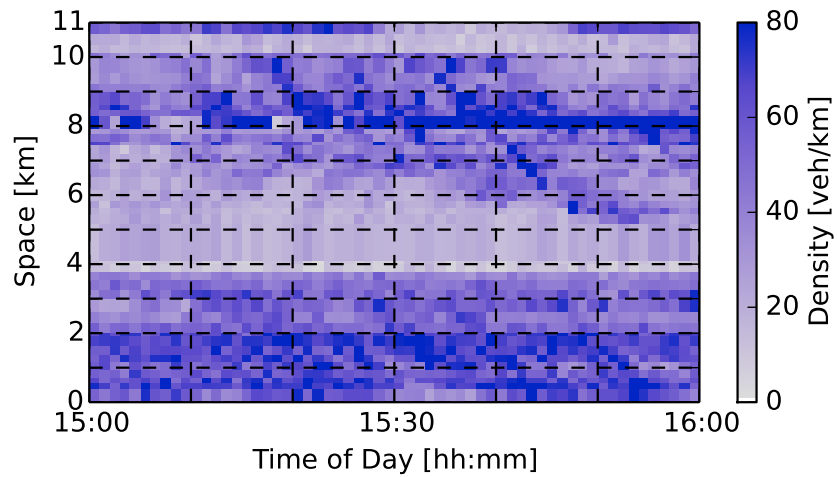
Figure 6.3: Time–space diagram of density in C1 as observed by the detectors.

Figure 6.4: Preparation of probe vehicles and equipments.

6.1.2 Probe vehicle data

Twenty standard-sized passenger vehicles with non-professional drivers were employed as the probe vehicles. The vehicles were equipped with mono-eye cameras and GPS loggers on their dashboards to identify and record the spacing and position. The survey section was limited to the cruising lane of the 0–11 km section because of law restrictions[*3] and the GPS function. Most of the probe vehicles drove three laps on C1, and a total of 59 laps were performed during the experiment period. This corresponded to 42.1 veh/h/lane. The flow of all vehicles in the survey section of C1 was 1255.2 veh/h/lane according to the detector data. Therefore, the PR was roughly calculated to 3.5%. Probe vehicle data, including positions and spacing, were collected at intervals of 15 s. Thus, an average number of 38.8 data points was recorded per lap. Fig 6.4 shows preparation of probe vehicles and data collection equipments.

(1) Position data

Vehicle positions were identified by the GPS data and simple map-matching procedure. The procedure is described as follows:

1. a digital map consists of the experiment site of links and nodes was acquired from an external source,

---

[*3]According to Japan's Road Traffic Act, vehicles should drive in the cruising lane unless changing routes, overtaking within the speed limit, or avoiding danger.
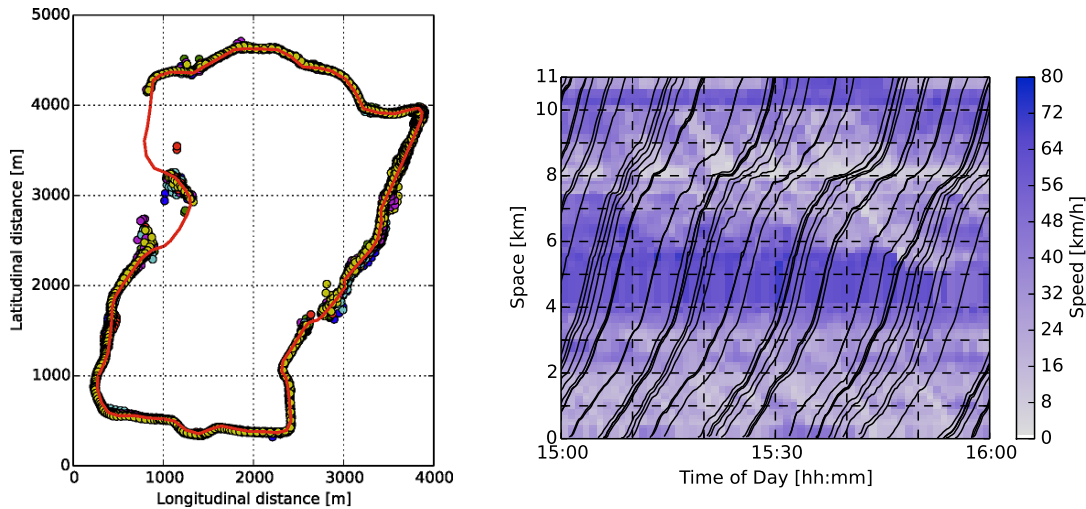
(a) Raw data of trajectories plotted on a (b) Map-matched trajectories on time–space diagram of speed
map

Figure 6.5: Trajectories of probe vehicles.

2. vehicle coordinates identified by GPS were matched to their closest point on the links,

3. data points located at 11–14.2 km section where the series of tunnels exist were removed.

Fig 6.5 shows the trajectories of the probe vehicles. Fig 6.5a shows the raw data plotted on a map of C1 where the red solid line indicates the shape of C1 and small circles indicate the vehicle coordinates. According to the figure, the measurement errors were not significant excluding tunnels. Fig 6.5b shows the map-matched data on the time–space diagram with speed; the trajectories seemed to be reasonable. For example, the probe vehicles tended to be slow (i.e., the slopes of trajectories decreased) when they went through the bottleneck at the 8 km point just like other vehicles (i.e., the plot color was dark). Although small errors were found in the GPS measurement and map-matching, the proposed traffic state estimation method is not significantly affected by such small errors as mentioned in section 3.6.

(2)   Spacing data

This experiment employs a spacing measurement method using a mono-eye camera equipped on the dashboard of the probe vehicles. Fig 6.6 shows some images taken by the cameras on the probe vehicles during the experiment; typical road environments and vehicle characteristics at the C1 are shown. The procedure of the spacing measurement method is described as follows:

1. the leading vehicles of the probe vehicles in the image were identified,

2. the apparent size of the leading vehicles' body width were measured,

3. the spacing were calculated based on the apparent size, its assumed actual size, angle of view of camera, etc.

The reason for the simple method is because implementation is relatively easy and they satisfy the requirement for this experiment. That is, the method is

- capable of detecting the leading vehicle at relatively long distance that often appears in highways,

- capable of determining the lane driven by the probe vehicle and the leading vehicle, and

- based on a clear logic (i.e., not a black box).

Note that any methods of measuring spacing are considerable for the proposed traffic state estimation methodology as long as the measurement method satisfies the required capability.

Specifically, the spacing s was estimated from images taken by the probe vehicles based on the following pinhole camera model assuming that the road is not curved.

$$s = \frac{2wp_0}{p\tan(\theta_0/2)} + l, \tag{6.1}$$

where w is the actual body width of the leading vehicle, p_0 is the width of the image, p is the apparent size of the body width of the leading vehicle in the image, θ_0 is the horizontal angle of view of the camera, and l is the actual body length of the leading vehicle. Here,

Figure 6.6: Examples of images taken by the cameras on the probe vehicles.

the variables p_0 and θ_0 were known. The actual body width w was assumed to be 1.92 m. This assumption comes from prior knowledge on the average width of a standard vehicle (1.8 m), large vehicle (2.4 m), and the average ratio of large vehicles on the route (20%). The actual body length l was assumed to be the same as that of the probe vehicles (5 m). Variable p was manually measured from the images. If these variables have errors (i.e., wrong assumptions on w and l, measurement error in p), the estimated spacing may be biased. The errors affect biases almost proportionally: therefore, the biases are not very significant. If the spacing was not measurable (i.e., the leading vehicle was not visible), a value of 100 m was assumed for the value. The most frequently appeared reason of the failure in spacing measurement was too large distance to leading vehicles. Therefore, the large value that is close to the maximum detectable range was substituted for the missing spacing data. Such cases occurred for 1.86% of all the data.

Fig 6.7 shows a part of the probe vehicle data as a time–space diagram. A dot represents a position datum collected by a probe vehicle. Data between two data points are linearly interpolated. Red areas represent areas between probe vehicles and their leading vehicles.
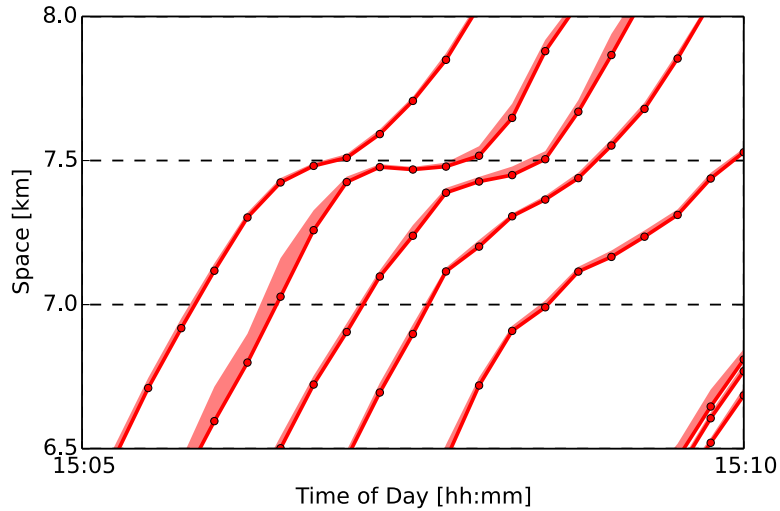
Figure 6.7: Part of the probe vehicle data.

If the assumed or measured variables have errors, the estimated spacing will have errors. We cannot determine the amount of the errors directly; because the ground truth data for the vehicle size during the experiment do not exist. However, the method may not be biased significantly and practicable for the experimental measurement because the assumed variables were based on common knowledge on statistics and regulations and detector data. In addition to that, the measurement was based on high resolution images.

(3)   Basic validation

In order to validate the probe vehicle data, we compared the data with the spacing and spot speed of all of the vehicles at four specific locations as calculated by the detectors' pulse data[*4]. Figures 6.8 and 6.9 show the speed and spacing distributions. Their statistics (mean μ, standard deviation σ, and Kolmogorov–Smirnov (K–S) test value $\sqrt{n}D_n$) are summarized in Table 6.1. If the K–S test value is larger than 1.36, the difference between probe vehicle data and detector data is statistically significant at the 5% level. According to these comparisons, there considered to be differences between the two data at some

---

[*4]The detectors' pulse data include every individual vehicle's spot speed, body length, and time headway at the detector location.

(a) At 0.390 km point. (b) At 2.980 km point. (c) At 7.140 km point. (d) At 8.640 km point.
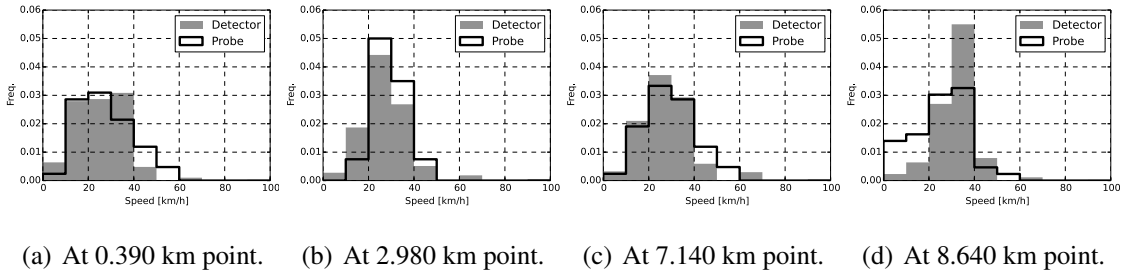
Figure 6.8: Spot speed distributions in probe vehicle data and detector data.

(a) At 0.390 km point. (b) At 2.980 km point. (c) At 7.140 km point. (d) At 8.640 km point.
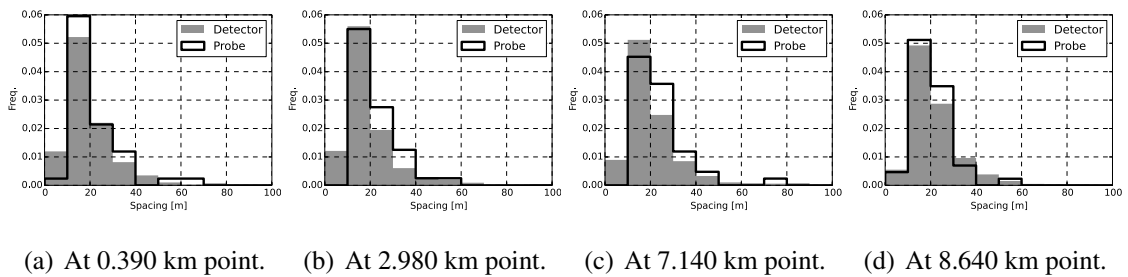
Figure 6.9: Spacing distributions in probe vehicle data and detector data.

locations. The probe vehicles had slightly faster speed and larger spacing at the three points (0.390 km, 2.980 km and 7.140 km points), and the reverse occurred at the 8.640 km point. The probe vehicles' routes were assigned to maintain cruising lane, therefore, their driving behavior may have slightly differed from that of other vehicles of which paths were going to diverge or had just merged. For example, the 8.640 km point was located downstream of the merging at Edobashi JCT (c.f., Fig 6.2). At this location, vehicles from C1 are often required to slow down to merge because of its road alignment. Therefore, the probe vehicles may have tended to be slower than other vehicles. Because of these reasons, the probe vehicle data may contain location-specific biases. This means that the random sampling assumption was not rigorously satisfied in the experiment.

6.2 The basic method

We quantitatively analyzed the traffic state estimation results of the basic method presented in chapter 3. Section 6.2.1 visualize examples of estimation results as

Table 6.1: Spot speed and spacing statistics of probe vehicle data and detector data.

		0.390 km point	2.980 km point	7.140 km point	8.640 km point
	Detector data (μ, σ) [km/h]	(24.2, 10.7)	(25.8, 10.5)	(26.3, 11.4)	(29.7, 9.3)
Speed	Probe vehicle data (μ, σ) [km/h]	(27.7, 11.8)	(28.4, 6.8)	(29.5, 10.2)	(26.2, 11.0)
	K–S test value $\sqrt{n}D_n$	0.684	1.248	0.763	1.568
	Detector data (μ, σ) [m]	(19.4, 11.2)	(19.2, 11.7)	(20.7, 12.3)	(21.5, 11.8)
Spacing	Probe vehicle data (μ, σ) [m]	(21.8, 11.5)	(22.4, 9.9)	(24.5, 11.4)	(19.7, 8.5)
	K–S test value $\sqrt{n}D_n$	1.008	1.784	1.503	0.518

time–space diagrams in order to investigate how well the traffic phenomena can be reproduced by the proposed method. Section 6.2.2 summarizes indices for accuracy and precision of the proposed method for various settings of the PR and the resolution. Section 6.2.3 describes relation between accuracy and precision of the proposed method and the traffic state.

6.2.1   Visualizations of estimation results

Fig 6.10 visualizes traffic states estimated by the proposed method (left side: a, c, e), as well as ones observed by the detectors (right side: b, d, f). The time and space resolution of the estimation were set to 5 min and 500 m, respectively, that is close to average distance between detectors and detector's data aggregation time interval in urban expressways in Japan. The PR was 3.5%. At this resolution and PR, the expected number of probe vehicles per region was 3.83; therefore, bias in the estimator is expected to be small (c.f., section 3.3). Traffic phenomena that were observed in the traffic detector data could be recognized in this estimation result. For example, Fig 6.10c shows a significant queue whose head was at the 8 km point and that propagated to a length of around 3 km at 15:50. There were other congested areas whose heads were at around the 3.5 km and 10 km points. These characteristics were almost identical to those described in chapter 3 and Fig 6.10d by the detector data.

The resolution of the estimation can be set flexibly corresponding to the objective of the analysis and PR (c.f., section 3.6). Lower PR scenarios were generated from

(a) Flow estimated by the proposed method.

(b) Flow observed by the detectors.

(c) Density estimated by the proposed method.

(d) Density observed by the detectors.

(e) Speed estimated by the proposed method.

(f) Speed observed by the detectors.
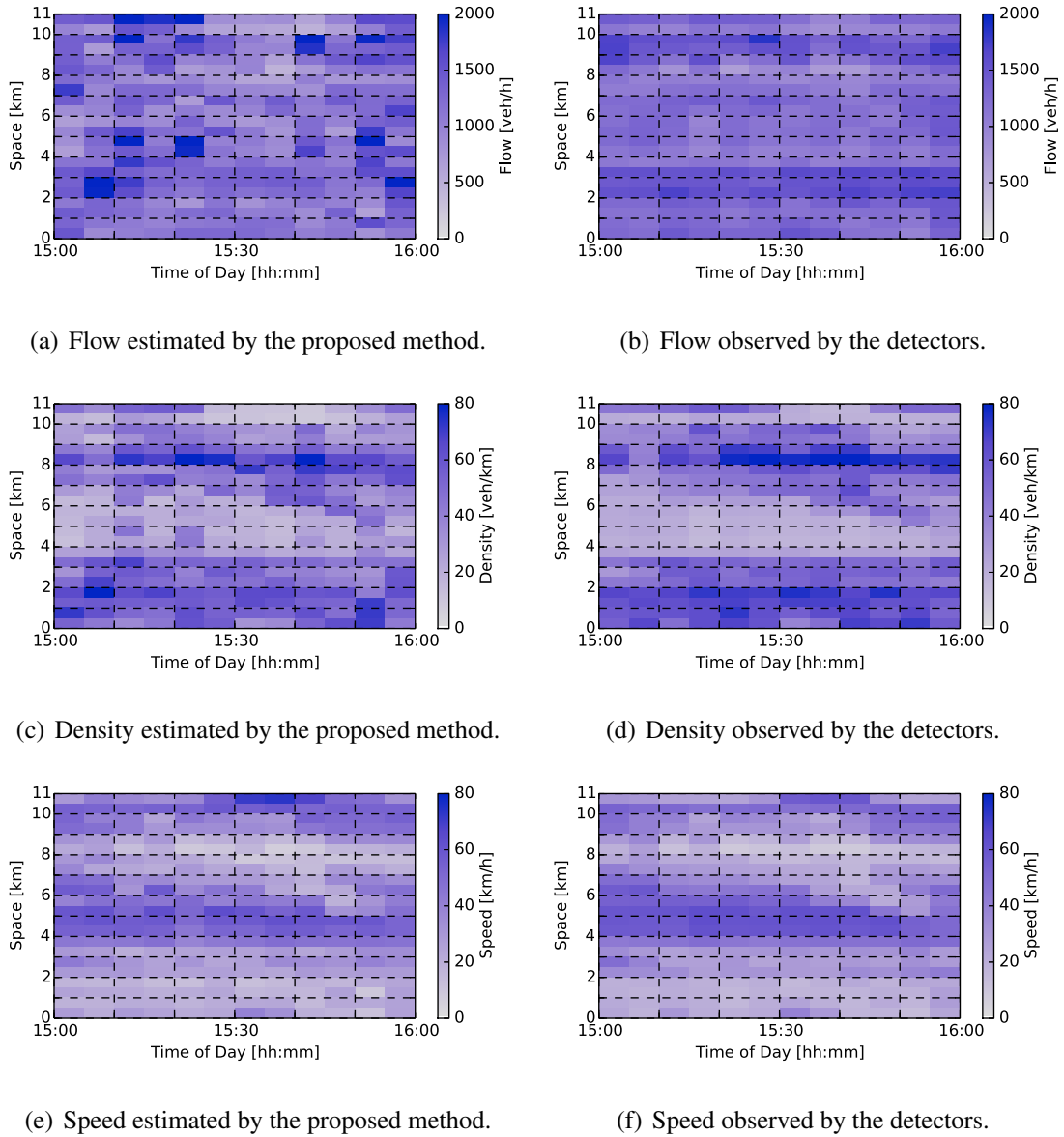
Figure 6.10: Visualization of estimated flow, density, and speed.

random sampling of the probe vehicles. Fig 6.11a shows the density estimation result at a resolution of 30 min and 4 km with a 1% PR; Fig 6.11b shows the density observed by the detectors aggregated with the corresponding resolution. The estimation results showed the tendencies of the traffic flow at lower resolutions. For example, the 0–4 km section had a relatively dense traffic flow, while the 4–8 km section tended to have sparse traffic at 15:00–15:30 and dense traffic at 15:30–16:00.

(a) Density estimated by the proposed method

(b) Density observed by the detectors
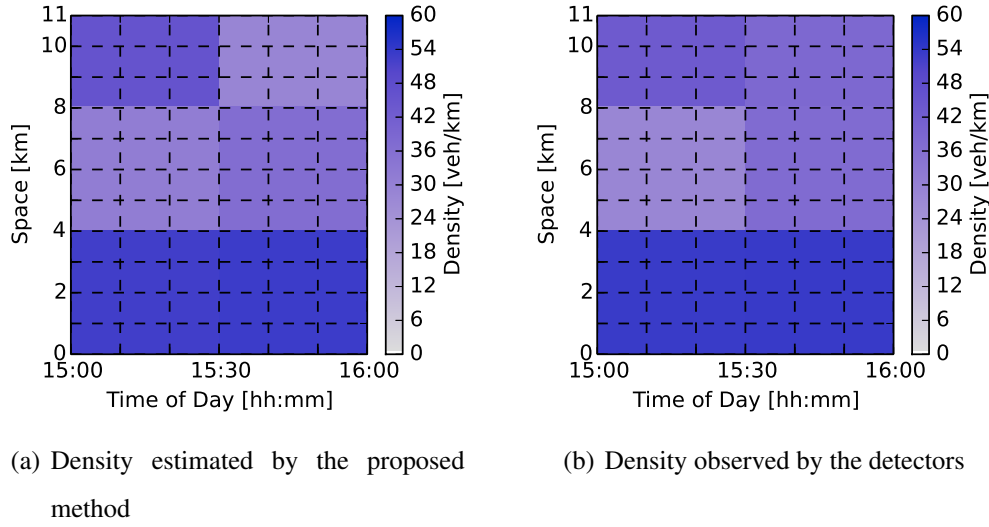
Figure 6.11: Visualization of estimated density with lower PR and lower resolution.

6.2.2   Effect of time–space resolution and PR

To quantify the relations among accuracy and precision of the estimation, time and space resolution, and PR, we compared accuracy and precision indices for the estimation scenarios. The bias and the root mean square percentage error (RMSPE) are employed as accuracy and precision indices, where $\text{Bias}(\hat{\theta}) = E[\hat{\theta} - \theta]$ and $\text{RMSPE}(\hat{\theta}) = \sqrt{E[((\hat{\theta} - \theta)/\theta)^2]}$. Variable θ denotes a traffic flow variable (one of q, k and v) at a certain time and space observed by the detectors; and variable $\hat{\theta}$ is one of those estimated from the probe vehicle data. In addition to that, analytically expected bias and precision shown in eq (3.21)–(3.24), that is, $\widehat{\text{Bias}}(\hat{\theta})$ and $\widehat{\text{RMSPE}}(\hat{\theta})$, were estimated for every scenario. The estimation was based on eqs (3.21)–(3.24) by estimating expectation of mean and variance spacing and time headway from the probe vehicle data. The parameters set for scenarios were PR P (%), time resolution Δt (min), and space resolution Δx (km). The PR P was 3.5% or 0.2%. In scenarios where $P = 3.5\%$, data from all of the probe vehicles were used for the estimation. In scenarios where $P = 0.2\%$, data from two randomly sampled laps were used on average (i.e., the expected flow of probe vehicles is 2 veh/h). The indices for the lower PR scenarios were calculated from the results of 20 estimation iterations. In each iteration, probe vehicle data for the estimation were

composed of different combinations of probe vehicles' laps whose PR was expected to be the scenario parameter P. The time resolution Δt was 5 min or 60 min, which corresponded to the resolutions used for Japanese highway traffic management and traffic census data, respectively. The space resolution Δx was 0.5 km or 11 km, which roughly corresponded to the usual detector interval and entire survey section length, respectively.

Table 6.2 summarizes the results of above estimation. Note that the mean values of the flow, density, and speed observed by the detectors were 1255.2 veh/h, 40.7 veh/km and 30.8 km/h, respectively.

The biases were affected by three different factors: the analytical characteristics of the estimators (c.f., sections 3.3 and 5.1), biases in the probe vehicles' driving behavior (c.f., sections 3.6 and 6.1.2), and biases in the spacing measurement method (c.f., section 6.1.2). According to Table 6.2, amounts of the analytical expected biases, $\widehat{\text{Bias}}(\hat{\theta})$, were almost negligible compared with the amounts of states for most of scenarios. It is also confirmed by the simulation-based validation shown in section 5.1. However, the actual biases on the flow and density calculated from the detector data were not identical to the analytically expected ones. For example, most of the actual biases were negative while the analytical expected one is positive. This can be explained by the probe vehicles' driving behavior biases as follows. In the (3.5%, 60 min, 11 km) scenario, whose analytically expected bias is small, slightly underestimated the flow, density, and speed. This suggests that the probe vehicles' driving behavior was slightly biased compared with the rest of traffic (section 3.6): the probe vehicles had 10% slower speed than other vehicles on average, and they had almost the same spacing with other vehicles on average. The amount of bias caused by the spacing measurement method can be expected to be small as mentioned in section 6.1.2. As consequence, the results implied that the amount of bias decreases as P, Δt and Δx increased, as the analytical results suggested. However, in the field experiment, the probe vehicles' driving behavior was slightly biased; therefore, the amount of bias is significantly smaller than the analytical result. The results of simulation-based validation shown in section 5.1 support this interpretation.

The tendencies in the precision RMSPE can be found as analytically expected; the

Table 6.2: Precision and bias indices over estimation scenarios.

(a) Flow.

Scenario parameters			Errors against the detector data		Analytically expected errors	
P (%)	Δt (min)	Δx (km)	RMSPE($\hat{q}$) (%)	Bias($\hat{q}$) (veh/h)	$\widehat{\text{RMSPE}}(\hat{q})$ (%)	$\widehat{\text{Bias}}(\hat{q})$ (veh/h)
0.2	5	0.5	43	21.1	67	111.5
0.2	5	11	33	−48.7	25	26.6
0.2	60	0.5	25	−59.9	27	37.3
0.2	60	11	16	−159.0	13	29.6
3.5	5	0.5	26	−82.4	17	42.6
3.5	5	11	14	−151.9	7	5.2
3.5	60	0.5	14	−147.1	6	4.5
3.5	60	11	13	−161.4	3	1.2

(b) Density.

Scenario parameters			Errors against the detector data		Analytically expected errors	
P (%)	Δt (min)	Δx (km)	RMSPE($\hat{k}$) (%)	Bias($\hat{k}$) (veh/km)	$\widehat{\text{RMSPE}}(\hat{k})$ (%)	$\widehat{\text{Bias}}(\hat{k})$ (veh/km)
0.2	5	0.5	49	−0.1	69	4.1
0.2	5	11	45	2.1	27	3.3
0.2	60	0.5	28	−2.9	44	1.3
0.2	60	11	13	−1.1	17	1.1
3.5	5	0.5	28	−2.6	17	1.2
3.5	5	11	15	−0.6	11	0.5
3.5	60	0.5	14	−4.2	7	0.2
3.5	60	11	3	−1.4	4	0.1

(c) Speed.

Scenario parameters			Errors against the detector data	
P (%)	Δt (min)	Δx (km)	RMSPE($\hat{v}$) (%)	Bias($\hat{v}$) (km/h)
0.2	5	0.5	43	0.4
0.2	5	11	31	−0.3
0.2	60	0.5	23	0.7
0.2	60	11	11	−3.1
3.5	5	0.5	18	−0.7
3.5	5	11	13	−3.0
3.5	60	0.5	12	−0.6
3.5	60	11	10	−3.0

precision improves as P, Δt and Δx increased. However, the actual precision was lower than the analytically expected one in most of the scenarios. This is also able to be explained by the probe vehicles' driving behavior biases. Therefore, if biases in the probe vehicle data did not exist (i.e., if the random sampling assumption were satisfied), RMSPE is expected to improve.

6.2.3   Effect of traffic situation

Fig 6.12 compares the estimated variables and the corresponding values observed by the detectors based on the results of the (3.5%, 5 min, 0.5 km) scenario. The colors represent the number of cases. The estimated variables correlated well with the corresponding values observed by the detectors in most cases. However, the relative error for the density tended to be larger when the density was low. This may be due to the variances in the mean headway. The variances tended to be larger at lower densities than at higher densities, and the accuracy and precision may have suffered, as suggested by eqs (3.21)–(3.24) in section 3.3. This means that the estimation accuracy and precision depend on the traffic state, although the amount of error was not significant among traffic states from free-flow to congested state.

Note that the data do not contain situations where the flow was low, such as sparse traffic, extremely congested traffic, and signalized traffic. Therefore, the capabilities of the method in such situations were not validated with this data. According to section 3.3, the accuracy and precision may decrease for sparse traffic and signalized traffic because of the larger variance in the mean headway distribution.

6.3   The method with CL

In order to investigate the applicability of the proposed method to the real world, the proposed method was validated by using data collected from a field experiment at an actual road.

(a) Flow.
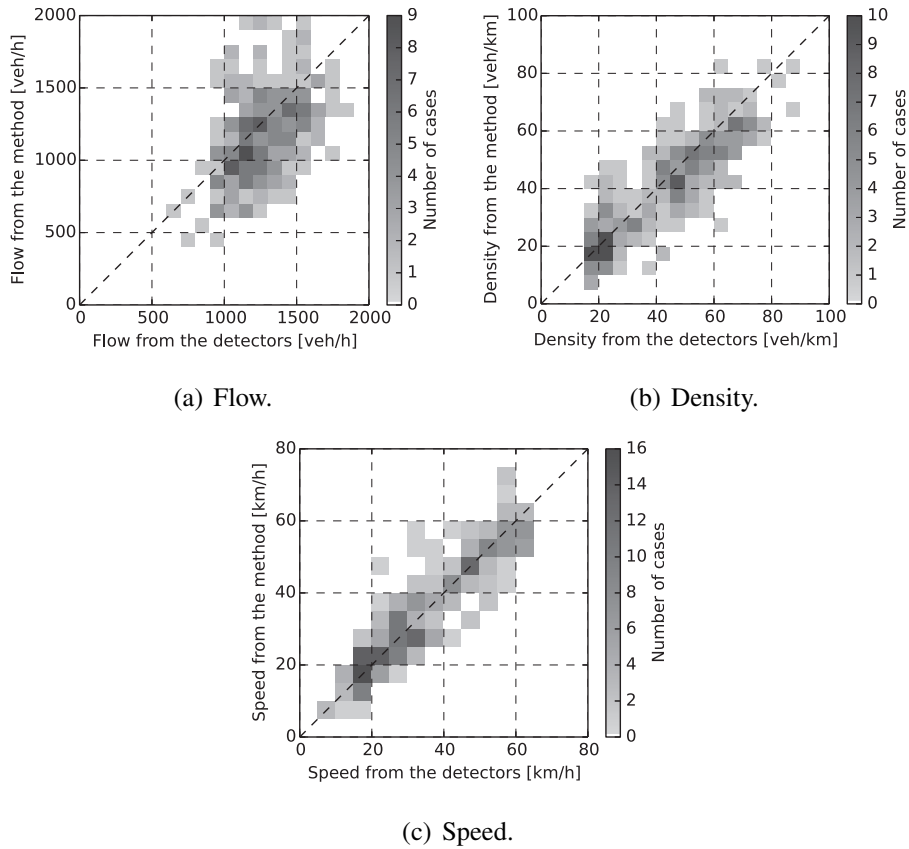
(b) Density.

(c) Speed.

Figure 6.12: Scatter plots of estimated variables versus the corresponding values observed by the detectors.

6.3.1   Ground truth

For a comparison purpose, Fig 6.13a–d show the state (flow q, density k, speed v) observed by the detectors (basically, they means the same state with Fig 6.10b, d, f) and cumulative flow $\tilde{N}$ as time–space diagrams. The contour lines of $\tilde{N}$ were drawn at intervals of 200 veh. The cumulative flow was calculated from the flow observed by detectors with a probe vehicle's trajectory as a reference point. Discontinuities in the contour lines present junctions (merging/diverging sections from/to other highway routes) in C1; these are represented as arrows on the upper side in Fig 6.2. Note that the cumulative flow $\tilde{N}$ did not always increase as t increased and x decreased when there were no discontinuities. This is because of the on/off-ramps, lane-change by vehicles, and systematic errors in the measurements of the detectors.

6.3.2   Results

The estimation targets were the traffic state at certain time and space resolutions and the cumulative flow in the survey section. The cumulative flow was calculated at 1 min time intervals and 100 m space intervals according to eq (4.5). The density $\hat{k}$ was calculated based on central differences at 100 m intervals according to eq (4.6). In order to compare the estimated states with the detector data, the estimated states were averaged at a time resolution of 5 min and space resolution of 500 m. The proposed method requires the positions of the discontinuity points to be specified. In this estimation, only junctions were considered to be discontinuity points. Thus, on/off-ramps and lane-change were ignored.

Fig 6.13e–h show the estimated traffic state $(\hat{q}, \hat{k}, \hat{v})$ with a 5 min × 500 m resolution and cumulative flow $\hat{\tilde{N}}$ as a time–space diagram. The contour lines of $\hat{\tilde{N}}$ were drawn at intervals of 200 veh. Through a comparison with Fig 6.13a–d, the estimation can be used to acquire the tendencies of the detectors' observed variables (e.g., a queue propagation from the 8 km point). Fig 6.14 compares the estimated variables and detectors' observed variables as scatter diagrams. According to the figures, the estimated variables and detectors' observed variables correlated well. However, the values tended to be underestimated. One of the reasons was a bias in the probe vehicles' driving behavior (i.e., their driving behaviors tended to be safer, which meant a slower speed and larger spacing than for other vehicles).

Table 6.3 summarizes the error indices of the traffic state estimation for different PRs. The 0.2% PR was reproduced by randomly sampling all of the probe vehicles. This corresponded to roughly 2 probe veh/h. The error indices of scenarios with a 0.2% PR were calculated from 25 iterations under different sampling conditions of the probe vehicles. According to the results, the estimation precision clearly increased with the PR. Note that most of the scenarios underestimated the states, similar to Fig 6.14 and for the same reasons. Table 6.4 compares results of the proposed method and the method without considering the CL; the precision was improved with the proposed method.
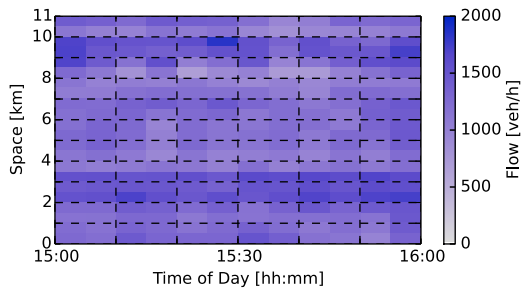
(a) Flow q observed by detectors.
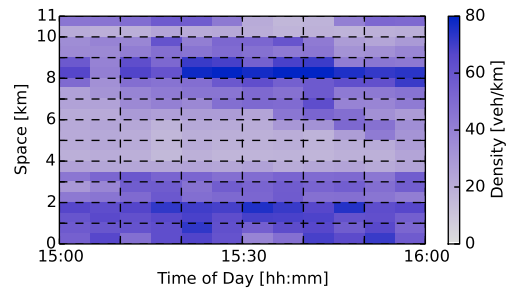
(b) Density k observed by detectors.
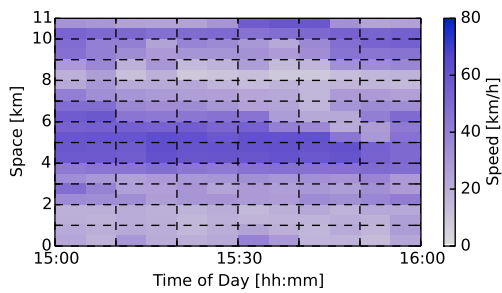
(c) Speed v observed by detectors.
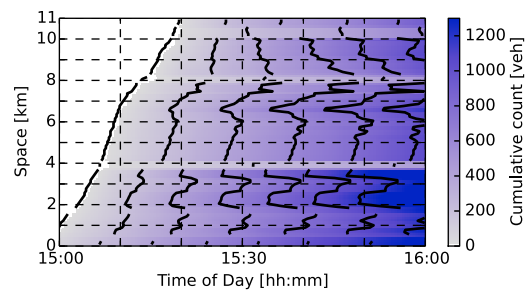
(d) Cumulative flow $\tilde{N}$ observed by the detectors.
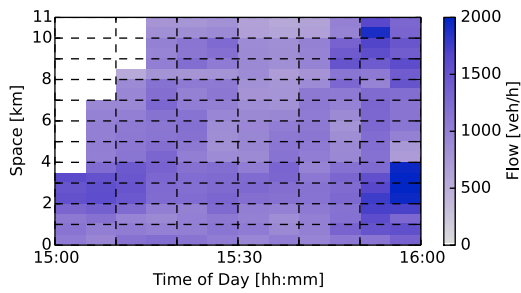
(e) Flow $\hat{q}$ estimated with proposed method.
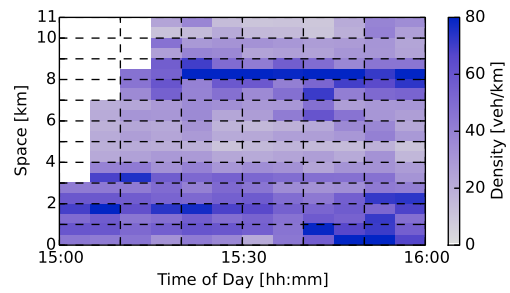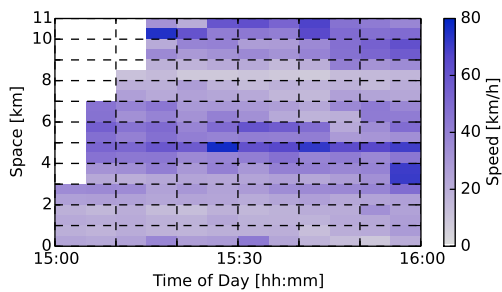
(f) Density $\hat{k}$ estimated with proposed method.

(g) Speed $\hat{v}$ estimated with proposed method.
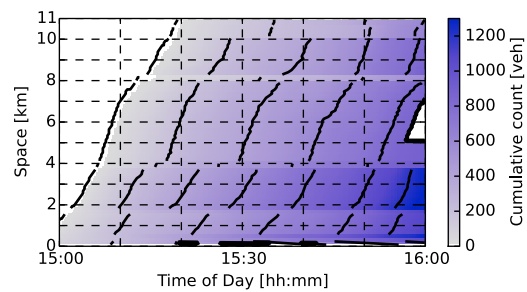
(h) Cumulative flow $\hat{\tilde{N}}$ estimated with proposed method.

Figure 6.13: Time–space diagrams of traffic state and cumulative flow in field experiment.

(a) Flow q.

(b) Density k.

(c) Speed v.

(d) Cumulative flow $\tilde{N}$.
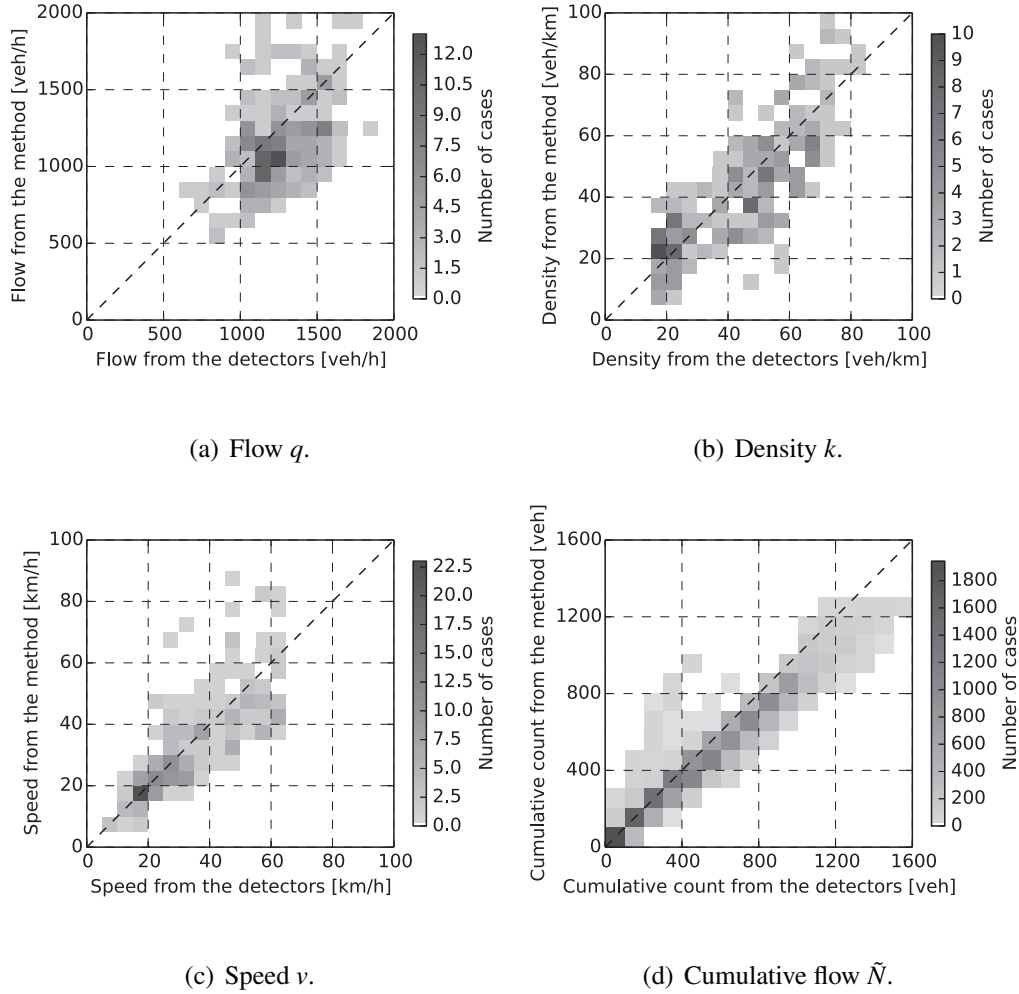
Figure 6.14: Scatter diagrams of estimated variables vs. detectors' observed variables in field experiment.

Table 6.3: Error indices for scenarios with proposed method in field experiment.

PR	Flow (veh/h)		Density (veh/km)		Speed (km/h)	
P	RMSPE($\hat{q}$)	Bias($\hat{q}$)	RMSPE($\hat{k}$)	Bias($\hat{k}$)	RMSPE($\hat{v}$)	Bias($\hat{v}$)
0.2%	30%	−158.9	39%	−4.9	60%	0.9
3.5%	23%	−133.9	30%	−2.3	24%	−2.1

Table 6.4: Comparison between results of field experiment with the method with CL and the basic method.

P	RMSPE($\hat{q}$)	RMSPE($\hat{q}_{\text{withoutCL}}$)	PoI
0.2%	30%	43%	30%
3.5%	23%	26%	13%

Table 6.5: Difference between validations based on simulation experiment and field experiment.

	The simulation experiment	The field experiment
FIFO condition	Always satisfied	Not always satisfied
CL	Always satisfied	Not always satisfied
Traffic flow model	Car-following model of Gipps (1981)	Actual traffic
Traffic condition	Synthetic scenario	Actual traffic
Driving behavior of probe vehicles	Not biased	Slightly biased
Ground truth	Available	Detectors
RMSPE($\hat{q}$) at P=0.2%	59%	30%
RMSPE($\hat{q}$) at P=3.5%	42%	23%
Bias($\hat{q}$) at P=0.2%	151.0 veh/h	-158.9 veh/h
Bias($\hat{q}$) at P=3.5%	83.6 veh/h	-133.9 veh/h
PoI due to incorporating CL at P=0.2%	12%	30%
PoI due to incorporating CL at P=3.5%	27%	13%

6.3.3 Comparison between simulation experiment- and field experiment-based validations

Table 6.5 summarizes the difference between the simulation experiment (section 5.2) and this field experiment. The simulation experiment was conducted under traffic conditions where the assumptions of the proposed method were always satisfied. On the other hand, the field experiment-based validation had some limitations, such as slight violations of the assumption. However, it allowed the proposed method's characteristics to be validated under actual traffic conditions. This advantage is important for validating the proposed method's practical characteristics because of the proposed method's strong dependence on the spacing, which was determined by a synthetic model (i.e., car-following model) in the simulation experiment.

The validation results suggest that the proposed method works well in an actual traffic environment, although the assumptions of the proposed method (i.e., the CL) were not exactly satisfied because of the on/off-ramps and lane-changing. For example, the precision increased with the PR in both the simulation (Table 5.5) and field experiment (Table 6.3). In fact, the proposed method showed better precision in the field experiment than in the simulation experiment. Ironically, one of the reasons is existence of lane-changing. They decrease the variance in the mean headway; then the estimation precision of the cumulative flow improved (c.f., eq (3.23)).

The notable difference between the two validation is a sign of the biases. The simulation-based validation (Table 5.5) and analytical approximation eq (3.21) showed positive biases, while the field experiment-based validation showed negative biases. This may be due to biases in the probe vehicles' driving behaviors. The probe vehicles tended to be slower than other vehicles, according comparison between the probe vehicle's speed and traffic speed observed by detectors.

Incorporating the CL improved the precision in both validations (Tables 5.6 and 6.4). However, in the field experiment scenario, the PoI decreased as the PR was increased; this tendency was the inverse of that in the simulation-based validation. This may be due to violations of the assumptions. If a large amount of probe vehicle data is available (i.e., the traffic state can be estimated precisely even without the CL being incorporated) the non-exact assumptions of the CL will negatively affect the precision.

Chapter 7 Conclusions

Traffic data are crucial for today's civilization as they are required for understanding behavior of traffic, developing traffic control measures, and executing the measures. However, current situation of traffic data collection is far from perfect, due to practical and theoretical limitations. Current Eulerian data collection method, namely, detectors, only work at its installed point, while the number of installed points are limited. Current Lagrangian data collection method, namely, GPS-equipped probe vehicles, cannot collect quantity-related information. To address this issue, this dissertation proposed traffic state estimation methods utilizing probe vehicle with spacing measurement equipment, which can be applicable in the near future due to technological advancement.

7.1   Achievements

This dissertation proposed traffic state estimation methods utilizing probe vehicle with spacing measurement equipment. First, our literature survey outlined that capability of existing traffic data collection/state estimation methods by defining traffic data generally. Second, methods of estimating traffic states and/or traffic flow model parameters from the collected data were formulated and analytically investigated. Third, the formulated methods are empirically validated based on data obtained via a field experiment in the real world, as well as synthetic simulation experiments. As a result, methodology that enables us to estimate traffic state for vast time–space domain, is established. It may contribute to monitoring traffic in everywhere, enhancing its efficiency, and understanding wide-ranging traffic dynamics in the near future.

In chapters 1 and 2, from both perspectives of academic and practical, a challenging task remained in traffic and transportation field is clarified: traffic state estimation with probe vehicles. Traffic state estimation—estimating flow, density and speed from partially observed and/or partially unreliable data—is essential to understand and manage

automobile-based movements of people and goods (i.e., traffic) in modern civilization. Academic research on traffic and transportation engineering is identical to understanding traffic; and managing traffic is important in terms of economical and environmental efficiency in practical. However, estimating traffic state in anytime and anywhere is not an easy task due to observation cost, required theoretical assumptions and privacy issues. Fixed observation such as detectors cannot collect data from wide range with feasible cost; and conventional probe vehicles require strong exogenous assumptions or violate privacy to estimate traffic state. As possible solution for this problem is found in recent advancement in vehicle technologies: on-vehicle spacing measurement equipment.

In chapters 3 and 4, methodology of estimating traffic state using probe vehicles with spacing measurement equipment is formulated. The basic method in chapter 3 is formulated as requires less exogenous assumptions as possible. It is consistent with traditional definition in traffic flow theory. These characteristics enable the method possible to be applied in various situations without theoretical discrepancies. Qualitative characteristics of the method is analytically investigated in detail. The method's accuracy and precision are expected to improves as time–space resolution of estimation lowered and probe vehicles penetration rate increased.

The methods in chapter 4 are formulated based on the basic method considering additional assumptions that are often accepted by traditional traffic flow theory. These assumptions are integrated to the methods in order to improve the proposed methodology's reasonability in common traffic situations, as well as to improve accuracy and precision of its estimation. Namely, one of the methods considers a conservation law of traffic. A conservation law is incorporated with the estimation method by utilizing information of probe vehicles trajectories, which is ignored by the basic method. The other method in chapter 4 considers a fundamental diagram of traffic as well: a functional form of a fundamental diagram is given exogenously but the parameters are estimated endogenously. A fundamental diagram is a key concept describing traffic dynamics (i.e., time–space transition of traffic state) and vehicle behavior. The method estimates traffic states and fundamental diagrams simultaneously; then they are integrated by using a data

assimilation framework.

In chapters 5 and 6, the proposed methodology is empirically validated; and practical performance of the proposed methodology is clarified. In chapter 6, actual probe vehicle data were collected via a field experiment conducted in an urban expressway in the real world. The actual data are preferable for validating the proposed methodology because spacing calculated by synthetic models is not always realistic. On the other hand, the actual data contain unpreferable factors such as probe vehicle's bias and measurement errors. These unpreferable factors are complemented by validating the proposed methodology using synthetic data generated by simulation experiment in chapter 5. As a result of the validation, relation among the estimation methods' precision and accuracy, time–space resolution and penetration rate of probe vehicles is clarified quantitatively. It is confirmed that the basic method's characteristics are fairly consistent with the analytical investigation. The effect of incorporating traffic dynamics into the basic method is also confirmed. For example, the methods' precision improves as resolution lowered and penetration rate increased, as analytical results suggested. In partially congested urban expressway, the basic method can estimate 5 min traffic volume fairly well with 3.5% penetration rate; and it can estimate 1 hour traffic volume precisely with 0.2% penetration rate (i.e., 2 probe vehicle/h/lane). The integration of a conservation law and a fundamental could improve precision by 10–30%. As results, the methods' applicability in actual traffic environment is shown[*1].

Summary of the proposed traffic state estimation methods is as follows. The methods estimate traffic state based on data collected by probe vehicles with spacing measurement equipment. The basic method relies only on random sampling and error free assumptions. It means that the method can be applicable to general traffic without theoretical discrepancies. The other two methods employ existence of conservation law and/or a fundamental diagram as additional assumption(s), in order to incorporate traffic dynamics. Therefore, they can get reasonable results (i.e., accurate and precise estimation results) if

---

[*1]Another field experiment in an arterial road with mixed traffic also supports this. See appendix B for its summary.

the assumptions are actually satisfied. The validation result suggested that the proposed methodology can estimate precise traffic state, which can be applicable for traffic control, with few percentages of probe vehicle penetration rate in partially congested highway. On the other hand, the proposed methods can estimate lower resolution traffic state like hourly traffic volume, which can be applicable for transportation planning, with few probe vehicles per hour.

7.2 Future directions

The future works to this dissertation are twofold: to sophisticate the proposed TSE methods and to extend the proposed methodology for other general transportation fields.

7.2.1 The proposed TSE methods themselves

Following improvements are considerable to the proposed TSE methods.

Less biased estimators. The basic estimators (3.14) and (3.15) are biased. The third-order term in the Taylor series may be valuable in formulating less biased estimators, since the approximation was shown to be reasonable (c.f., sections 3.5, 5.1 and 6.2).

Unbiased estimations method that can be applied to biased probe vehicle data. It will relax the random sampling assumption. It is an important topic because the advanced technologies may cause biases in the probe vehicles' driving behavior. Use of information on the surrounding vehicles of the probe one, which are expected to be not biased, may be valuable to obtain the unbiased estimation.

Adaptive estimation of FD parameters in the method with FD and CL. It will relax the assumption of constant FD and improve estimation capability. To achieve this, two approaches are considerable: automatic clusterization of region **B** based on probe vehicle data and adaptive parameter estimation through data assimilation (c.f., 樋口, 2011).

Incorporation of Lagrangian traffic flow model. It will improve reasonability and performance of a TSE method, since the Lagrangian coordinate system can utilize information of vehicle trajectories (c.f., Yuan et al., 2012; Laval and Leclercq, 2013; Wada et al., 2015). However, it requires explicit consideration of non-FIFO (multi-lane) and multi-class traffic, which is ignored by the existing studies.

Incorporation of node conservation law. It is required to make the method applicable in networks; and requires merging/diverging models. Since probe vehicle data can be available throughout a network (and some links may not have probe vehicles at a moment), considering a node conservation law may improve reasonability and performance of estimation (c.f., Castillo et al., 2013).

Consideration of practical problems. In a real world application, several problems that are almost ignored by the proposed TSE methods may arise. For example, first, leading vehicles cannot be always recognized because of excessive distances, curves, etc., as described at section 3.6. Therefore, imputation methods for such missing spacing are required. Second, exact vehicle length is not known. This problem can be solved with on-line estimation of vehicle length distribution by measuring it in neighbor lanes. Third, the proposed TSE methods may have low precision at surface streets which have intersections, signals, parking, etc. Current methods require lowering time–space resolution in order to get high precision under such situations. However, low resolution information is sometimes useful, such as hourly traffic volume and annual average daily traffic for planning purposes and MFD for possible area-wide traffic managements. Nevertheless, if the signal timing information is known, the information can be incorporated with the method with FD and CL (c.f., Mehran et al., 2012; Wada et al., 2015).

7.2.2   Transportation system estimation with travelers observing other travelers

In chapter 1, it was mentioned that information is a key to enhance efficiency of a transportation system; and the challenging problem is to collect information from the entire system so that the system becomes understandable and controllable. As a solution to the problem, this dissertation proposed methodology for estimating transportation system's states and traveler's model parameters using travelers who observe other travelers in the system.

This dissertation formulated and validated a special case of the problem, namely, traffic state estimation, where travelers' movement is one-dimensional (in spatial). This methodology can be generalized for network-wide movement, two-dimensional movement and day-to-day movement, such as traffic network, pedestrian space, multi-mode urban transportation, and day-to-day learning/adaptation, at least in theoretical[*2]. It may be worth to be investigated, though it will arise (have arose) a lot of difficult problems in technological and ethical.

[*2]Simple examples exist for traffic networks and mixed traffic. See appendices A and B for their summaries.

Appendix A Expansion to Network: OD Flow

This appendix[*1] describes how the proposed method can be expanded for estimation of network traffic. Specifically, OD flow estimation method using PVSME data is developed and validated using simulation experiment.

OD flow, demand and matrix are valuable information for transportation planning. Typical approach in existing studies is to estimate current (dynamic) OD matrix using current partial collected traffic data and prior information on OD matrix, assuming UE conditions (Bell, 1991; Yang et al., 1992; Wei and Asakura, 2013). Yamamoto et al. (2009) applied GPS-equipped probe vehicle data for the approach by assuming FDs. Other approach estimates dynamic OD flow using AVI data without prior information on an OD matrix (Asakura et al., 2000).

In the spirit of this dissertation, the method should be containing assumptions as less as possible (e.g., prior knowledge on OD matrix and route choice principles must be eliminated). In fact, it is possible by simply expanding the basic method described in chapter 3.

A.1   Formulation

Probe vehicles are assumed

- to measure position and spacing without errors,
- to be randomly sampled from all the vehicles, and
- to report their OD pairs.

The third condition is added compared to the basic method. Network schematics are assumed to be known. An example of probe vehicle data under above conditions are

---

[*1]This appendix is mainly based on joint research with Prof. Yasuo Asakura, published in *the 49th Conference of JSCE Infrastructure Planning and Management* (瀬尾・朝倉, 2014).
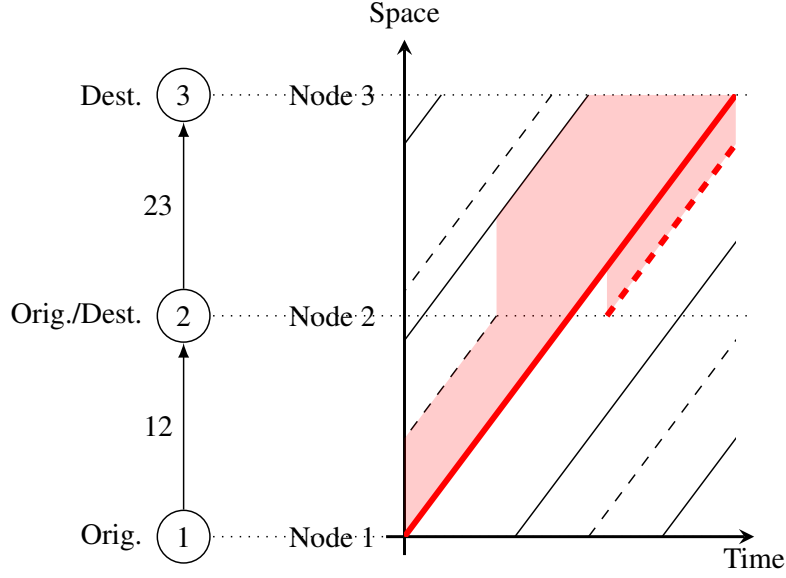
Figure A.1: Example of probe vehicle data in network

shown in Fig A.1. The network is consists of three nodes and two links. Node 1 is a producing node, node 2 is a producing and attracting node, and node 3 is an attracting node, of traffic; therefore, OD pairs are $1 \to 2$, $1 \to 3$ and $2 \to 3$. Red thick lines represent probe vehicles' trajectories; red filled areas represent observed time–space regions by probe vehicles; black lines represent non-probe vehicles' trajectories; solid lines represent vehicles' trajectories whose OD pair is $1 \to 3$; and dashed lines represent vehicles' trajectories whose OD pair is $1 \to 2$ or $2 \to 3$.

The objective is to estimate link flow who has an particular OD pair in a network. By expanding the basic estimator of flow (3.14), estimator for flow per OD pair can be easily defined as

$$\hat{q}^{(uw)}(\mathbf{A}) = \frac{\sum_{m \in \mathbf{P}^{(uw)}(\mathbf{A})} d_m(\mathbf{A})}{\sum_{m \in \mathbf{P}(\mathbf{A})} |\mathbf{a}_m(\mathbf{A})|}, \tag{A.1}$$

where $q^{(uw)}(\mathbf{A})$ is a flow in a time–space region $\mathbf{A}$ whose OD pair is uw, and $\mathbf{P}^{(uw)}(\mathbf{A})$ is a set of probe vehicles in $\mathbf{A}$ whose OD pair is uw. By substituting $\mathbf{A}$ with $\mathbf{A}_{ij}^{(t)}$, that is, a time–space region that covers link ij and time t in eq (A.1), a link OD flow can be estimated—in the following part, the flow is represented as q_{ij}^{uw} if the time can be ignored.
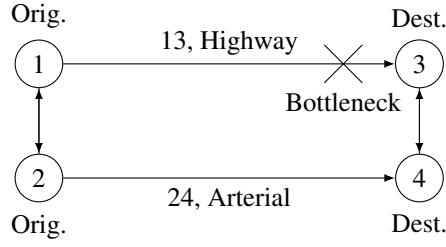
Figure A.2: Network for simulation experiment.

Table A.1: OD matrix for simulation experiment.

	3	4
1	600	300
2	300	600

Note that following relation is satisfied by the definition:

$$\hat{q}(\mathbf{A}) = \sum_{uw} \hat{q}^{(uw)}(\mathbf{A}). \tag{A.2}$$

A.2   Simulation experiment-based validation

Numerical characteristics of the proposed method are validated using simulation experiment.

Aimsun (TSS-Transport Simulation Systems) is employed as a simulator; where vehicle behavior is described by the car-following model of Gipps (1981), route choice behavior is described by quasi dynamic user optimum, and vehicle departure is described as Poisson arrival. The network schematics and OD matrix are shown in Fig A.2 and Table A.1 that simulate a highway with a bottleneck and a parallel arterial road. The time width of **A** is set to one hour.

An estimation result with 5% of PR is shown in Fig A.3; the estimated variables are well corresponded to the ground truth. The RMSE of flow calculated from 10 iterations is 36.6 veh/h.
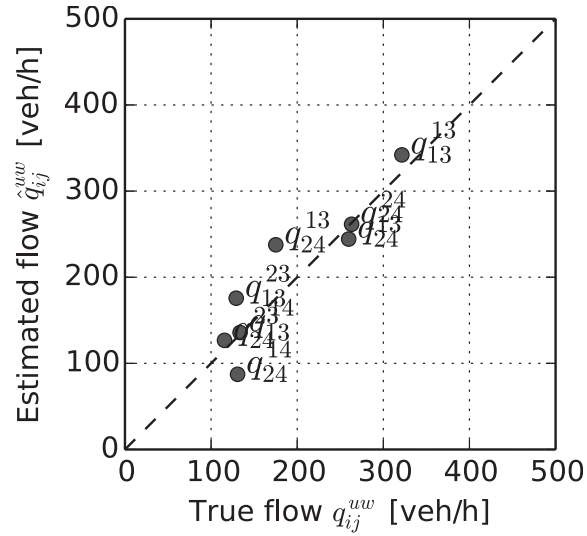
Figure A.3: Comparison between estimated flow and ground truth.

A.3   Remarks

This appendix demonstrated expansion of the basic method of chapter 3 to network flow estimation. Only additional assumption is availability of information on probe vehicles' OD pair. The validation results with small toy network suggested that the proposed method works well. Even if number of combination of OD pairs are large, the method may work by aggregating OD pairs appropriately.

Network traffic information such as OD flow is often employed for transportation planning purposes, which require relatively low resolution data, such as hourly traffic volume of a link and annual average daily traffic volume. As shown in section 6.2, data from PVSMEs with quite low PR can be utilized for precise estimation of low resolution traffic information. Therefore, this application of PVSME data may be feasible in the very near future, compared with traffic control-motivated TSE.

As a future direction, the method with FD and CL can be expanded to network flow estimation. To do so, a conservation law at a node should be considered so that traffic states in unobserved links can be interpolated.

Appendix B Field Experiment at Arterial Road with Mixed Traffic

In this appendix[*1], we focus on mixed traffic flow formed by car (i.e., four-wheeled-vehicle) and motorcycle which is very popular in many Asian cities of developing countries. Under the mixed traffic condition, motorcycles in small sizes which do not need to follow the lane disciplines, could travel alongside with lane-based driving cars, follow obliquely a lead cars with short headways (Robertson, 2002), swerve away to overtake or to avoid collision with the preceding cars (Lee et al., 2009; Nguyen et al., 2012, 2014). Therefore, the occurrence of motorcycles may weaken the lane discipline of the cars and could make the traffic flow difficult to be observed.

B.1   Field experiment environment

Pasteur Str. located in central area of Ho Chi Minh City, Vietnam was chosen for the survey location, as shown in Fig B.1a. The road is a one-way road with 3 lanes: two outer lanes for cars and one inner lane for motorcycles. However, cars and motorcycles could share their lanes each other. The experimental road segment is approximately 1.5 km long with 7 signalized intersections. Four fixed cameras were set at two different places on the both sidewalk of the road, as illustrated by circles in Fig B.1a to obtain validation data of car flow rate. Probe vehicles were asked to run on the road segment and return to the starting point for the next round by using Nam Ky Khoi Nghia Str. parallel to this road.

Taxis were employed as probe vehicle, equipped with a GPS logger and a video camera. A GPS logger is put inside the taxi to log GPS coordinates every 15 seconds to a file. Then a logger application opens the file to provide data of position and speed. The

---

[*1]This appendix is mainly based on joint research with Dr. Long Xuan Nguyen, Dr. Takahiko Kusakabe, Dr. Hong Tan Van and Prof. Yasuo Asakura, published in *19th HKSTS Conference* (Nguyen et al., 2014).
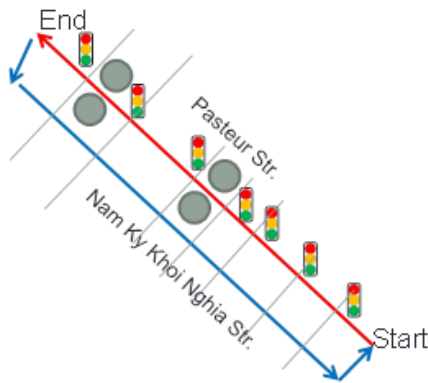
(a) Map of Pasteur Str.   (b) View from probe vehicle
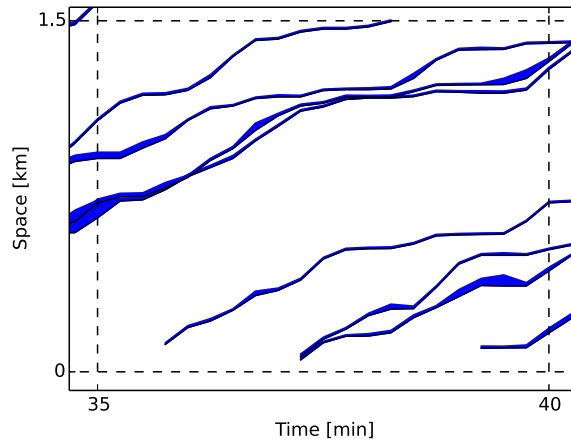
(c) Part of probe vehicle data

Figure B.1: Experiment at Pasteur Str.

video camera is fixed on the dashboard of the front passenger seat to record movies. The images extracted from the movies contain information utilized for measuring distances between the probe vehicle and other vehicles in its surroundings. An example of the images and part of the probe vehicle data are shown in Fig B.1b and c, respectively.

The survey was conducted on March, 7th 2014 for 1.5 hours from 4:00 pm to 5:30 pm in the dry weather. Ten taxis equipped with video cameras and GPS loggers gathered on the Tan Cang parking area near the survey location. At 4:00 pm, the probe vehicles departed one-by-one every five minutes and ran on the course. In addition, four fixed cameras on the sidewalk were used to observe the real traffic state of the traffic flow. At

(a) 800 m point

(b) 1350 m point
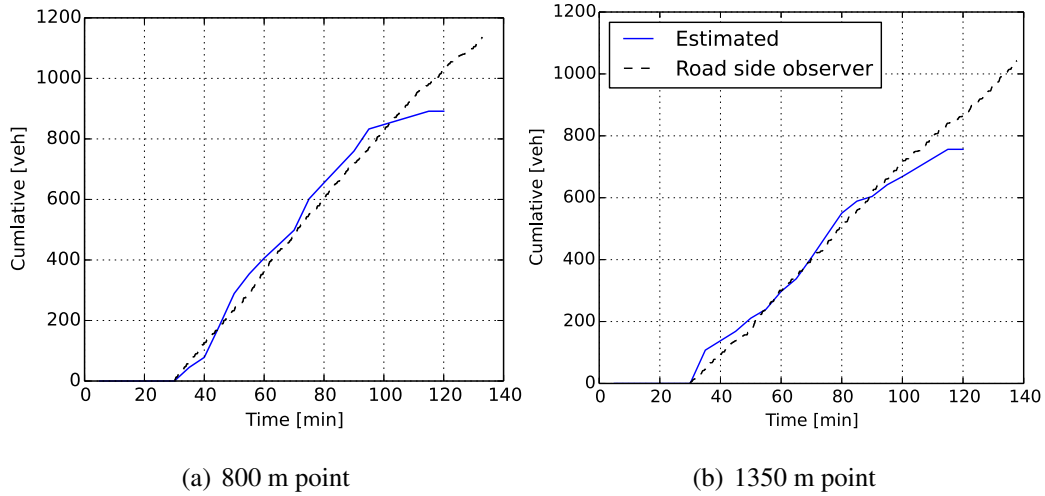
Figure B.2: Cumulative curves at Pasteur Str.

5:30 pm, the probe vehicles left the course at the same time and returned to the parking area. Regarding the behaviors of taxi drivers, they were asked to run normally as desiring. It means that each driver could run with their desired speed when the traffic flow is free, or overtake the preceding vehicles to attain a higher speed when traffic become congested. The flow of all the cars was about 600 veh/h. The flow of all the motorcycles was about 4500 veh/h.

B.2   Results of TSE on cars

The traffic state of cars was estimated using the basic method.

Fig B.2 shows cumulative curves at two locations of Pasteur Str. Dashed lines represent ground truth obtained by road side observer, and blue lines represent estimated values by all the probe vehicle with 5 min time resolution. According to the figure, the rough tendency of estimated cumulative curves are close to observed ones. However, errors in high resolution state such as 5 min flow are relatively large. This characteristic is similar to the results of sections 5.1 and 6.2.

Table B.1 summarizes estimation performance at Pasteur Str. The same tendency to sections 5.1 and 6.2 can be found: accuracy and precision improves as P, Δt increases.

Table B.1: Flow estimation results at Pasteur Str.

P	Δt (min)	RMSPE($\hat{q}$)	Bias($\hat{q}$) (veh/h)
0.2%	5	57.9%	63.8
0.2%	60	42.0%	91.0
1.0%	5	52.7%	52.9
1.0%	60	18.4%	−11.4
2.5%	5	55.4%	14.3
2.5%	60	7.9%	−20.5

However, in quantitatively, the precision is lower than the field experiment in the urban expressway. It may be due to larger variance in headway due to the higher fluctuation of the mixed traffic and signals.

References

Antoniou, C. and Polydoropoulou, A.: The value of privacy: Evidence from the use of mobile devices for traveler information systems, *Journal of Intelligent Transportation Systems*, 2015.

Asakura, Y. and Hato, E.: Tracking survey for individual travel behaviour using mobile communication instruments, *Transportation Research Part C: Emerging Technologies*, Vol. 12, No. 3–4, pp. 273–291, 2004.

Asakura, Y. and Iryo, T.: Analysis of tourist behaviour based on the tracking data collected using a mobile communication instrument, *Transportation Research Part A: Policy and Practice*, Vol. 41, No. 7, pp. 684–690, 2007.

Asakura, Y., Hato, E., and Kashiwadani, M.: Origin-destination matrices estimation model using automatic vehicle identification data and its application to the Han-Shin expressway network, *Transportation*, Vol. 27, No. 4, pp. 419–438, 2000.

Ashton, W. D.: Gap-acceptance problems at a traffic intersection, *Applied Statistics*, pp. 130–138, 1971.

Ban, X. J., Hao, P., and Sun, Z.: Real time queue length estimation for signalized intersections using travel times from mobile sensors, *Transportation Research Part C: Emerging Technologies*, Vol. 19, No. 6, pp. 1133–1156, 2011.

Bell, M. G. H.: The estimation of origin-destination matrices by constrained generalised least squares, *Transportation Research Part B: Methodological*, Vol. 25, No. 1, pp. 13–22, 1991.

Bengler, K., Dietmayer, K., Farber, B., Maurer, M., Stiller, C., and Winner, H.: Three decades of driver assistance systems: Review and future perspectives, *Intelligent Transportation Systems Magazine, IEEE*, Vol. 6, No. 4, pp. 6–22, 2014.

Bertozzi, M. and Broggi, A.: GOLD: a parallel real-time stereo vision system for generic obstacle and lane detection, *IEEE Transactions on Image Processing*, Vol. 7, No. 1, pp. 62–81, 1998.

Braess, D.: Über ein paradoxon aus der verkehrsplanung, *Unternehmensforschung*, Vol. 12, pp. 258–268, 1968.

Cassidy, M. J.: Bivariate relations in nearly stationary highway traffic, *Transportation Research Part B: Methodological*, Vol. 32, No. 1, pp. 49–59, 1998.

Castillo, E., Nogal, M., Rivas, A., and Sanchez-Cambronero, S.: Observability of traffic networks. optimal location of counting and scanning devices, *Transportmetrica B: Transport Dynamics*, Vol. 1, No. 1, pp. 68–102, 2013.

Chiabaut, N., Buisson, C., and Leclercq, L.: Fundamental diagram estimation through passing rate measurements in congestion, *Intelligent Transportation Systems, IEEE Transactions on*, Vol. 10, No. 2, pp. 355–359, 2009.

Choudhury, C. F. and Ben-Akiva, M. E.: Modelling driving decisions: a latent plan approach, *Transportmetrica A: Transport Science*, Vol. 9, No. 6, pp. 546–566, 2013.

Coifman, B.: Vehicle re-identification and travel time measurement in real-time on freeways using existing loop detector infrastructure, *Transportation Research Record: Journal of the Transportation Research Board*, No. 1643, pp. 181–191, 1998.

Coifman, B.: Estimating travel times and vehicle trajectories on freeways using dual loop detectors, *Transportation Research Part A: Policy and Practice*, Vol. 36, No. 4, pp. 351–364, 2002.

Coifman, B.: Revisiting the empirical fundamental relationship, *Transportation Research Part B: Methodological*, Vol. 68, pp. 173–184, 2014.

Coifman, B.: Empirical flow-density and speed-spacing relationships: Evidence of vehicle length dependency, *Transportation Research Part B: Methodological*, Vol. 78, pp. 54–65, 2015.

Coifman, B. and Hall, H.: An overview of the on-going OSU instrumented probe vehicle research,Technical report, The Ohio State University, 2014.

Coifman, B., Beymer, D., McLauchlan, P., and Malik, J.: A real-time computer vision system for vehicle tracking and traffic surveillance, *Transportation Research Part C: Emerging Technologies*, Vol. 6, No. 4, pp. 271–288, 1998.

Coifman, B., McCord, M., Mishalani, R. G., Iswalt, M., and Ji, Y.: Roadway traffic monitoring from an unmanned aerial vehicle, *Intelligent Transport Systems, IEE Proceedings*, Vol. 153, No. 1, pp. 11–20, 2006.

Comert, G.: Simple analytical models for estimating the queue lengths from probe vehicles at traffic signals, *Transportation Research Part B: Methodological*, Vol. 55, pp. 59–74, 2013.

Daganzo, C. F.: The cell transmission model: A dynamic representation of highway traffic consistent with the hydrodynamic theory, *Transportation Research Part B: Methodological*, Vol. 28, No. 4, pp. 269–287, 1994.

Daganzo, C. F.: Requiem for second-order fluid approximations of traffic flow, *Transportation Research Part B: Methodological*, Vol. 29, No. 4, pp. 277–286, 1995.

Daganzo, C. F.: *Fundamentals of Transportation and Traffic Operations*, Pergamon Oxford, 1997.

Daganzo, C. F.: A behavioral theory of multi-lane traffic flow. part I: Long homogeneous freeway sections, *Transportation Research Part B: Methodological*, Vol. 36, No. 2, pp. 131–158, 2002.

Daganzo, C. F.: A variational formulation of kinematic waves: basic theory and complex boundary conditions, *Transportation Research Part B: Methodological*, Vol. 39, No. 2, pp. 187–196, 2005a.

Daganzo, C. F.: A variational formulation of kinematic waves: Solution methods, *Transportation Research Part B: Methodological*, Vol. 39, No. 10, pp. 934–950, 2005b.

Daganzo, C. F.: In traffic flow, cellular automata = kinematic waves, *Transportation Research Part B: Methodological*, Vol. 40, No. 5, pp. 396–403, 2006.

Daganzo, C. F.: Urban gridlock: Macroscopic modeling and mitigation approaches, *Transportation Research Part B: Methodological*, Vol. 41, No. 1, pp. 49–62, 2007.

Daganzo, C. F. and Geroliminis, N.: An analytical approximation for the macroscopic fundamental diagram of urban traffic, *Transportation Research Part B: Methodological*, Vol. 42, No. 9, pp. 771–781, 2008.

Daganzo, C. F., Gayah, V. V., and Gonzales, E. J.: Macroscopic relations of urban traffic variables: Bifurcations, multivaluedness and instability, *Transportation Research Part B: Methodological*, Vol. 45, No. 1, pp. 278–288, 2011.

Daganzo, C. F., Gayah, V. V., and Gonzales, E. J.: The potential of parsimonious models for understanding large scale transportation systems and answering big picture questions, *EURO Journal on Transportation and Logistics*, Vol. 1, No. 1-2, pp. 47–65, 2012.

Darwish, T. and Bakar, K. A.: Traffic density estimation in vehicular ad hoc networks: A review, *Ad Hoc Networks*, Vol. 24, Part A, pp. 337–351, 2015.

Delpiano, R., Laval, J., Coeymans, J. E., and Herrera, J. C.: The kinematic wave model with finite decelerations: A social force car-following model approximation, *Transportation Research Part B: Methodological*, Vol. 71, pp. 182–193, 2015.

Deng, W., Lei, H., and Zhou, X.: Traffic state estimation and uncertainty quantification based on heterogeneous data sources: A three detector approach, *Transportation Research Part B: Methodological*, Vol. 57, pp. 132–157, 2013.

Diakaki, C., Papageorgiou, M., Papamichail, I., and Nikolos, I.: Overview and analysis of vehicle automation and communication systems from a motorway traffic management perspective, *Transportation Research Part A: Policy and Practice*, Vol. 75, pp. 147–165, 2015.

Diaz, J. J. V., Llorca, D. F., Gonzalez, A. B. R., Minguez, R. Q., Llamazares, A. L., and Sotelo, M. A.: Extended floating car data system: Experimental results and application for a hybrid route level of service, *Intelligent Transportation Systems, IEEE Transactions on*, Vol. 13, No. 1, pp. 25–35, 2012.

Edie, L. C.: Car-following and steady-state theory for noncongested traffic, *Operations Research*, Vol. 9, No. 1, pp. 66–76, 1961.

Edie, L. C.: Discussion of traffic stream measurements and definitions, in Almond, J. ed. *Proceedings of the 2nd International Symposium on the Theory of Traffic Flow*, pp. 139–154, 1963.

El Faouzi, N.-E., Leung, H., and Kurian, A.: Data fusion in intelligent transportation systems: Progress and challenges–a survey, *Information Fusion*, Vol. 12, No. 1, pp. 4–10, 2011.

Evensen, G.: Sequential data assimilation with a nonlinear quasi-geostrophic model using Monte Carlo methods to forecast error statistics, *Journal of Geophysical Research: Oceans*, Vol. 99, No. C5, pp. 10143–10162, 1994.

Gayah, V. V. and Dixit, V. V.: Using mobile probe data and the macroscopic fundamental diagram to estimate network densities, *Transportation Research Record: Journal of the Transportation Research Board*, Vol. 2390, No. 1, pp. 76–86, 2013.

Gazis, D. C. and Knapp, C. H.: On-line estimation of traffic densities from time-series of flow and speed data, *Transportation Science*, Vol. 5, No. 3, pp. 283–301, 1971.

Gazis, D. C., Herman, R., and Rothery, R. W.: Nonlinear follow-the-leader models of traffic flow, *Operations Research*, Vol. 9, No. 4, pp. 545–567, 1961.

Geroliminis, N. and Daganzo, C. F.: Existence of urban-scale macroscopic fundamental diagrams: Some experimental findings, *Transportation Research Part B: Methodological*, Vol. 42, No. 9, pp. 759–770, 2008.

Geroliminis, N. and Sun, J.: Properties of a well-defined macroscopic fundamental diagram for urban traffic, *Transportation Research Part B: Methodological*, Vol. 45, No. 3, pp. 605–617, 2011.

Gipps, P. G.: A behavioural car-following model for computer simulation, *Transportation Research Part B: Methodological*, Vol. 15, No. 2, pp. 105–111, 1981.

Gipps, P. G.: A model for the structure of lane-changing decisions, *Transportation Research Part B: Methodological*, Vol. 20, No. 5, pp. 403–414, 1986.

Goodall, N. J., Smith, B. L., and Park, B.: Microscopic estimation of freeway vehicle positions from the behavior of connected vehicles, *Journal of Intelligent Transportation Systems*, 2014.

Greenshields, B. D.: A study of traffic capacity, in *Highway Research Board Proceedings*, Vol. 14, pp. 448–477, 1935.

Hao, P., Sun, Z., Ban, X. J., Guo, D., and Ji, Q.: Vehicle index estimation for signalized intersections using sample travel times, *Transportation Research Part C: Emerging Technologies*, Vol. 36, pp. 513–529, 2013.

Hara, Y. and Kuwahara, M.: Traffic monitoring immediately after a major natural disaster as revealed by probe data – a case in Ishinomaki after the Great East Japan Earthquake, *Transportation Research Part A: Policy and Practice*, Vol. 75, pp. 1–15, 2015.

Hartenstein, H. and Laberteaux, K.: A tutorial survey on vehicular ad hoc networks, *Communications Magazine, IEEE*, Vol. 46, No. 6, pp. 164–171, 2008.

Helbing, D.: Traffic and related self-driven many-particle systems, *Reviews of Modern Physics*, Vol. 73, pp. 1067–1141, 2001.

Herrera, J. C. and Bayen, A. M.: Incorporation of Lagrangian measurements in freeway traffic state estimation, *Transportation Research Part B: Methodological*, Vol. 44, No. 4, pp. 460–481, 2010.

Herrera, J. C., Work, D. B., Herring, R., Ban, X. J., Jacobson, Q., and Bayen, A. M.: Evaluation of traffic data obtained via GPS-enabled mobile phones: The Mobile Century field experiment, *Transportation Research Part C: Emerging Technologies*, Vol. 18, No. 4, pp. 568–583, 2010.

Hilbert, E. E., Rennie, P. A., and Kneidl, W. A.: A sensor for control of arterials and networks, *Vehicular Technology, IEEE Transactions on*, Vol. 29, No. 2, pp. 208–215, 1980.

Hornby, A. S. et al.: eds. *Oxford advanced learner's dictionary*, Oxford University Press, 2010.

Jin, W.-L.: On the existence of stationary states in general road networks, *Transportation Research Part B: Methodological*, 2015.

Jin, W.-L., Gan, Q.-J., and Gayah, V. V.: A kinematic wave approach to traffic statics and dynamics in a double-ring network, *Transportation Research Part B: Methodological*, Vol. 57, pp. 114–131, 2013.

Kalman, R. E. and Bucy, R. S.: New results in linear filtering and prediction theory, *Journal of Basic Engineering*, Vol. 83, No. 3, pp. 95–108, 1961.

Karlaftis, M. G. and Vlahogianni, E. I.: Statistical methods versus neural networks in transportation research: Differences, similarities and some insights, *Transportation Research Part C: Emerging Technologies*, Vol. 19, No. 3, pp. 387–399, 2011.

Katakura, M.: Time headway distribution of traffic flow, *Proceedings of the Japan Society of Civil Engineers*, No. 189, pp. 107–115, 1971.

125

Kataoka, S., Yasuda, M., and Tanaka, K.: Bayesian reconstruction of missing observations, *Interdisciplinary Information Sciences*, Vol. 21, No. 1, pp. 11–23, 2015.

Kikuchi, S., Uno, N., and Tanaka, M.: Impacts of shorter perception-reaction time of adapted cruise controlled vehicles on traffic flow and safety, *Journal of Transportation Engineering*, Vol. 129, No. 2, pp. 146–154, 2003.

Kita, H.: A merging–giveway interaction model of cars in a merging section: a game theoretic analysis, *Transportation Research Part A: Policy and Practice*, Vol. 33, No. 34, pp. 305–312, 1999.

Klein, L. A., Mills, M. K., and Gibson, D. R. P.: Traffic detector handbook—volume I and II,Technical report, Federal Highway Administration, 2006.

Kometani, E. and Sasaki, T.: On the stability of traffic flow, *Journal of the Operations Research Society of Japan*, Vol. 2, No. 1, pp. 11–26, 1958.

Kometani, E. and Sasaki, T.: Dynamic behaviour of traffic with a non-linear spacing–speed relationship, in Herman, R. ed. *Proceedings of the Symposium on Theory of Traffic Flow, Research Laboratories, General Motors*, Elsevier, pp. 105–119, 1961.

Kusakabe, T., Iryo, T., and Asakura, Y.: Data mining for traffic flow analysis: Visualization approach, in Barcelo, J. and Kuwahara, M. eds. *Traffic Data Collection and its Standardization*, Springer, pp. 57–72, 2010.

Laval, J. A.: Hysteresis in traffic flow revisited: An improved measurement method, *Transportation Research Part B: Methodological*, Vol. 45, No. 2, pp. 385–391, 2011.

Laval, J. A. and Daganzo, C. F.: Lane-changing in traffic streams, *Transportation Research Part B: Methodological*, Vol. 40, No. 3, pp. 251–264, 2006.

Laval, J. A. and Leclercq, L.: The Hamilton–Jacobi partial differential equation and the three representations of traffic flow, *Transportation Research Part B: Methodological*, Vol. 52, pp. 17–30, 2013.

Laval, J. A., Castrillón, F., and Zhou, Y.: Stochastic approximations for the macroscopic fundamental diagram of urban networks, in *Transportation Research Board 94th Annual Meeting*, 2015.

Laval, J. A., He, Z., and Castrillon, F.: Stochastic extension of Newell's three-detector method, *Transportation Research Record: Journal of the Transportation Research Board*, Vol. 2315, No. 1, pp. 73–80, 2012.

Lebacque, J. P.: The Godunov scheme and what it means for first order traffic flow models, in Lesort, J. B. ed. *Transportation and Traffic Theory. Proceedings of the 13th International Symposium on Transportation and Traffic Theory*, pp. 647–677, 1996.

Leclercq, L. and Geroliminis, N.: Estimating MFDs in simple networks with route choice, *Transportation Research Part B: Methodological*, Vol. 57, pp. 468–484, 2013.

Leclercq, L., Laval, J. A., and Chevallier, E.: The Lagrangian coordinates and what it means for first order traffic flow models, in Allsop, R., Bell, M., and Heydecker, B. eds. *Transportation and Traffic Theory 2007*, pp. 735–753, Elsevier, 2007.

Leclercq, L., Laval, J. A., and Chiabaut, N.: Capacity drops at merges: An endogenous model, *Transportation Research Part B: Methodological*, Vol. 45, No. 9, pp. 1302–1313, 2011.

Lee, T.-C., Polak, J. W., and Bell, M. G.: New approach to modeling mixed traffic containing motorcycles in urban areas, *Transportation Research Record: Journal of the Transportation Research Board*, Vol. 2140, No. 1, pp. 195–205, 2009.

Lee, S., Wong, S. C., and Li, Y. C.: Real-time estimation of lane-based queue lengths at isolated signalized junctions, *Transportation Research Part C: Emerging Technologies*, Vol. 56, pp. 1–17, 2015.

Lei, H. and Zhou, X.: Linear programming model for estimating high-resolution freeway traffic states from vehicle identification and location data, *Transportation Research Record: Journal of the Transportation Research Board*, Vol. 2421, pp. 151–160, 2014.

Lighthill, M. J. and Whitham, G. B.: On kinematic waves. II. a theory of traffic flow on long crowded roads, *Proceedings of the Royal Society of London. Series A. Mathematical and Physical Sciences*, Vol. 229, No. 1178, pp. 317–345, 1955.

Liu, K., Yamamoto, T., and Morikawa, T.: Feasibility of using taxi dispatch system as probes for collecting traffic information, *Journal of Intelligent Transportation Systems*, Vol. 13, No. 1, pp. 16–27, 2009.

Makigami, Y., Newell, G. F., and Rothery, R.: Three-dimensional representation of traffic flow, *Transportation Science*, Vol. 5, No. 3, pp. 302–313, 1971.

McCord, M. R., Yang, Y., Jiang, Z., Coifman, B., and Goel, P. K.: Estimating annual average daily traffic from satellite imagery and air photos: Empirical results, *Transportation Research Record: Journal of the Transportation Research Board*, Vol. 1855, No. 1, pp. 136–142, 2003.

Mehran, B., Kuwahara, M., and Naznin, F.: Implementing kinematic wave theory to reconstruct vehicle trajectories from fixed and probe sensor data, *Transportation Research Part C: Emerging Technologies*, Vol. 20, No. 1, pp. 144–163, 2012.

Messelodi, S., Modena, C. M., Zanin, M., Natale, F. G. D., Granelli, F., Betterle, E., and Guarise, A.: Intelligent extended floating car data collection, *Expert Systems with Applications*, Vol. 36, No. 3, Part 1, pp. 4213–4227, 2009.

Mori, U., Mendiburu, A., lvarez, M., and Lozano, J. A.: A review of travel time estimation and forecasting for advanced traveller information systems, *Transportmetrica A: Transport Science*, Vol. 11, No. 2, pp. 119–157, 2015.

Moskowitz, K.: Discussion of 'freeway level of service as influenced by volume and capacity characteristics' by D. R. Drew and C. J. Keese, *Highway Research Record*, Vol. 99, pp. 43–44, 1965.

Muñoz, L., Sun, X., Horowitz, R., and Alvarez, L.: Traffic density estimation with the cell transmission model, in *American Control Conference*, Vol. 5, pp. 3750–3755, 2003.

Murakami, E. and Wagner, D. P.: Can using global positioning system (GPS) improve trip reporting? *Transportation Research Part C: Emerging Technologies*, Vol. 7, No. 2-3, pp. 149–165, 1999.

Nanthawichit, C., Nakatsuji, T., and Suzuki, H.: Application of probe-vehicle data for real-time traffic-state estimation and short-term travel-time prediction on a freeway, *Transportation Research Record: Journal of the Transportation Research Board*, Vol. 1855, No. 1, pp. 49–59, 2003.

National Highway Traffic Safety Administration: Preliminary Statement of Policy Concerning Automated Vehicles, Press release, 2013.

Newell, G. F.: Theories of instability in dense highway traffic, *Journal of the Operations Research Society of Japan*, Vol. 5, No. 5, pp. 9–54, 1962.

Newell, G. F.: A simplified theory of kinematic waves in highway traffic, part I: General theory, *Transportation Research Part B: Methodological*, Vol. 27, No. 4, pp. 281–287, 1993a.

Newell, G. F.: A simplified theory of kinematic waves in highway traffic, part II: Queueing at freeway bottlenecks, *Transportation Research Part B: Methodological*, Vol. 27, No. 4, pp. 289–303, 1993b.

Newell, G. F.: A simplified theory of kinematic waves in highway traffic, part III: Multi-destination flows, *Transportation Research Part B: Methodological*, Vol. 27, No. 4, pp. 305–313, 1993c.

Newell, G. F.: A simplified car-following theory: a lower order model, *Transportation Research Part B: Methodological*, Vol. 36, No. 3, pp. 195–205, 2002.

Nguyen, L. X., Hanaoka, S., and Kawasaki, T.: Describing non-lane-based motorcycle movements in motorcycle-only traffic flow, *Transportation Research Record: Journal of the Transportation Research Board*, Vol. 2281, No. 1, pp. 76–82, 2012.

Nguyen, L. X., Hanaoka, S., and Kawasaki, T.: Traffic conflict assessment for non-lane-based movements of motorcycles under congested conditions, *IATSS Research*, Vol. 37, No. 2, pp. 137–147, 2014.

Nguyen, L. X., Seo, T., Van, H. T., Kusakabe, T., and Asakura, Y.: Mixed flow observation using video cameras on probe vehicles: A case study in Ho Chi Minh City, in *Proceedings of the 19th International Conference of Hong Kong Society for Transportation Studies*, pp. 374–381, 2014.

Oh, S., Byon, Y.-J., Jang, K., and Yeo, H.: Short-term travel-time prediction on highway: A review of the data-driven approach, *Transport Reviews*, 2015.

Ohba, Y., Ueno, H., and Kuwahara, M.: Travel time calculation method for expressway using toll collection system data, in *Intelligent Transportation Systems, 1999. Proceedings. 1999 IEEE/IEEJ/JSAI International Conference on*, pp. 471–475, 1999.

Panmungmee, C., Wongsarat, M., and Tangamchit, P.: Automatic traffic estimation system using mobile probe vehicles, in *Knowledge and Smart Technology (KST), 2012 4th International Conference on*, pp. 11–15, 2012.

Payne, H. J.: Models of freeway traffic and control, *Mathematical Models of Public Systems*, Vol. 1, No. 1, pp. 51–61, 1971.

Pipes, L. A.: An operational analysis of traffic dynamics, *Journal of Applied Physics*, Vol. 24, No. 3, pp. 274–281, 1953.

Qu, X., Wang, S., and Zhang, J.: On the fundamental diagram for freeway traffic: A novel calibration approach for single-regime models, *Transportation Research Part B: Methodological*, Vol. 73, pp. 91–102, 2015.

Quddus, M. A., Ochieng, W. Y., and Noland, R. B.: Current map-matching algorithms for transport applications: State-of-the art and future research directions, *Transportation Research Part C: Emerging Technologies*, Vol. 15, No. 5, pp. 312–328, 2007.

Rabie, T., Shalaby, A., Abdulhai, B., and El-Rabbany, A.: Mobile vision-based vehicle tracking and traffic control, in *Intelligent Transportation Systems, 2002. Proceedings. The IEEE 5th International Conference on*, pp. 13–18, 2002.

Rajamani, R. and Shladover, S. E.: An experimental comparative study of autonomous and co-operative vehicle-follower control systems, *Transportation Research Part C: Emerging Technologies*, Vol. 9, No. 1, pp. 15–31, 2001.

Redmill, K. A., Coifman, B., McCord, M., and Mishalani, R. G.: Using transit or municipal vehicles as moving observer platforms for large scale collection of traffic and transportation system information, in *Intelligent Transportation Systems (ITSC), 2011 14th International IEEE Conference on*, pp. 1089–1095, 2011.

Richards, P. I.: Shock waves on the highway, *Operations Research*, Vol. 4, No. 1, pp. 42–51, 1956.

Robertson, S.: Motorcycling and congestion: Definition of behaviours, *Contemporary Ergonomics*, pp. 273–277, 2002.

Saneyoshi, K.: Drive assist system using stereo image recognition, in *Proceedings of the IEEE Intelligent Vehicles Symposium*, pp. 230–235, IEEE, 1996.

Sanwal, K. K. and Walrand, J.: Vehicles as probes, *California Partners for Advanced Transit and Highways (PATH), Working Paper*, 1995.

Sarvi, M. and Kuwahara, M.: Microsimulation of freeway ramp merging processes under congested traffic conditions, *Intelligent Transportation Systems, IEEE Transactions on*, Vol. 8, No. 3, pp. 470–479, 2007.

Seo, T. and Kusakabe, T.: Probe vehicle-based traffic state estimation method with spacing information and conservation law, *Transportation Research Part C: Emerging Technologies*, 2015, in press. doi:10.1016/j.trc.2015.05.019.

Seo, T., Kusakabe, T., and Asakura, Y.: Estimation of flow and density using probe vehicles with spacing measurement equipment, *Transportation Research Part C: Emerging Technologies*, Vol. 53, pp. 134–150, 2015a.

Seo, T., Kusakabe, T., and Asakura, Y.: Traffic state estimation with the advanced probe vehicles using data assimilation, in *Intelligent Transportation Systems (ITSC), 2015 18th International IEEE Conference on*, 2015b, accepted.

Sheffi, Y.: *Urban Transportation Networks*, 1985.

Shiomi, Y., Taniguchi, T., Uno, N., Shimamoto, H., and Nakamura, T.: Multilane first-order traffic flow model with endogenous representation of lane-flow equilibrium, *Transportation Research Part C: Emerging Technologies*, 2015.

Shiomi, Y., Yoshii, T., and Kitamura, R.: Platoon-based traffic flow model for estimating breakdown probability at single-lane expressway bottlenecks, *Transportation Research Part B: Methodological*, Vol. 45, No. 9, pp. 1314–1330, 2011.

Sivaraman, S. and Trivedi, M. M.: Looking at vehicles on the road: A survey of vision-based vehicle detection, tracking, and behavior analysis, *Intelligent Transportation Systems, IEEE Transactions on*, Vol. 14, No. 4, pp. 1773–1795, 2013.

Srivastava, A., Jin, W.-L., and Lebacque, J.-P.: A modified cell transmission model with realistic queue discharge features at signalized intersections, *Transportation Research Part B: Methodological*, 2015.

Sumalee, A., Wang, J., Jedwanna, K., and Suwansawat, S.: Probabilistic fusion of vehicle features for reidentification and travel time estimation using video image data, *Transportation Research Record: Journal of the Transportation Research Board*, Vol. 2308, No. 1, pp. 73–82, 2012.

Sumalee, A., Zhong, R. X., Pan, T. L., and Szeto, W. Y.: Stochastic cell transmission model (SCTM): A stochastic dynamic traffic model for traffic state surveillance and assignment, *Transportation Research Part B: Methodological*, Vol. 45, No. 3, pp. 507–533, 2011.

Sun, Z. and Ban, X. J.: Vehicle trajectory reconstruction for signalized intersections using mobile traffic sensors, *Transportation Research Part C: Emerging Technologies*, Vol. 36, pp. 268–283, 2013.

Sun, Z., Jin, W.-L., and Ritchie, S. G.: Simultaneous state and parameter estimation in newell's simplified kinematic wave model with heterogeneous data, in *Transportation Research Board 94th Annual Meeting*, 2015.

Talebpour, A. and Mahmassani, H.: Influence of autonomous and connected vehicles on stability of traffic flow, in *Transportation Research Board 94th Annual Meeting*, 2015.

Treiterer, J. and Myers, J.: The hysteresis phenomenon in traffic flow, in Buckley, D. J. ed. *Transportation and Traffic Theory*, Springer, pp. 13–38, 1974.

TSS-Transport Simulation Systems: Aimsun. http://www.aimsun.com.

van Lint, J. W. C. and Hoogendoorn, S. P.: A robust and efficient method for fusing heterogeneous data from traffic sensors on freeways, *Computer-Aided Civil and Infrastructure Engineering*, Vol. 25, No. 8, pp. 596–612, 2010.

van Lint, J. W. C., Hoogendoorn, S. P., and Hegyi, A.: Dual EKF state and parameter estimation in multi-class first-order traffic flow models, in *Proceedings of the 17th IFAC World Congress*, pp. 14078–14083, 2008.

van Wageningen-Kessels, F., van Lint, H., Hoogendoorn, S. P., and Vuik, K.: Lagrangian formulation of multiclass kinematic wave model, *Transportation Research Record: Journal of the Transportation Research Board*, Vol. 2188, pp. 29–36, 2010.

van Wageningen-Kessels, F., van Lint, H., Vuik, K., and Hoogendoorn, S.: Genealogy of traffic flow models, *EURO Journal on Transportation and Logistics*, 2014.

van Wageningen-Kessels, F., Yuan, Y., Hoogendoorn, S. P., van Lint, H., and Vuik, K.: Discontinuities in the Lagrangian formulation of the kinematic wave model, *Transportation Research Part C: Emerging Technologies*, Vol. 34, pp. 148–161, 2013.

Vlahogianni, E. I., Karlaftis, M. G., and Golias, J. C.: Short-term traffic forecasting: Where we are and where we're going, *Transportation Research Part C: Emerging Technologies*, Vol. 43, Part 1, pp. 3–19, 2014.

Wada, K., Ohata, T., Kobayashi, K., and Kuwahara, M.: Traffic measurements on signalized arterials from vehicle trajectories, *Interdisciplinary Information Sciences*, Vol. 21, No. 1, pp. 77–85, 2015.

Wang, Y. and Papageorgiou, M.: Real-time freeway traffic state estimation based on extended Kalman filter: a general approach, *Transportation Research Part B: Methodological*, Vol. 39, No. 2, pp. 141–167, 2005.

Wang, Y., Papageorgiou, M., Messmer, A., Coppola, P., Tzimitsi, A., and Nuzzolo, A.: An adaptive freeway traffic state estimator, *Automatica*, Vol. 45, No. 1, pp. 10–24, 2009.

Wardrop, J. G.: Some theoretical aspects of road traffic research, in *ICE Proceedings: Engineering Divisions*, Vol. 1, pp. 325–362, Thomas Telford, 1952.

Wardrop, J. G. and Charlesworth, G.: A method of estimating speed and flow of traffic from a moving vehicle, in *ICE Proceedings: Engineering Divisions*, Vol. 3, pp. 158–171, Thomas Telford, 1954.

Wei, C. and Asakura, Y.: A Bayesian approach to traffic estimation in stochastic user equilibrium networks, *Transportation Research Part C: Emerging Technologies*, Vol. 36, pp. 446–459, 2013.

Wilby, M. R., Diaz, J. J. V., Gonzlez, A. B. R., and Sotelo, M. A.: Lightweight occupancy estimation on freeways using extended floating car data, *Journal of Intelligent Transportation Systems*, Vol. 18, No. 2, pp. 149–163, 2014.

Yamamoto, T., Miwa, T., Takeshita, T., and Morikawa, T.: Updating dynamic origin-destination matrices using observed link travel speed by probe vehicles, in *Transportation and Traffic Theory 2009: Golden Jubilee*, Springer, pp. 723–738, 2009.

Yanagihara, M., Uno, N., and Nakamura, T.: Latent class analysis for driving behavior on merging section, in *Transportation Research Procedia*, Vol. 6, pp. 259–271, 2015.

Yang, H., Sasaki, T., Iida, Y., and Asakura, Y.: Estimation of origin-destination matrices from link traffic counts on congested networks, *Transportation Research Part B: Methodological*, Vol. 26, No. 6, pp. 417–434, 1992.

Yokoi, K., Suzuki, Y., Sato, T., Abe, T., Toda, H., and Ozaki, N.: A camera-based probe car system for traffic condition estimation, in *Proceedings of 20th ITS World Congress*, 2013.

Yuan, Y., van Lint, J. W. C., Wilson, R. E., van Wageningen-Kessels, F., and Hoogendoorn, S. P.: Real-time Lagrangian traffic state estimator for freeways, *Intelligent Transportation Systems, IEEE Transactions on*, Vol. 13, No. 1, pp. 59–70, 2012.

Zhang, H. M.: Traffic flow theory in an era of automated vehicles, in *Transportation Research Board 94th Annual Meeting*, 2015.

Zhang, G., Wang, Y., Wei, H., and Chen, Y.: Examining headway distribution models with urban freeway loop event data, *Transportation Research Record: Journal of the Transportation Research Board*, Vol. 1999, pp. 141–149, 2007.

Zheng, Z.: Recent developments and research needs in modeling lane changing, *Transportation Research Part B: Methodological*, Vol. 60, pp. 16–32, 2014.

Zito, R., D'Este, G., and Taylor, M. A. P.: Global positioning systems in the time domain: How useful a tool for intelligent vehicle-highway systems? *Transportation Research Part C: Emerging Technologies*, Vol. 3, No. 4, pp. 193–209, 1995.

上田大樹, 井料隆雅, 朝倉康夫: 長期 ETC 統計データによる異なるランプ間 OD 交通量と旅行時間の相関分析, 交通工学, Vol. 49, No. 3, pp. 43–52, 2014.

小谷益男, 古市朋輝, 児島正之, 岩崎征人: 高速道路単路部における連続的な交通容量推定手法とその有効性, 土木学会論文集, No. 737/IV-60, pp. 125–131, 2003.

白石智良, 赤羽弘和, 森田綽之, 堀口良太: 都市高速道路の感知交通量のバイアス補正手法の開発, 第 32 回交通工学研究発表会講演論文集, 2012.

瀬尾亨, 日下部貴彦, 朝倉康夫: 車間距離を計測するプローブカーを前提とした交通状態の推定手法, 土木学会論文集 D3（土木計画学）, Vol. 69, No. 5, pp. I_809–I_818, 2013.

瀬尾亨, 朝倉康夫: 車間距離測定プローブカーの長期観測に基づくネットワーク交通流のノンパラメトリック推定, 土木計画学研究・講演集, Vol. 49, 2014.

瀬尾亨, 日下部貴彦, 朝倉康夫: 車間距離測定プローブカーを用いた都市高速道路の交通流観測実験報告, 第 34 回交通工学研究発表会論文集, pp. 277–283, 2014.

成岡尚哉, 瀬尾亨, 日下部貴彦, 朝倉康夫: ノンパラメトリック手法による車両感知器データからの突発的ボトルネック検出法, 交通工学論文集, Vol. 1, No. 1, pp. 11–20, 2015.

花岡洋平, 安田宗樹, 桑原雅夫, 原祐輔: ガウシアングラフィカルモデルを用いたネットワーク交通状況の補間推定に関する研究, 土木計画学研究・講演集, Vol. 47, 2013.

樋口知之（編）データ同化入門, 朝倉書店, 2011.

和田健太郎, 佐津川功季: 動的利用者均衡状態における MFD の解析：1 起点多終点ネットワークの場合, 土木計画学研究・講演集, Vol. 50, 2014.